Synthesis, Characterization and Photo-physical Properties of Zinc(II) and Ruthenium(II) Complexes with 2-(4′-*N*,*N*-dimethylaminophenylazo) pyridine Ligand

Wasana Runrueng

A Thesis Submitted in Partial Fulfillment of the Requirements for the Degree of Master of Science in Inorganic Chemistry

Prince of Songkla University

2013

Thesis Title	Synthesis, Characterization and Photo-physical Properties of Zinc (II) and Ruthenium (II) Complexes with 2-(4′-*N*,*N*-dimethylaminophenylazo)pyridine Ligand
Author	Miss Wasana Runrueng
Major Program	Chemistry

Major Advisor

…….…….....

(Dr. Nararak Leesakul)

Examining Committee

….……..…Chairperson

(Asst.Prof.Dr.Yuthana Tantirungrotechai)

…….…….....

(Asst.Prof.Dr.Kanidtha Hansongnern)

…….....

(Dr. Walailak Puetpaiboon)

…….....

(Dr.Nararak Leesakul)

The Graduate School, Prince of Songkla University, has approved this thesis as partial fulfillment of the requirements for the Master of Science Degree in Chemical Studies.

…….....

(Assoc. Prof. Dr. Teerapol Srichana)
Dean of Graduate School

This is to certify that the work here submitted is the result of the candidate's own investigations. Due acknowledgement has been made of any assistance received.

…….Signature

(Dr.Nararak Leesakul)

Major Advisor

…….Signature

(Wasana Runrueng)

Candidate

I hereby certify that this work has not been accepted in substance for any degree, and is not being currently submitted in candidature for any degree.

…… Signature

(Wasana Runrueng)

Candidate

ชื่อวิทยานิพนธ์ การสังเคราะห์ ศึกษาโครงสร้างและศึกษาคุณสมบัติเชิงแสงของสารประกอบเชิงซ้อนของโลหะสังกะสี (II) และรูทีเนียม (II) กับลิแกนด์ 2-(4′-*N,N*- dimethylaminophenylazo)pyridine

ผู้เขียน นางสาว วาสนา รื่นเริง

สาขาวิชา เคมีอนินทรีย์

ปีการศึกษา 2556

บทคัดย่อ

สารประกอบเชิงซ้อนของโลหะ Zn(II) และ Ru(II), [(Zn(dmazpy)Cl_2)], [Ru(dmazpy)(*p*-cymene)Cl]Cl, Ru(dmazpy)(dcbpyH_2)$_2$ และ Ru(dmazpy)(dcbpyH_2)(SCN)$_2$ เมื่อ dmazpy คือ 2-(4′-*N,N*-dimethylaminophenylazo)pyridine และ (dcbpyH_2) คือ 4-4′-dicarboxylic acid-2,2′-bipyridine ถูกสังเคราะห์ขึ้นเพื่อศึกษาโครงสร้าง ด้วยเทคนิคการวิเคราะห์ปริมาณธาตุและเทคนิคทางสเปกโตรสโกปีต่างๆ ได้แก่ IR, การวัดการดูดกลืนแสงและการเปล่งแสงในช่วง UV-vis, NMR, ES-MS และX-ray diffraction พบว่าสารประกอบเชิงซ้อนของ Zn(II) เมื่อใช้อัตราส่วนในการ ทำปฏิกิริยาของสารตั้งต้น $ZnCl_2.3H_2O$ กับลิแกนด์ dmazpy เป็น 1:1 พบว่าเกิดสารประกอบเชิงซ้อนสีชมพูแดง ของ Zn(dmazpy)Cl_2 มีโครงสร้างผลึกเป็นทรงเหลี่ยมสี่หน้าบิดเบี้ยว (distorted tetrahedral) ดูดกลืนแสงที่ความยาวคลื่นสูงสุดประมาณ 552 nm สามารถเปล่งแสงที่ความยาวคลื่น 620 nm เมื่อกระตุ้นด้วยความยาวคลื่น 550 nm สารประกอบเชิงซ้อนของ Zn(dmazpy)Cl_2 ที่สังเคราะห์ได้ จึงเป็นสารที่มีคุณสมบัติเชิงแสง (photo active compound) ส่วนสารประกอบเชิงซ้อน Ru(dmazpy)(dcbpyH_2)(SCN)$_2$ สังเคราะห์จากปฏิกิริยาระหว่างสารตั้งต้น [Ru-(*p*-cymene)(dmazpy)Cl]Cl กับลิแกนด์ dcbpyH_2 ส่วนสารประกอบเชิงซ้อน[(Ru(dmazpy)(dcbpyH_2)$_2$)(PF_6)$_2$ สังเคราะห์จากปฏิกิริยาระหว่าง $RuCl_3$.3 H_2O กับลิแกนด์ dcbpyH_2 และ dmapy ตามลำดับ พบว่า สารประกอบเชิงซ้อนทั้งสองชนิดมีคุณสมบัติทางเคมีที่ซับซ้อนจากธรรมชาติของลิแกนด์เอง ซึ่งไม่สามารถทำให้บริสุทธิ์เพื่อยืนยันโครงสร้างที่แท้จริงได้ แต่อย่างไรก็ตามได้ประสบผลสำเร็จในการสังเคราะห์สารตั้งต้นสังเคราะห์ [Ru(*p*-cymene)(dmazpy)(Cl)]Cl และรายงานการศึกษาโครงสร้างด้วยเทคนิคทางสเปกโตรสโกปีต่างๆรวมถึงคุณสมบัติเชิงแสงและสมบัติทางไฟฟ้าเคมีด้วยเทคนิคไซคลิกโวลแทมเมตรี

Thesis Title Synthesis, Characterization and Photo-physical Properties of Zinc(II) and Ruthenium(II) Complexes with 2-(4′-*N,N*-

dimethylaminophenylazo)pyridine Ligand

Author Miss Wasana Runrueng

Major Program Inorganic Chemistry

Academic Year 2013

ABSTRACT

Complexes of Zn(II) and Ru(II), (ZndmazpyCl_2), [Ru(dmazpy)(*p*-cymene) Cl]Cl, Ru(dmazpy)(dcbpyH_2)$(SCN)_2$ and Ru(dmazpy)(dcbpyH_2)$_2$ where dmazpy is 2-(4′-*N*,*N*-dimethylaminophenylazo)pyridine, *p*-cymene is *p*-isopropyl methylbenzene and dcbpyH_2 is 4,4′-dicarboxylic-2,2′-bipyridine were synthesized and characterized by using elemental analysis and spectroscopic techniques (IR, NMR, ES-MS, X-ray diffraction and UV-Vis absorption). It has been found that the Zn(dmazpy)Cl_2 was formed by 1:1 reaction between $ZnCl_2.3H_2O$ and dmazpy ligand. The pinkish red of Zn(dmazpy)Cl_2 crystal structrure is a distorted tetrahedral geometry. It displays absorption band at 552 nm and emits at 610 nm (λex=550 nm). The Zn(dmazpy)Cl_2 is a photo active complex. [Ru(dmazpy)(dcbpyH_2)$(SCN)_2$] complex was obtained from the reaction between the [Ru(dmazpy)(*p*-cymene)(dmazpy)Cl]Cl precursor and dcbpyH_2 ligand while the complex of [Ru(dcbpyH_2)$_2$(dmazpy)]$(PF_6)_2$ was synthesized from the reaction between $RuCl_3.3H_2O$ with dmazpy and dcbH_2, respectively. It is unfortunately that both complexes have the complicated chemistry by the nature of ligands. They could not be purified enough to study the real structure. Nevertheless, the precursor of [Ru(*p*-cymene)(dmazpy)Cl]Cl is sported for its structure by spectroscopic techniques, its electrochemistry property.

CONTENTS

LIST OF TABLES

LIST OF FIGURES

\

LIST OF FIGURES (continued)

LIST OF FIGURES (continued)

LIST OF FIGURES (continued)

LIST OF FIGURES (continued)

LIST OF FIGURES (continued)

CHAPTER 1
INTRODUCTION

1.1 Introduction

Compounds of azo (–N=N–) group are well known photoactive materials (Ho *et al.,* 1995). They are widely used as dyes in the textile industry, as substrates for photo aligning for liquid crystals (Gibbon *et al.,* 1991), in optical data storage devices and light sensitizers in dye-sensitized solar cells (Sharma *et al.,* 2008).A modification of azo compounds is connecting azo group to an imine (-C=C-N=C–) function yielding azo-imine (–N=C-N=N–) moiety. The azo-imine compounds are frequently as the powerful ligands of transition metal complexes owing to their great σ-donor and π-accepter property. Besiders their low-lying π*- molecular orbitals are extensively chelating ligands with metal ions such as Ru(II) and Os(II) (Mondal *et al.,* 2007). The applications of azo-imine compounds and the complexes with metal ions mostly are on the textile coloring (Millington *et al*., 2007) and photochromic agent (Byabarlta *et al*., 2001). There has been a substantial examination of the chemistry of Zn(II) complexes of N-donor heterocycles (Das *et al*., 2006 and Chand *et al*., 2003) as possible optical materials.

In the present study, the synthesis of an azo-imine, 2-(4′-*N,N*-dimethylamino phenylazo)pyridine (dmazpy) (Figure 1a) and its Zn (II) and Ru (II) complexes are investigated. The structure of Zn(II) complex ($Zn(dmazpy)Cl_2$) is shown in Figure 1b. Other complexes as of Ru(II) are the [Ru(*p*-cymene)(dmazpy)Cl]Cl (cpx3, Figure 1c), $Ru(dmazpy)(dcbH_2)(SCN)_2$ cpx 4 (Figure 1d) and $[Ru(dmazpy)(dcbH_2)_2](PF_6)_2$ (cpx 5, Figure 1e) where $dcbH_2$ is 4,4′-dicarboxylic acid-2,2′-bipyridine which was expected to be a sensitizer in dye-sensitized solar cell (DSSC). The precursor of Ru(*p*-cymene)$(dmazpy)Cl_2$ (Figure 1c) is synthesized and used to prepare the neutral complex of Ru (II), $Ru(dmazpy)(dcbH_2)(SCN)_2$. The consisting of $dcbH_2$ ligand is for anchoring with TiO_2 while the existing of dmazpy is objected to enhancing the

absorption property in the visible region. All compounds are characterized by spectroscopic techniques and the photo-physical properties are investigated.

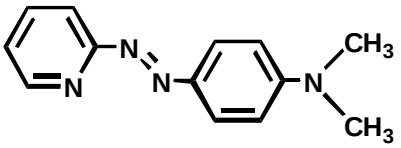

Figure 1a

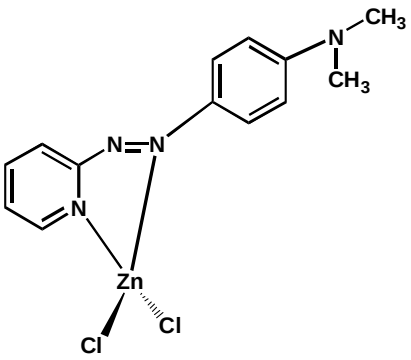

Figure 1b

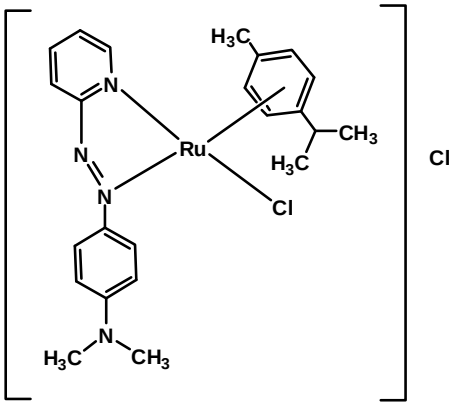

Figure 1c

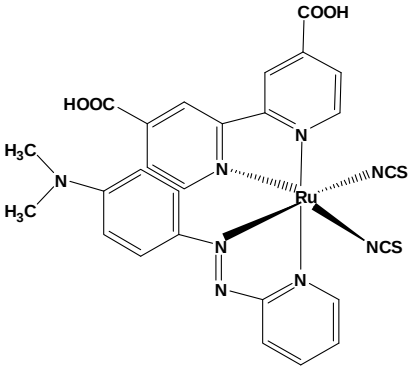

Figure 1d

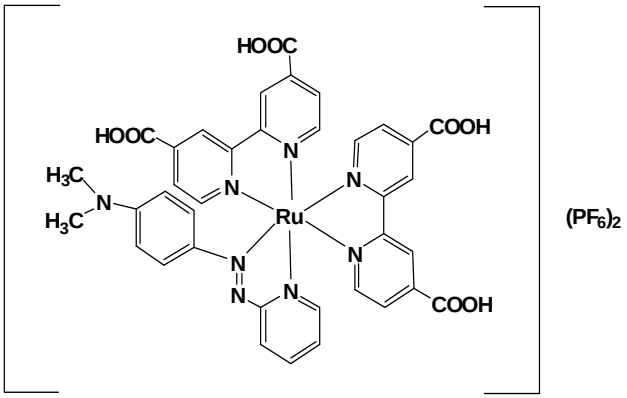

Figure 1e

Figure 1 a. 2-(4′-*N,N*-dimethylaminophenylazo)pyridine ligand (dmazpy)

b. [Zn(dmazpy)Cl_2] (cpx 1)

c. [Ru(*p*-cymene)(dmazpy)Cl_2] (cpx 2)

d. [Ru(dmazpy)(dcbpy)$(SCN)_2$] (cpx 3)

e. [Ru(dmazpy)$(dcbH_2)_2$]$(PF_6)_2$ (cpx 4)

Dye-sensitized solar cells (DSSCs) have attracted much attention as they can offer high-energy conversion efficiencies. DSSCs are easy to fabricate, and the manufacturing cost is lower compared to silicon solar cells (Gratzel *et al*, 1997).

The working scheme of a typical cell is illustrated in Figure 2, showing a TiO_2 layer deposited on a conductive ITO glass. The dye is placed over this semiconductor film, in contact with an electrolyte. The excitation of the dye upon irradiation is followed by injection of the resulting electrons into the CB of the semiconductor, from where they reach the cell anode (usually a conductive glass or plastic). Regeneration of electrons occur through donation from a redox electrolyte in contact with the dye. This typically occurs through an organic solvent containing an iodide/triiodide couple. Triiodide is reduced in turn at the counter electrode, while electron migration from the anode to the counter electrode closes the circuit.

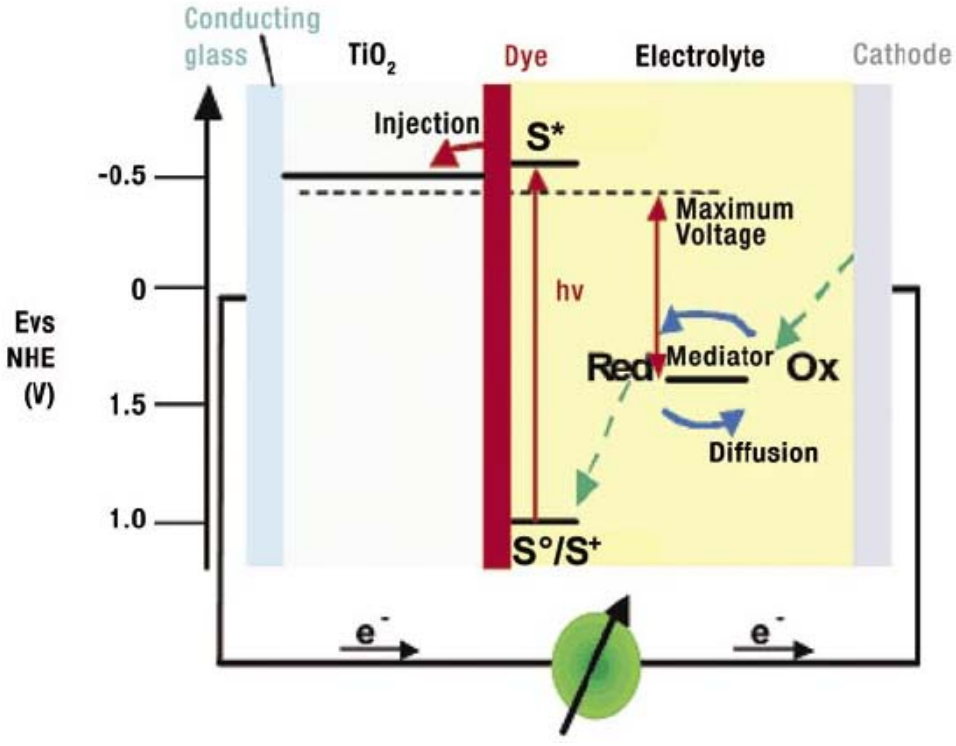

Figure 2 Scheme of manipulating a typical dye-sensitised solar cell.
Picture from Photovoltaics International journal

1.2 Review of Literature

Nag *et al.*, (2001) synthesized 2-(Arylazo)pyridines (aap) (R-C_6H_4-N=N-C_5H_4N, **1**) 2-(arylazo)pyrimidines (aapm) (R-C_6H_4-N=N-$C_4H_3N_2$, **2**); R=H, *o*-Me, *m*-Me, *p*-Me, *p*-Cl and dichloro-(2-(phenylazo)pyrimidine)zinc(II)·CH_3OH. The complexes were characterized by elemental analyses, IR, UV–Vis absorption and ^1H NMR spectral data. Single-crystal X-ray structure of dichloro-(2-(arylazo)pyrimidine)zinc(II) ·CH_3OH (Figure 3) suggests that the complex is a distorted trigonal bipyramidal symmetric around Zn(II), and Cl(1), Cl(2), N(4) (N (azo)) make the trigonal plane. Zn(II) moves downwards by 0.12 Å from the centre of gravity of the plane. Two axial positions are occupied by N(1) (N(pyrimidine)) and methanol-O. Molecular packing shows one-dimensional infinite chain via hydrogen bonding.

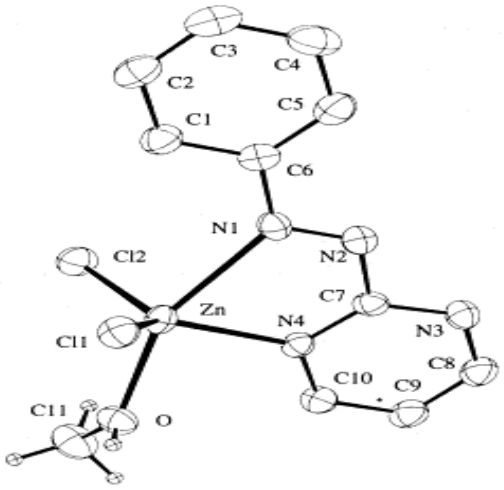

Figure 3 Single-crystal X-ray structure of Zn(papm)Cl_2·CH_3OH.

Source: Nag *et al*., (2001)

Santra *et al*., (2001) studied the reaction of 2-(arylazo)pyrimidine (aapm) with $Ru(PPh_3)_3Cl_2$ in CH_2Cl_2 solution affords $[Ru(PPh_3)_2(aapm)Cl_2]$ (**2**) while the reaction under refluxing conditions in EtOH isolates $[Ru(PPh_3)_2(aapm)_2]$ $(ClO_4)_2·H_2O$(**3**/**4**). Single crystal X-ray diffraction study of dichloro-bis(triphenylphosphine){2-(phenylazo)pyrimidine}ruthenium(II) (Figure 4) has assigned a *cis*-$Ru(PPh_3)_2$ motif to the complex. Isomers of $[Ru(PPh_3)_2(aapm)_2](ClO_4)_2$ have been characterized by ^1H NMR. They exist in *cis–trans–cis* and *cis–cis–cis* configurations in which

coordination is considered with reference to three pairs of sequence of P, P (PPh_3 abbreviated as P), N, N (N is N(pyrimidine)) and N′, N′ (N′ is N(azo)). The complexes exhibit MLCT transitions in the visible region. Redox studies show the Ru(III)/Ru(II) couple is in the range 0.8–1.2 V vs. SCE and $[Ru(PPh_3)_2(aapm)_2](ClO_4)_2$ exhibits a higher potential value than that of $[Ru(PPh_3)_2(aapm)Cl_2]$.

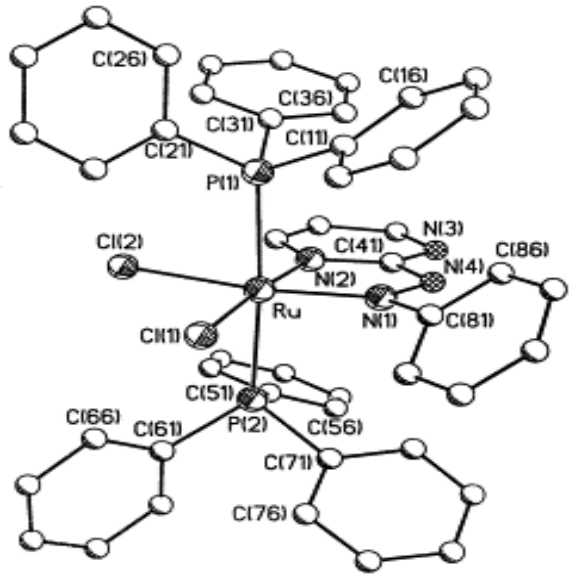

Figure 4 Single crystal X-ray structure and the atom-labelling scheme for $Ru(P)_2(papm)Cl_2$ (**2a**). For clarity, all hydrogen atoms have been omitted.

Source: Santra *et al*., (2001)

Arslan *et al*., (2007) synthesized aqua(azobispyridine)bis(salicylato)zinc(II) monohydrate complex (**1**) as shown in Figure 5 and characterized by means of elemental analysis, IR and UV-vis spectroscopy, thermal analysis and X-ray diffraction techniques. The crystal structure analysis indicates that the mononuclear **1** shows an *s-cis*/*E*/*s-cis* configured azobispyridine ligand, with the distortion from square pyramidal toward trigonal bipyramidal. Zn(II) ion was coordinated to N from pyridyl and azo N atom together with two oxygen atoms from carboxylate and one oxygen from the aqua ligand. The crystal packing involves both hydrogen-bonding and π–π interactions. The title complex undergoes a thermochromic phase transition at *ca*. 189 °C, changing from **1** (brown) to **2** (purple) and the thermal decomposition of **1** proceeds in four stages.

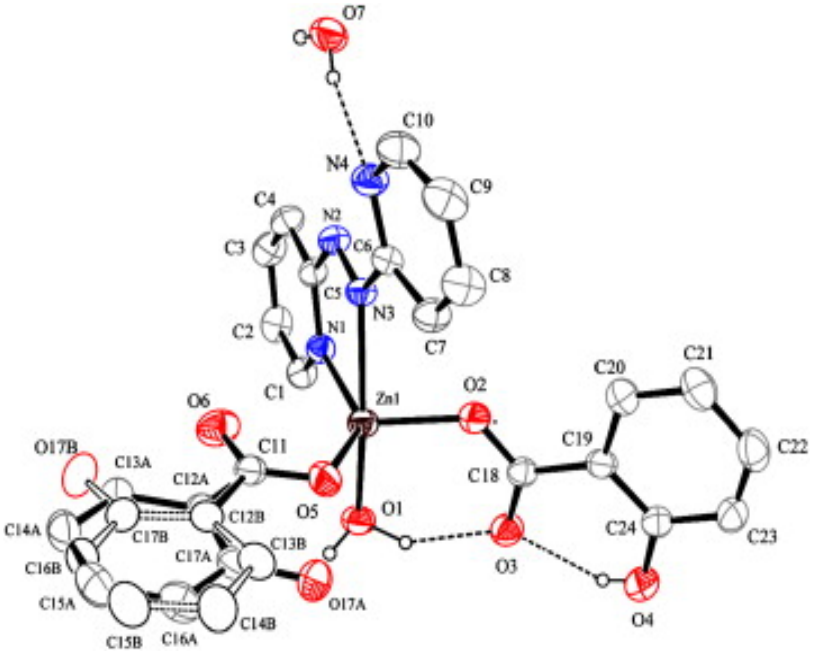

Figure 5 The molecular structure of **1**, showing the atom-numbering scheme. Displacement ellipsoids are drawn at the 30% probability level and H atoms are shown as small spheres of arbitrary radii.

Source: Arslan *et al*., (2007)

Samanta *et al*., (2007) synthesized four new coordination complexes, $Ni^{II}(L)_2$ (**1**), $[Co^{III}(L)_2]ClO_4$ (**2**), $[Zn(HL)(L)]ClO_4 \cdot H_2O$ (**3**) and $[Zn(L)_2][Zn(L)(HL)]ClO_4 \cdot 7H_2O$ (**4**) (where L is a monoanion of a Schiff base ligand, *N*′-[(2-pyridyl) methylene]salicyloylhydrazone (HL) with NNO tridentate donor set) as shown in Figure 6, have been synthesized and systematically characterized by elemental analysis, spectroscopic studies and room temperature magnetic susceptibility measurements. Single crystal X-ray diffraction analysis reveals that **1** is a neutral complex, while **2**–**4** are cationic complexes. Among them, **4** is a rare type of cationic complex with two molecules in the asymmetric unit. The ligand chelates the metal centre with two nitrogen atoms from the pyridine and imino moieties and one oxygen atom coming from its enolic counterpart. All the reported complexes show distorted octahedral geometry around the metal centres, with the two metal–N (imino) bonds being significantly shorter than the two metal–N (Py) bonds.

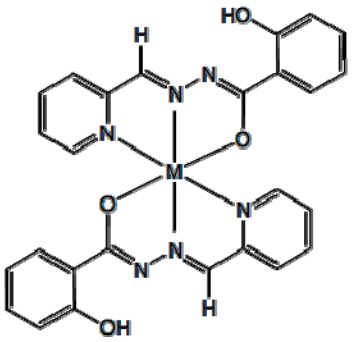

Central metal ion	Complex
Ni(II)	$Ni^{II}(L)_2$ (1)
Co(III)	$[Co^{III}(L)_2]ClO_4$ (2)
Zn(II)	$[Zn(HL)(L)]ClO_4 . H_2O$ (3)
Zn(II)	$[Zn(L)_2][Zn(L)(HL)]ClO_4 . 7H_2O$ (4)

Figure 6 Scheme of synthesis of the ligand and the complexes.

Source: Samanta *et al*., (2007)

Khalighi *et al*., (2008) synthesized $[ZnCl_2(C_{12}H_{12}N_2)]$ as shown in Figure 7, It contains two independent molecules. The Zn^{II} atoms are four-coordinated in distorted tetrahedral configurations by two N atoms from 5,5′-dimethyl-2,2′-bipyridine and two terminal Cl atoms. In the crystal structure, intermolecular C—H···Cl hydrogen bonds link the molecules. There are C—H···π contacts between the methyl groups and the pyridine and five-membered rings containing Zn^{II} atoms; π–π contacts also exist between the pyridine rings [centroid–centroid distances = 3.665 (5) and 3.674 (5) Å].

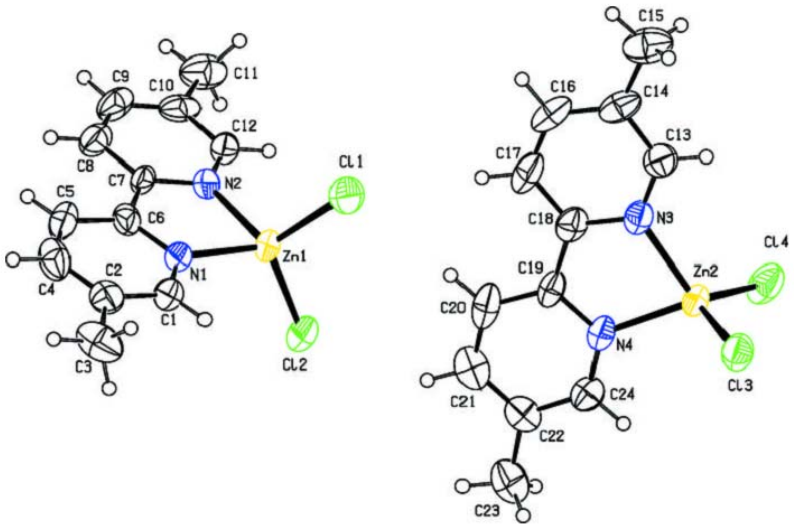

Figure 7 The molecular structure of the $[ZnCl_2(C_{12}H_{12}N_2)]$, with the atom-numbering scheme. Displacement ellipsoids are drawn at the 40% probability level.

Source: Khalighi *et al*., (2008)

Kalateh *et al*., (2010) synthesized [$ZnBr_2(C_{11}H_{10}N_2)$] as shown in Figure 8, The Zn^{II} atom is four-coordinated in a distorted tetrahedral configuration by two N atoms from a 6-methyl-2,2′-bipyridine ligand and two terminal Br atoms. Weak inter-molecular C—H···Br hydrogen bonds and π–π stacking interactions between the pyridine rings [centroid–centroid distances = 3.763 (5) and 3.835 (6) Å] contribute to crystal-packing effects.

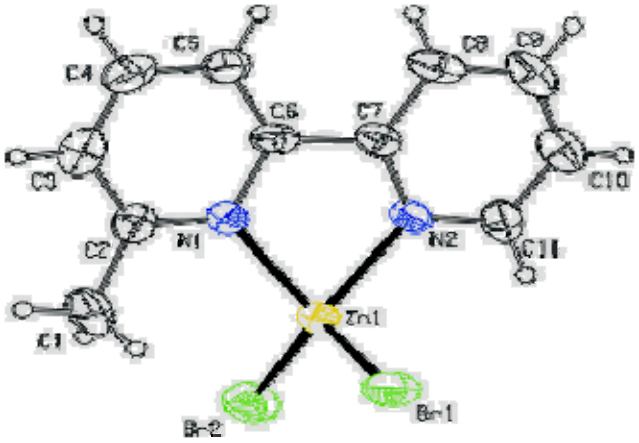

Figure 8 The molecular structure of [$Zn(C_{11}H_{10}N_2)Br_2$], with the atom-numbering scheme. Displacement ellipsoids are drawn at the 30% probability level.

Source: Kalateh *et al*., (2010)

Pramanik *et al*., (2010) studied the formation of a series of Cu(II), Zn(II) as shown in Figure 9 and Cd(II) complexes using the *p*-substituted aryl azo system has been reported. Presence of electron donating –Me, –OMe groups impart some unusual coordination behaviors in Cu(II) complexes. Varying coordination mode and electron density in the ligand results in the formation of an unusual Cu–S bond in complex **1** and an unusual equatorial coordination of H_2O in Cu(II) complex **2** with a square-pyramidal geometry.

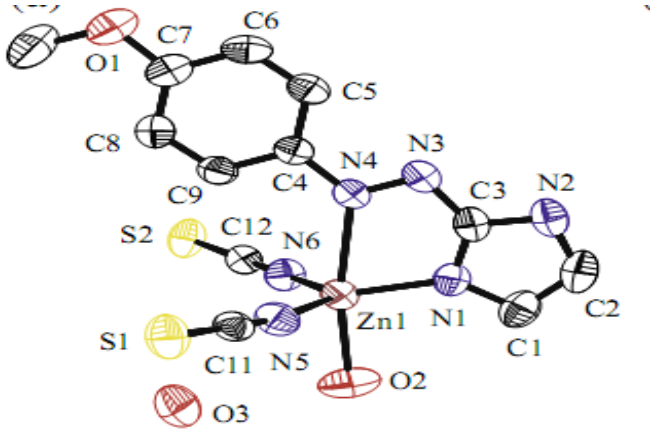

Figure 9 ORTEP plot of $[Zn(L_2)(NCS)_2(H_2O)]H_2O$**.**

Source: Pramanik *et al*., (2010)

Pramanik *et al*., (2010) synthesized aryl azo imidazole based building block and with the d^{10} metal [Zn(II), Cd (II) and Hg(II)] and counter anion (Cl, NO_3, SCN) in order to rationalize the effect of coordination behavior of the metal ion (Figure 10), the size of the anions and the substitution effects of ligands upon the structure adopted by theses metal complexes. Influences of halogen (Cl,Br and I) substitutions are reflected in the precise molecular level architecture in the individual complexes. The parameters related to the coordination sphere depend on the metal-to-ligand ratios and are also influenced by the solvent of crystallization. A competition between the coordinating capilities of the counter anion with ligands and its shape led to neutral and anionic metal complexes.

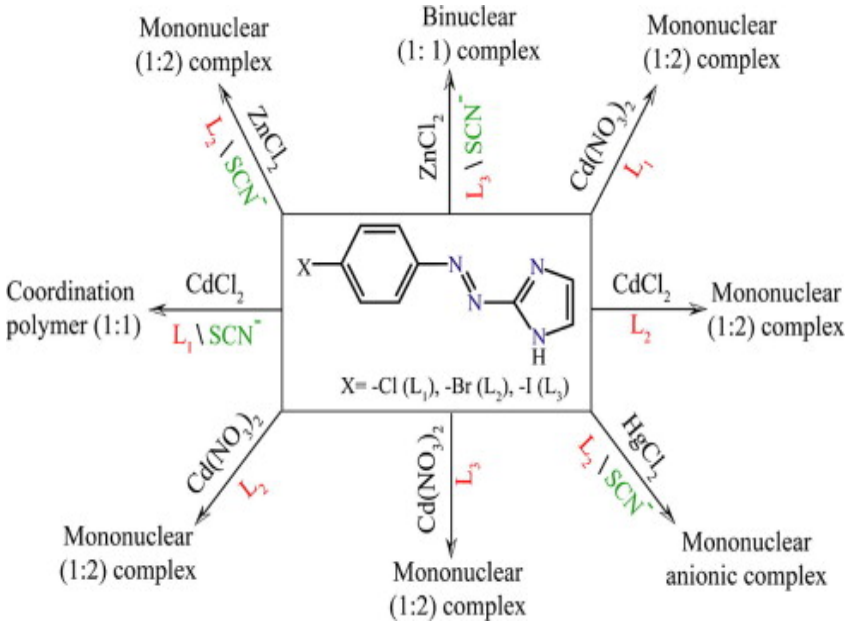

Figure 10 Effect of substituents and counter ions of self-assembly d^{10} metal complexes assisted by aryl azo system.

Source: Pramanik *et al*., (2010)

Leesakul *et al*., (2011) synthesized and characterized of a novel Zn^{II} complex with *N*,*N*-diethyl-4-[2-(pyridyl)diazenyl]aniline ($C_{30}H_{36}N_8$: deazpy), an azoimine ligand. The molecular structure of $Zn(C_{30}H_{36}N_8)Cl_2$ is a distorted tetrahedral complex (Figure 11). The *N*,*N*-diethyl-4-[2-(pyridyl)diazenyl] aniline ligand is a bidentate ligand. The chelated coordinations between Zn^{II} and N donor atoms of pyridine and azo moieties are generally observed in the crystal structure. However, the Zn^{II} coordinates to two unidentate deazpy ligands *via* N(py) atoms [Zn(1)—N(1) = 2.0513 (19) Å, Zn(1)—N(5) = 2.0439 (19) Å] and two Cl atoms [Zn(1)—Cl(1) = 2.2565 (6) Å, Zn(1)—Cl(2) = 2.2713 (6) Å]. These Zn—N bond distances are slightly longer than that of related Zn^{II} with two unidentate imidazole ligands giving the Zn—N distances = 2.003 (3) and 2.013 (3) Å.

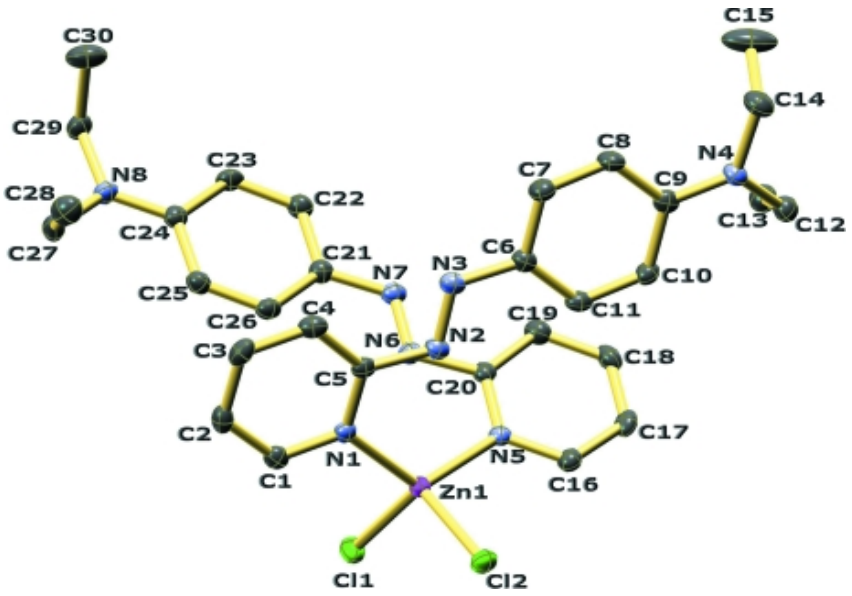

Figure 11 Molecular structure of $Zn(C_{30}H_{36}N_8)Cl_2$ complex with thermal ellipsoids plotted at the 50% probability level. H atoms are omitted.

Source: Leesakul *et al*., (2011)

Tan *et al*., (2011) synthesized $[ZnCl_2(C_8H_7N_3)_2]$ as shown in Figure 12, the Zn^{II} cation is coordinated by two Cl^- anions and two 4-(1*H*-pyrazol-3-yl)pyridine ligands in a distorted tetrahedral geometry. In the two 4-(1*H*-pyrazol-3-yl)pyridine ligands, the dihedral angles between the pyrazole and pyridine rings are 3.3 (3) and 13.3 (3)°. Intermolecular N—H···N and N—H···Cl hydrogen bonding is present in the crystal structure (Figure 13).

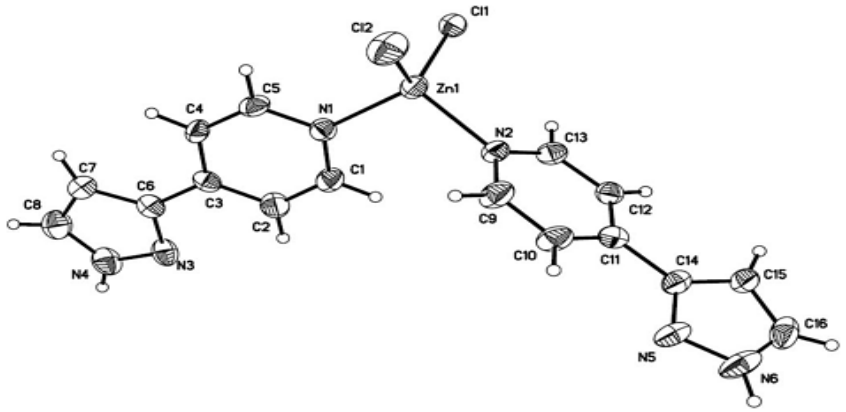

Figure 12 The structure of $[ZnCl_2(C_8H_7N_3)_2]$, showing the atomic numbering scheme with 30% probability displacement ellipsoids.

Source: Tan *et al*., (2011)

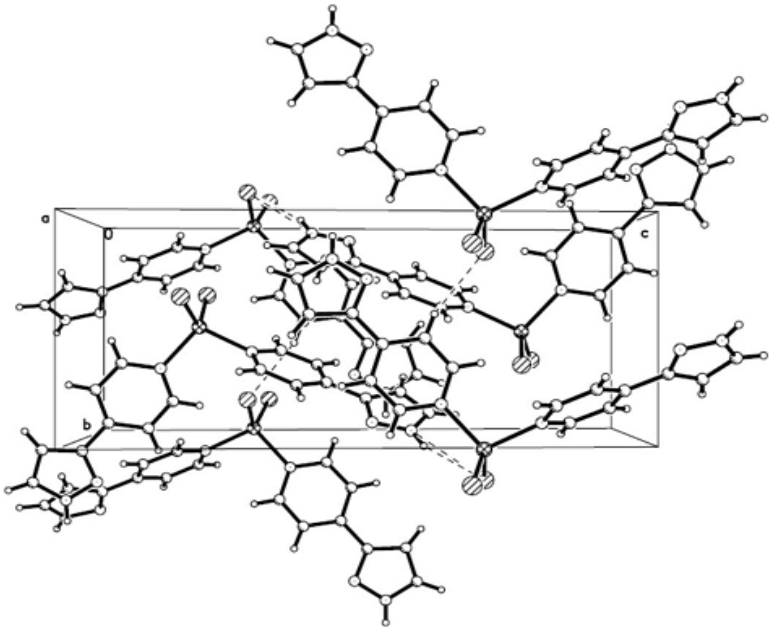

Figure 13 A view of the three-dimensional network of $[ZnCl_2(C_8H_7N_3)_2]$. Hydrogen bonds are shown as dashed lines.

Source: Tan *et al*., (2011)

Anitha *et al*., (2012) synthesized the Schiff base complexes of VO(II), Co(II), Ni(II), Cu(II) and Zn(II) derived from 3-(4-5-(4-chlorophenyl)diazenyl)-2-hydroxybenzylideneamino)phenylimino)methyl)-4H-chromen-4-one [CDHBPC] and characterized on the basis of analytical and spectral data. The results of this investigation support the suggested octahedral structure of the metal complexes as shown in Figure 14. This complex shows relatively strong solid state NLO properties with the relative SHG efficiency of the material 2.7 and 3.2 times more active than urea and KDP. The Schiff bases and their metal complexes were found to be highly active against the antibacterial and antifungal species. Presence of two azomethine, and a more extended conjugated system shows higher luminescence efficiency of the synthesized compounds. All the compounds are thermally very stable with high melting point and intense color and are attractive from the point of view of studying photoinduced effects in theory.

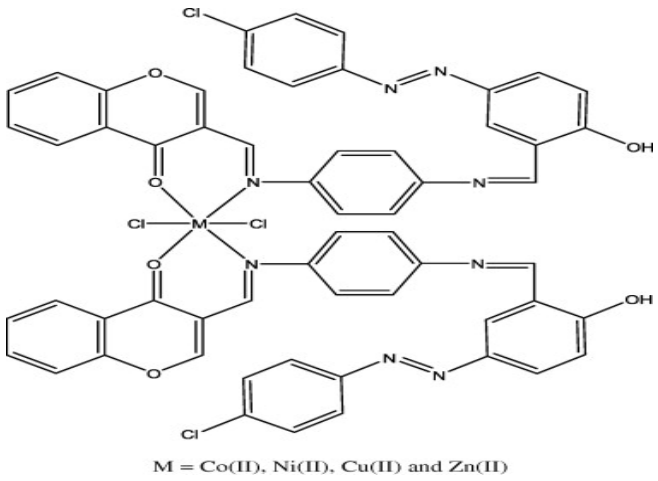

Figure 14 Proposed structure of metal (II) complexes with 3-(4-5-(4-chlorophenyl)diazenyl)-2-hydroxybenzylideneamino) phenylimino)methyl)-4H-chromen-4-one [CDHBPC] .

Source: Anitha *et al*., (2012)

Dharmalingam *et al*., (2012) synthesized [$ZnCl_2(C_{11}H_9N)_2$] as shown in Figure 15, the Zn^{2+} cation lies on a twofold axis and is coordinated by two Cl^- anions and the N atoms of two 2-phenylpyridine ligands, forming a ZnN_2Cl_2 polyhedron with a slightly distorted tetrahedral coordination geometry. The dihedral angle between the phenyl ring and the metal-bound pyridine ring is 50.3 (4)° for each 2-phenylpyridine ligand. This arranges the phenyl ring from one ligand in the complex above the pyridine ring of the other resulting in an intramolecular π–π interaction, with a centroid–centroid distance of 3.6796 (17) Å. Weak C—H···Cl hydrogen bonds stabilize the crystal packing, linking molecules into chains along the *c* axis (Figure 16).

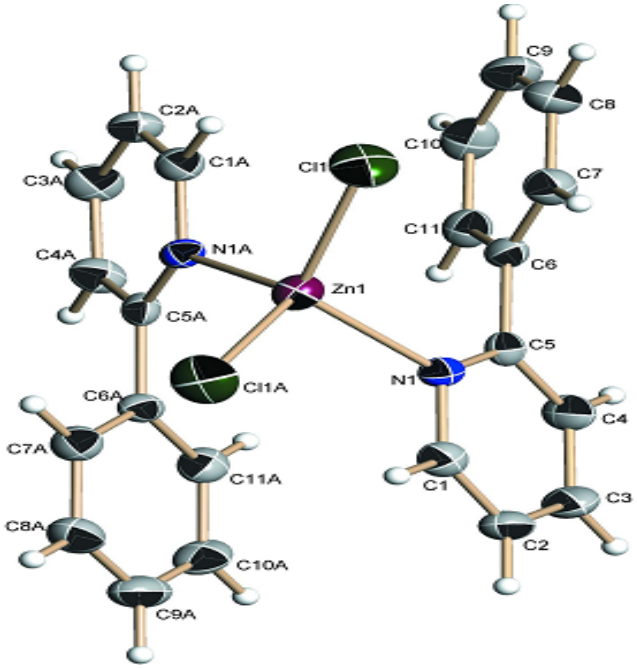

Figure 15 The molecular structure of [$ZnCl_2(C_{11}H_9N)_2$], showing the atom-numbering and with displacement ellipsoids drawn at the 50% probability level.

Source: Dharmalingam *et al*., (2012)

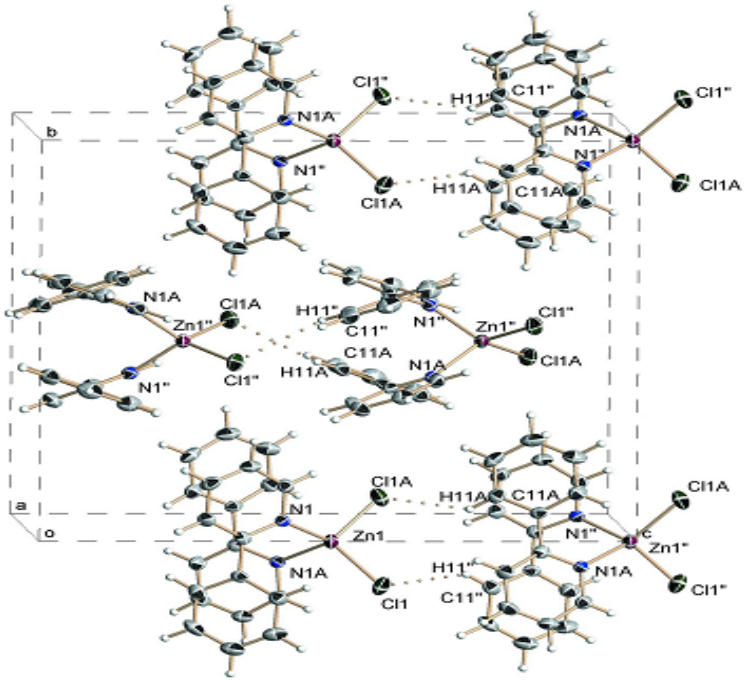

Figure 16 A crystal packing diagram of $[ZnCl_2(C_{11}H_9N)_2]$,, viewed along the a axis.

Source: Dharmalingam *et al*., (2012)

Leesakul *et al*., (2012) synthesized $(C_{13}H_{16}N_4)[ZnCl_4]$ as shown in Figure 17, consists of a tetrahedral $[ZnCl_4]^{2-}$ anion and a 2-{2-[4-(dimethylamino)phen-yl]diazen-1-ium-1-yl}pyridinium dication. The pyridinium-N atom is *syn* to the azo bond which allows for the formation of an intramolecular N—H···N hydrogen bond. In the crystal, the cation and anion are held together by N—H···Cl hydrogen-bond interactions involving the pyridinium and diazen-1-ium N atoms. The π–π stacking interactions occur between the pyridine and benzene rings of adjacent cations [centroid–centroid distances = 3.6270 (18) and 3.8685 (18) Å]; the stacks are parallel to the *a* axis.

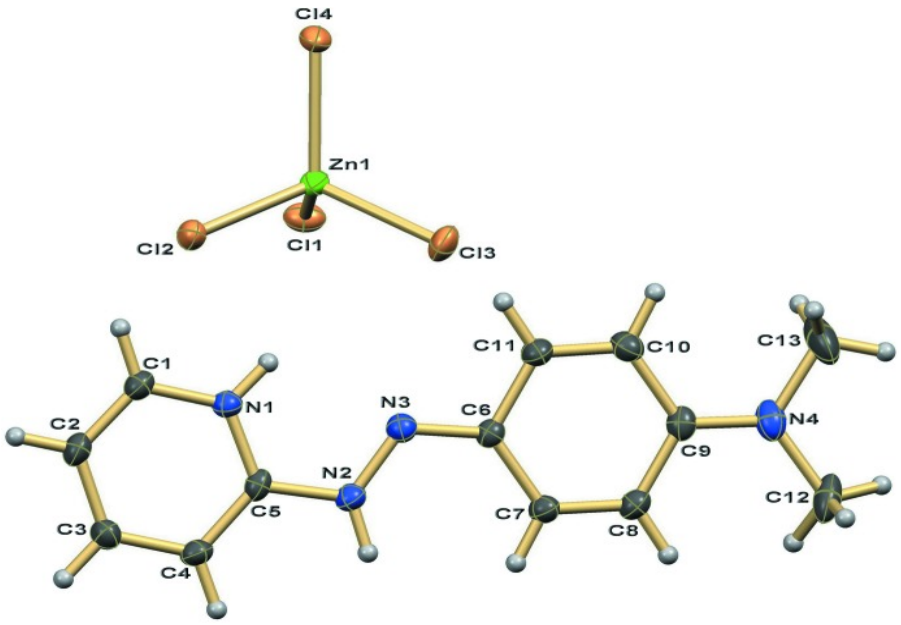

Figure 17 Molecular structure of [(H_2dmazpy)($ZnCl_4$)] with thermal ellipsoids plotted at the 50% probability level.

Source: Leesakul *et al*., (2012)

Synthesis and characterization of ruthenium (II) complexes and their for dye-sensitized solar cells were investigated intensively by researchers for decades. For example,

Huang *et al*., (2010) synthesized three novel heteroleptic ruthenium complexes, RD1 RD2 and RD3. When RD1 is [Ru (dcbpy)(1-methyl-2-(pyridin-2-yl)-1H-ben- zimidazole)$(NCS)_2$], RD2 is [Ru(dcbpy)(2-(pyridine-2-yl) benzothiazole) $(NCS)_2$] and RD3 is [Ru(dcbpy)(2-(pyridin-2-yl) benzoxazole)(NCS)]. Compared with the dcbpy ligand used in N3 dye, these unsymmetrical ligands were easy to synthesize with larger dye loading on TiO_2 surface than that of N719. RD1 reaches 80 % cell performance of N719, and it is the best among these three dyes due to its larger dye loading and broader IPCE action spectrum. Structures of the complexes are shown in Figure 18.

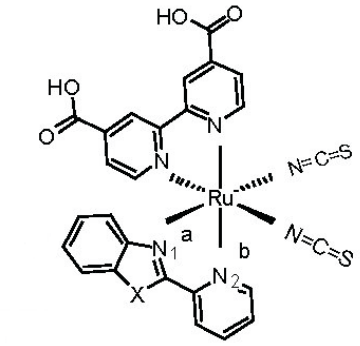

Figure 18 Structure of the complexes RD1 RD2 and RD3

Source: Huang *et al*., (2010)

Jiang *et al*., (2008) synthesized polypyridine ruthenium complex of the type *cis*-Ru(L1)(L2)$(NCS)_2$, (coded as HRD-2), When L1 is 4,4′-dicarboxylic acid-2,2′-bipyridine (dcbpy), L2 is 4,4′-bis[p-diethylamino]-a-styryl]-2,2′-bipyridine. The dye displays extremely high molar extinction coefficient, which is comparable with organic dye. Preliminary test shows the dye-sensitized TiO_2 solar cell gives high conversion efficiency up to 8.65% under 1 Sun, while 8.35% is given for N3 based DSCs under the same condition. Structure of the complex was shown in Figure 19.

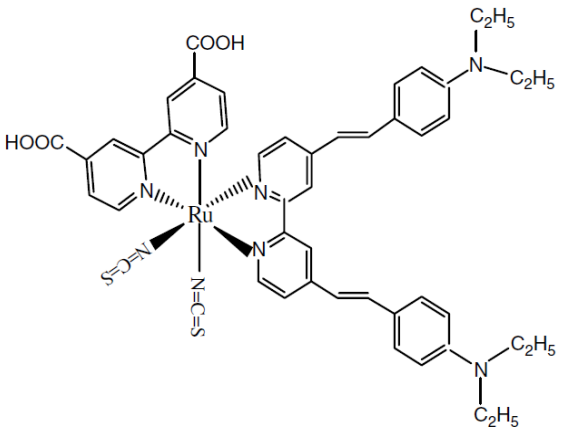

Figure 19 Structure of the HRD-2 complex

Source: Jiang *et al*., (2008)

Klein *et al*., (2004) synthesized amphiphilic ligands 4,4′-bis(1-adamantyl-aminocarbonyl)-2,2′-bipyridine (**L**^{1}), 4,4′-bis{5-{*N*-[2-(3*β*-cholest-5-en-3-ylcarba-mate-*N*-yl)ethyl]aminocarbonyl}}-2,2′-bipyridine (**L**^{2}), 4,4′-bis{5-{*N*-[2-(3*β*-cholest-5-en-3-ylcarbamate-*N*-yl)propyl] aminocarbonyl}}-2,2′-bipyridine (**L**^{3}), and 4,4′-bis (dodecan-12-ol)-2,2′-bipyridine (**L**^{4}) and their ruthenium(II) complexes of the type [Ru(II) (L)(L^{1})(NCS)$_2$] (**1**), [Ru(II)(L)(L^{2}) (NCS)$_2$] (**2**), [Ru(II) (L)(L^{3})(NCS)$_2$] (**3**), and [Ru(II)(L)(L^{4})(NCS)$_2$] (**4**), when L is 4,4′-bis(carboxylic acid)-2,2′-bipyridine . The performance of these complexes as charge-transfer photosensitizers in nanocrystalline TiO_2-based solar cells was studied. When complexes **1**-4 anchored onto a 12 + 4 μm thick nanocrystalline TiO_2 films, very efficient sensitization was achieved (85 ± 5% incident photon-to-current efficiencies in the visible region). Under standard AM 1.5 sunlight, the complex 4 yielded a short-circuit photocurrent density of 17 ± 0.5 mA/cm^2, the open-circuit voltage was 720 ± 50 mV, and the fill factor was 0.72 ± 0.05, corresponding to an overall conversion efficiency of 8.8 ± 0.5%. Structure of the complexes were shown in Figure 20.

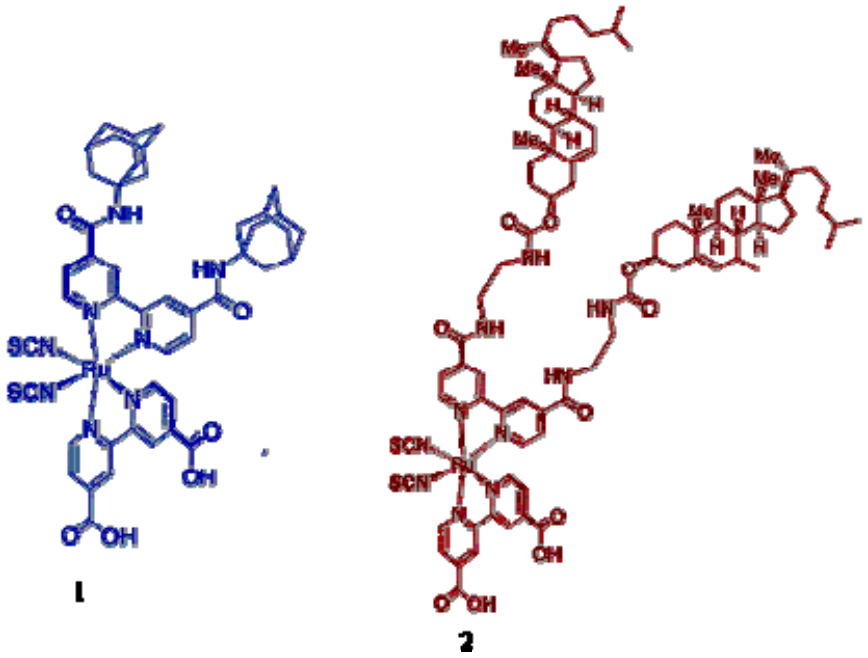

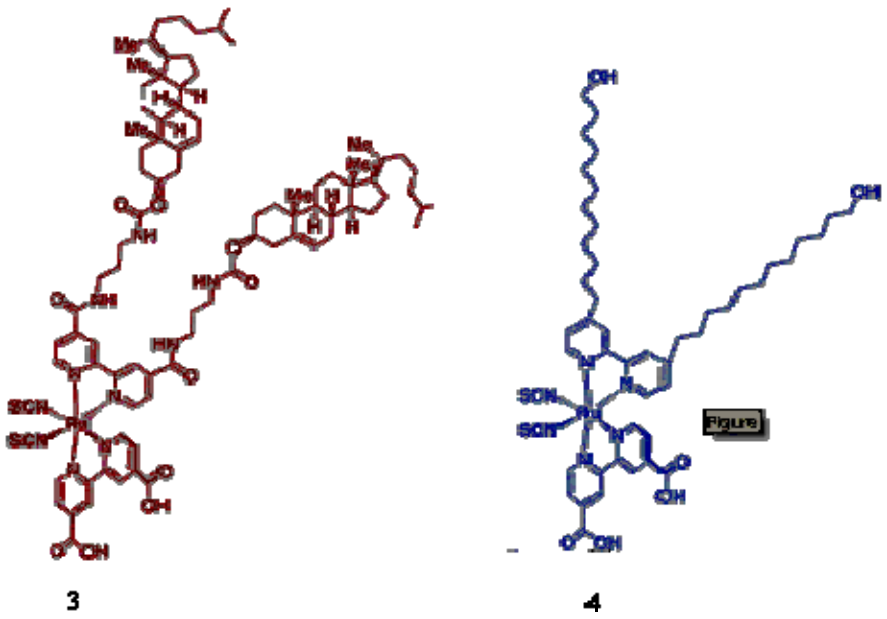

3 4

.

Figure 20 Structure of the complexes 1-4

1. [Ru(II)$LL^1(NCS)_2$]
2. [Ru(II)$LL^2(NCS)_2$]
3. [Ru(II)$LL^3(NCS)_2$]
4. [Ru(II)$LL^4(NCS)_2$]

Source: Klein *et al*., (2004)

Kuang *et al*., (2008) synthesized new ion-coordinating ruthenium polypyridyl sensitizer of the type NaRu(4-carboxylic acid-4′-carboxylate)(4,4′ bis[(triethylene glycolmethylether)heptylether]-2,2′-bipyridine)(NCS)2 (coded as K68). A power conversion efficiency of 6.6% was obtained for dye-sensitized solar cells (DSCs) based on the K68 dye and a newly developed binary ionic liquid electrolyte containing 1-propyl-3-methyl-imidazolium iodide (PMII) and 1-ethyl-3-methyl-imidazolium tetracyanoborate (EMIB(CN)4). For a non-volatile organic solvent based electrolyte, a photovoltaic power conversion efficiency of 7.7% was obtained under simulated full sun light and exhibited a good thermal stability during the accelerated test under 80 °C in the dark. Structures of the complexes are shown in Figure 21.

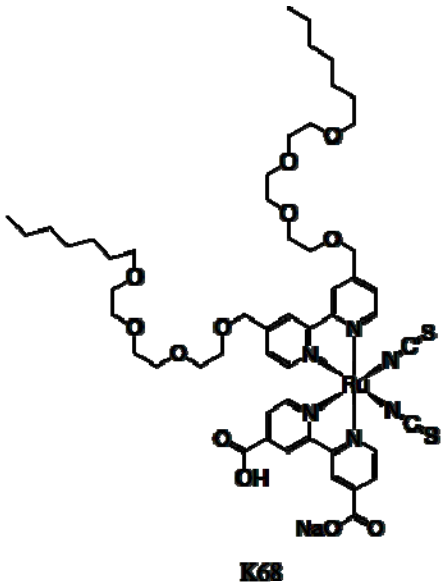

Figure 21 Structure of the K68 complex

Source: Kuang *et al*., (2008)

Nazeeruddin *et al*., (2004) synthesized amphiphilic heteroleptic ruthenium (II) complexes of the type $[Ru(H_2dcbpy)Cl(cymene)]NO_3$ (1) $[Ru(H_2dcbpy)(dmbpy)(NCS)_2]$ (2), $[Ru(H_2dcbpy)(dhbpy)(NCS)_2]$ (3) $[Ru(H_2dcbpy)(dnbpy)(NCS)_2]$ (4) and $[Ru(H_2dcbpy)(dtdbpy)(NCS)_2]$ (5), when H_2dcbpy is 4,4′-dicarboxy-2,2′- bipyridine, dmbpy is 4,4′-dimethyl-2,2′-bipyridine, dnbpy is 4,4′-dinonyl-2,2′-bipyridine , dnbpy is 4,4′- dinonyl-2,2′-bipyridine and tdbpy is 4,4′-tridecyl-2,2′-bipyridine. The performance of these complexes as charge-transfer photosensitizers in nanocrystalline TiO_2-based solar cells was studied. When anchored complexes 2–5 onto nanocrystalline TiO_2 films achieve very efficient sensitization over 85 ± 5% incident photon-to current efficiencies (IPCEs) in the visible region. Structures of the complexes are shown in Figure 22.

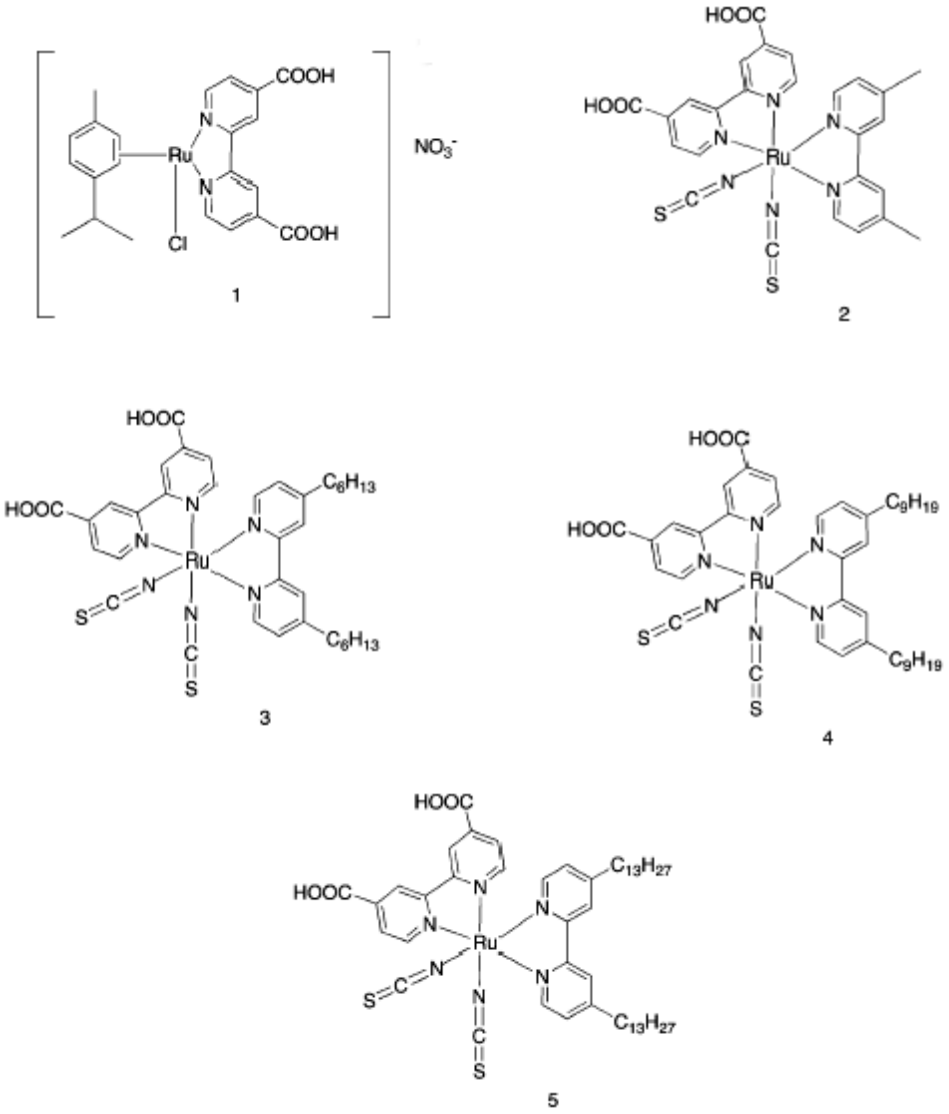

Figure 22 Structure of the complexe 1-5

1. [Ru(H_2dcbpy)Cl(cymene)]NO_3
2. [Ru(H_2dcbpy)(dmbpy)$(NCS)_2$]
3. [Ru(H_2dcbpy) (dhbpy)$(NCS)_2$]
4. [Ru(H_2dcbpy)(dnbpy)$(NCS)_2$]
5. [Ru(H_2dcbpy)(dtdbpy)$(NCS)_2$]

Source: Nazeeruddin *et al.,* (2004)

Nazeeruddin *et al*., (2005) synthesized ruthenium(II) complexes of the type [Ru(L2)$(NCS)_2$] (K8) and [Ru(L)(L9)$(NCS)_2$] (K9), when L is 4,4′-bis(carboxyvinyl)-2,2′-bipyridine and L9 is 4,4′-dinonyl-2,2′- bipyridine The performance of K8 and K9 complexes as charge transfer photosensitizers in nanocrystalline TiO_2 based solar cells was investigated. These complexes when anchored onto TiO_2 films exhibit very efficient sensitization yielding 75±5 % incident photon-to-current efficiencies (IPCE) in the visible region. At one sun the K8 complex gave a short circuit photocurrent density of 18±0.5 mA/cm^2, the open circuit voltage 640±50 mV and fill factor of 0.75±0.05, corresponding to an overall conversion efficiency of 8.64±0.5 %. Under similar conditions, the K9-sensitized solar cell gave a photocurrent density of 16.5±0.5 mA/cm^2, 666±50 mV open circuit potential and 0.71±0.05 fill factor yielding 7.81 %±0.6 % efficiency. Structure of the complexes are shown in Figure 23.

.

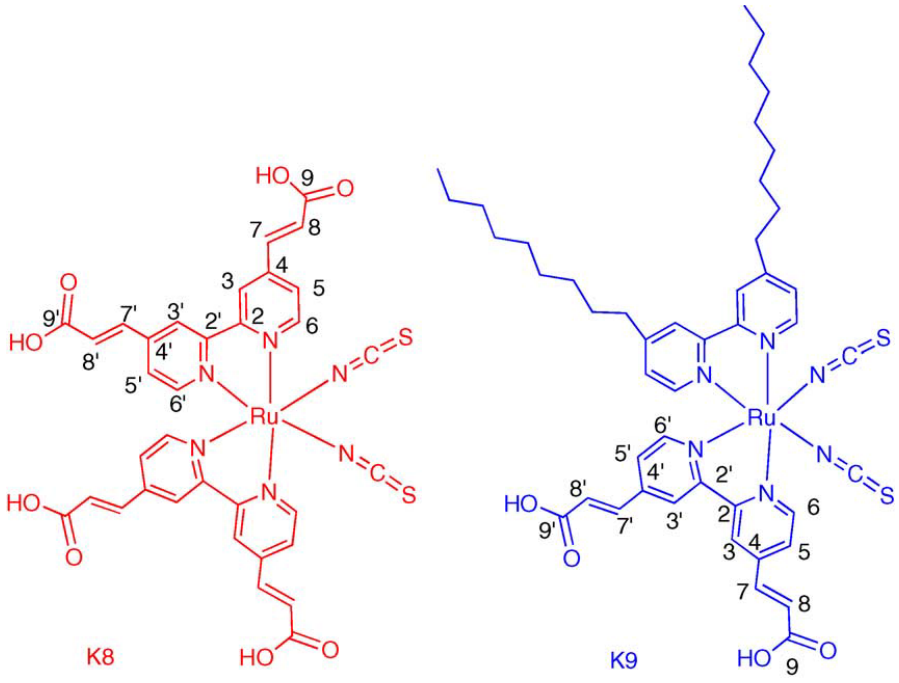

Figure 23 Structure of K8 and K9 complexes

Source: Nazeeruddin *et al*., (2005)

Ocakoglu *et al*., (2007) synthesized new ruthenium(II) complexes of the type $[Ru(L_2)(H_2dcbpy)(NCS)_2]$ [K27] and $[Ru(L1)(H_2dcbpy)(NCS)_2]$ [K30], when H_2dcbpy is 4,4′-dicarboxy-2,2′- bipyridine L1 is 4,5-diazafluoren-9-one, and L2 is 1,10-phenanthroline-5,6-dione. The resulting complexes were characterized by UV/VIS, emission, IR, TGA, NMR, elemental analysis and cyclic voltammetry. The low-energy MLCT absorption maxima of the complexes appear at 524 nm, and the luminescence consists of a single band with a maximum at 700 and 720 nm, respectively. The electrochemical behaviors of the complexes have been studied in CH_3CN by cyclic voltammetry. The LUMO energy levels of K27 and K30 were determined as -4.01 and -3.86 eV. Structures of the complexes are shown in Figure 24.

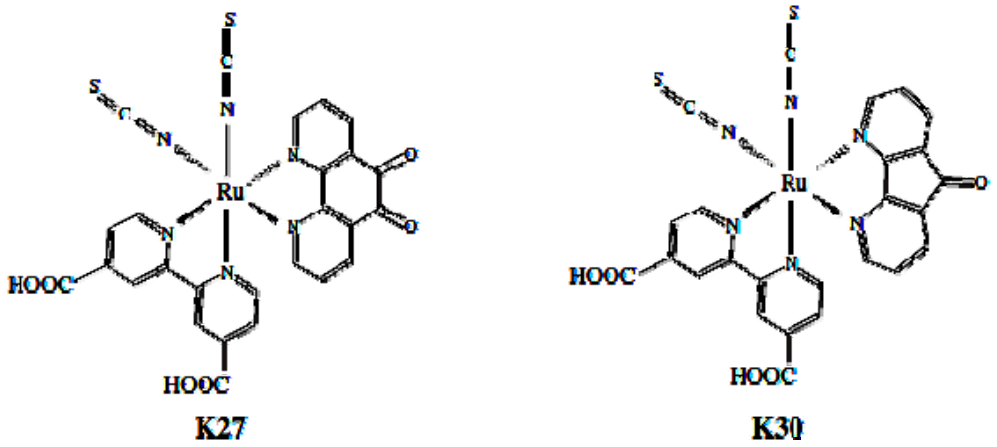

Figure 24 Structure of K27 and K30 complexes

Source: Ocakoglu *et al*., (2007)

Sahin *et al*., (2008) synthesized new ruthenium(II) complex with 4,4′-bis(dihexylmethyl)-2,2′-bipyridine ligand. The type of complex is $[Ru(L1)(L2)(NCS)_2]$ (CS9), when L1 is 4,4′- dicarboxy-2,2′-bipyridine and L2 is 4,4′-bis(dihexylmethyl)-2,2′-bipyridine. The complex was characterized by UV/Vis and FTIR spectrophotometers, ^{1}H-NMR spectroscopy and cyclic voltammetry. The performance of this complex as charge transfer photosensitizer in nc-TiO_2 based dye sensitized solar cells was studied under standard AM 1.5 sunlight. The complex, CS9 in DMF, gave a photocurrent density of 12.62 mA/cm^2, 630 mV open circuit potential

and 0.62 fill factor yielding 5.68 % efficiency. Structures of the complexes are shown in Figure 25.

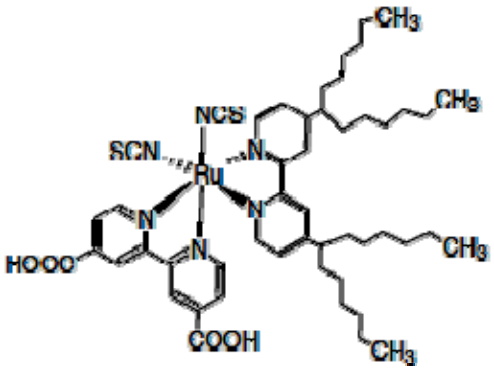

Figure 25 Structure of CS9 complex

Source: Sahin *et al*., (2008)

Sahin *et al*., (2010) synthesized new heteroleptic ruthenium(II) complex of the type $[Ru(L_1)(L_2)(NCS)_2]$ (CS23), when L_1 is 4,4′-dicarboxy-2,2′-bipyridine and L_2 is 1-(2,4,6-trimethylbenzyl)-2-(2′-pyridyl)benzimidazole. The complex was characterized using spectroscopic methods and cyclic voltammetry. Charge-separation was investigated within nanoporous titanium dioxide employing surface photovoltage spectroscopy. The novel complex had a photocurrent density of 9.47 mA/cm^2, 600 mV open circuit potential and 0.60 fill factor yielding an efficiency of 3.4%. The photovoltaic performance of the colorant was compared with that of *cis*-bis (isothiocyanato)(2,2′-bipyridyl-4,4′-dicarboxylato)(2,2′-bipyridyl-4,4′-di-nonyl)ruthenium(II); both compounds exhibited similar efficiency, while the fill factor value was higher than the novel dye. Structure of the complex was show in Figure 26.

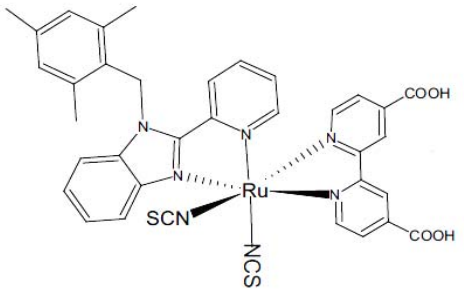

CS23

Figure 26 Structure of CS23 complex

Source: Sahin *et al*., (2008)

Song *et al*., (2009) synthesized a new ruthenium(II) complex with amphiphilic bipyridyl ligand. The type of complex is [Ru(dcbpy)(L)$(NCS)_2$] (S8), when dcbpy is 4,4′-dicarboxy-2,2′-bipyridine and L is *N,N*-di-(2-pyridyl)-dodecylamine or *N,N*-di-(2-pyridyl)-tetradecylamine. The complex was characterized by UV/Vis, IR and NMR spectroscopy. Aliphatic chains linking to carboxylate groups of S8 act as an effective electron donor and carboxylate groups act as an effective electron withdrawing between the TiO_2 layer and the carboxylate linking TiO_2 layer leading to increasing of electron density at this interface, which is attributed to increasing efficiency of electron injection to the TiO_2 conduction band from the excited state of dye. The complex, S8, gave a photocurrent density of 13.02 mA/cm^2, 0.60 V open circuit voltage and 0.69 fill factor yielding 5.36% efficiency. Structure of the complex was shown in Figure 27.

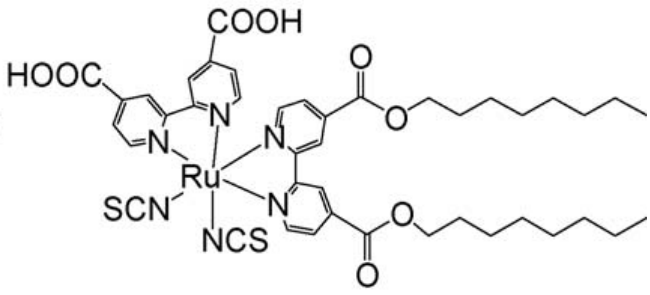

S8

Figure 27 Structure of S8 complex

Source: Song *et al*., (2009)

Objectives

1. To synthesize and to characterize 2-(4′-*N,N*-dimethylamino phenylazo)pyridine ligand (dmazpy) and [Zn(dmazpy)Cl_2]
2. To synthesize and to characterize [Ru (*p*-cymene)(dmazpy)Cl]Cl [Ru(dmazpy)(dcbpyH_2)$(SCN)_2$] and [Ru (dmazpy) (dcbH_2)$_2$](PF_6)]
3. To study the optical properties of the synthesized complexes.

CHAPTERT 2
MATERIALS AND METHODS

2.1 Materials

2.1.1 Chemical substances

Products from Fluka

1. 2-aminopyridine, $C_5H_6N_2$, A.R. grade
2. Tetrabutylammonium hexafluorophosphate (TBAH), $C_{16}H_{36}F_6NP$, A.R. grade

Products from MERCK

1. Sodium hydroxide, NaOH, A.R. grade
2. Silica gel 100 (0.063 – 0.200 mm), A.R. grade

Products from Sigma Aldrich

1. *N*,*N*-dimethyl-1,4-nitrosoaniline, $ONC_6H_4N(CH_3)_2$, A.R. grade
2. Dichloro(*p*-cymene)ruthenium(II) dimer, $C_{20}H_{28}C_{l4}Ru_2$, A.R. grade
3. Ferrocene, $Fe(C_5H_5)_2$, A.R. grade
4. Ruthenium(III)-chloride-3-Hydrate, A.R. grade

Product from BDH

Zinc chloride, A.R. grade

Product from Alfa Aesar

4,4′-dicarboxylic-2,2′-bipyridine ($dcbH_2$), A.R. grade

Product from GE Healthcare

Sephadex LH-20, A.R. grade

2.1.2 Solvents

Products from MERCK

1. Benzene, C_6H_6, A.R. grade
2. Hexane, C_6H_{14}, A.R. grade
3. Methanol, CH_3OH, A.R. grade
4. Dichloromethane, CH_2Cl_2, A.R. grade

Products from LAB SCAN

1. Acetone, CH_3COCH_3, A.R. grade
2. Acetonitrile, CH_3CN, A.R. grade
3. Chloroform, $CHCl_3$, A.R. grade
4. Dimethylformamide (DMF), $HCON(CH_3)_2$, A.R. grade
5. Diethyl ether, $(C_2H_5)_2O$, A.R. grade
6. Ethanol, C_2H_5OH, A.R. grade
7. Ethyl acetate, $CH_3COOC_2H_5$, A.R. grade
8. Hexane, C_6H_{14}, A.R. grade

Product from BDH

Dimethyl sulfoxide (DMSO), $(CH_3)_2SO$, A.R. grade

Product from Fluka

Dimethylformamide (DMF), $HCON(CH_3)_2$, A.R. grade

Product from MAY AND BAKER

Tratrahydrofuran (THF), C_4H_8O, A.R. grade

2.2 Instruments

2.2.1 Nuclear Magnetic Resonance Spectroscopy

1D and 2D NMR spectra were recorded in $CDCl_3$, DMSO-d_6 and CD_3OD solution depended on the studied compounds with a Varian BRUKER AVANCE 300 FT-NMR and 300 MHz spectrometer. Tetramethylsilane ($Si(CH_3)_4$) was used as an internal standard.

2.2.2 Elemental Analysis

Elemental analytical data were obtained by using a CHNS-O Analyzer, CEvInstruments Flash EA 1112 Series, Thermo Quest, Italy.

2.2.3 Infrared Spectroscopy

Infrared spectra were collected by using KBr pellets on a BX Perkin Elmer FTIR Spectrophotometer from 400 - 4,000 cm^{-1}

2.2.4 X-ray Diffractometry

The structures of $[Zn(dmazpy)Cl_2]$ complex were determined by Bruker APEX diffractometer with the SHLEXL97 programs.

2.2.5 Mass spectrometry

Mass spectra were recorded on a Liquid Chromatograph-Mass spectrometer, 2690, LCT, Micromass.U.K.by Electrospray Ionization Positive Mode.

2.2.6 UV-Visible Absorption Spectroscopy

UV-Visible absorption spectra were recorded on Specord S100 model with standard cuvette, path length 1 cm in the range 200-800 nm. Deuterium and tungsten were used as light sources covering wavelengths in UV and visible region respectively.

In addition, the UV- Visible Spectrometer, Lambda 45, PerkinElmer, United stated was also used for absorption properties.

2.2.7 Luminescence spectroscopy

Luminescence spectra were performed by Luminescence spectrometer LS 55.

2.2.8 Cyclic Voltammetry

Electrochemical experiments were proceed using cyclic voltammetric technique with Maclab controlled by Echem 1.5.1 program. Cyclic voltammograms were obtained by using a platinum wire as an auxiliary electrode, a glassy carbon as an working electrode and a platinum wire as an reference electrode. The supporting electrolyte was tetrabutylammonuim hexafluorophosphate (TBAH) in acetronitrile. At the end of each experiment, ferrocene was added as an internal standard. All potentials were quoted vs the ferrocene/ferrocenium ion in acetonitrile. A ferrocene–ferrocenium (Fc/Fc^{+}) reversible couple was observed at 0.44 V versus SCE at a scan rate of 0.1 Vs^{-1} in acetonitrile. The argon was bubbled through the solution prior to each measurement.

2.3 Synthesis of ligand

2.3.1 Synthesis of 2-(4′-*N*,*N*-dimethylaminophenylazo)pyridine ligand (dmazpy)

The 2-(4′-*N*,*N*-dimethylaminophenylazopyridine)(dmazpy) ligand was prepared by the reaction between 2-aminopyridine and *N*,*N*–dimethyl-1,4-nitro-soaniline. The *N*,*N*–dimethyl-1;4-nitrosoaniline (1.502 g, 0.01 mol) was slightly added to the warm solution of 2-aminopyridine (0.940 g, 0.01 mol) at 80°C in the presence of 6 mL 25 M NaOH in benzene. After this period the mixture was carried out under refluxing conditions for 11 h. The dark red ligand was soluble in benzene. Reaction mixture was filtered and extracted with 50 mL benzene. The mixture solution was evaporated to be small volume. Purification was carried out by column chromatography on silica column. The red ligand was eluted with 9:1, 8:2, 7:3

hexane:ethyl acetate, respectively. The solid ligand was washed with diethyl ether for three times. The yield of dmazpy ligand is 56.24 % .

2.4 Synthesis of complexes

2.4.1 Synthesis of [Zn(dmazpy)Cl_2] complex.

Zn (II) complex with 2-(4′-*N*,*N*- dimethylaminophenylazo) pyridine ligand was prepared by a typical one-pot synthesis. $ZnCl_2$ (0.30 mmol, 0.041 g) was dissolved in CH_3CN (20 mL) and synthesized dmazpy (0.60 mmol, 0.136 g) ligand was added. The reaction mixture was refluxed at 75 ^oC for 4 h. The solution turned from orange to pink. After the reaction, The mixture was filtered through a sintered glass. Then the solution was left for overnight. The resulting solution was crystallized and recrystallized in dichloromethane: methanol (2:1) mixture at room temperature**.** The yield of Zn(dmazpy)Cl_2 complex is 35.46 % .

2.4.2 Synthesis of [Ru(p-cymene)(dmazpy)Cl]Cl complex

The [Ru(*p*-cymene)(dmazpy)Cl]Cl complex was prepared by following pathway. Ru-*p*-cymene dimer (306 mg, 0.5 mmol) was added to a THF solution (8 mL) of dmazpy ligand (226 mg, 1.0 mmol). The color of the mixture immediately turned from red to green. The reaction mixture was stirred at room temperature for 2 h. The precipitate was filtered off, washed with THF and filtered off again, to remove un-reacted dmazpy. The residue was dissolved in CH_2Cl_2 (5 mL) and then precipitated with diethyl ether (10 mL) giving the green solid with 63 % yield.

2.4.3 Synthesis of [Ru(dmazpy) (dcbpyH_2)$(NCS)_2$] complex

The [Ru(dmazpy)(dcbpyH_2)$(NCS)_2$] complex was prepared by the reaction between [$RuCl_2$(*p*-cymene)]$_2$ and the ligands. In a typical synthesis, [$RuCl_2$ (*p*-cymene)]$_2$ (0.10 g, 0.16 mmol) was dissolved in DMF (50 mL) and synthesized ligand dmazpy (0.08 g, 0.32 mmol) was added. The reaction mixture was heated to 55-65 ^oC under argon for 4 h. with constant stirring. After this period, solid dcbpyH_2 (0.32 mmol, 0.08 g) was added and refluxed for 4 h. Then NH_4NCS (13 mmol, 0.11 g) was added to the reaction mixture and reflux was continued for 4 h. The reaction mixture was allowed to cool to room temperature and the solution was filtered

through a sintered glass crucible. The resulting solid was washed with water to remove an excess of NH_4NCS. The insoluble product was collected on a sintered glass crucible by suction filtration, washed with distilled water and diethyl ether, respectively. The crude complex was purified on a sephadex LH-20 column chlomatography using methanol as an eluent for 6 times.

2.4.4 Synthesis of $[Ru(dcbpyH_2)_2(dmazpy)](PF_6)_2$ complex

In a typical one-pot synthesis, $RuCl_3.3H_2O$ (0.042 g, 0.16 mmol) was dissolved in DMF (50 mL) and synthesized ligand dmazpy (0.04g, 0.16 mmol) was added. The reaction mixture was heated at 55-56 ºC under argon for 4 hrs and then $dcbpyH_2$ (0.08 g, 0.032 mmol) was added. The reaction mixture was refluxed at 155-156 ºC for another 4 hrs. Excess tetrabutylammonium haxafluorophoshate was added to the reaction mixture and heated for 1.5 h. After the reaction, the mixture was then collected on a sintered-glass crucible by suction filtration, washed with acetone and dried in air. The crude complex was purified on a sephadex LH-20 column chlomatography using methanol as an eluent for 5 times.

CHAPTER 3

RESULTS AND DISCUSSION

3.1 Synthesis and characterization of 2-(4′-*N,N*-dimethylaminophenylazo)pyridine (dmazpy) ligand

Synthesis of 2-(4′-*N,N* -dimethylaminophenylazo)pyridine ligand (dmazpy)

The 2-(4′-*N,N*′-dimethylaminophenylazo)pyridine ligand was obtained from the reaction of 2-aminopyridine and *N,N*–dimethyl-1,4-nitrosoaniline. The *N,N*–dimethyl-1,4-nitrosoaniline (1.502 g, 0.01 mol) was slightly added to the warm solution of 2-aminopyridine (0.940 g, 0.01 mol) at 80 °C in the presence of 6 mL of 25 M NaOH in benzene. After this period the mixture was carried out under refluxing conditions for 11 h.

Reaction mixture was filtered and extracted with 50 mL of benzene and water. The dark red ligand was soluble in benzene portion. The mixture solution was evaporated to be small volume. Purification was carried out by column chromatography on silicagel column. The red ligand was eluted with 9:1, 8:2, 7:3 of hexane: ethyl acetate, respectively. The reaction are followed by equation 1.

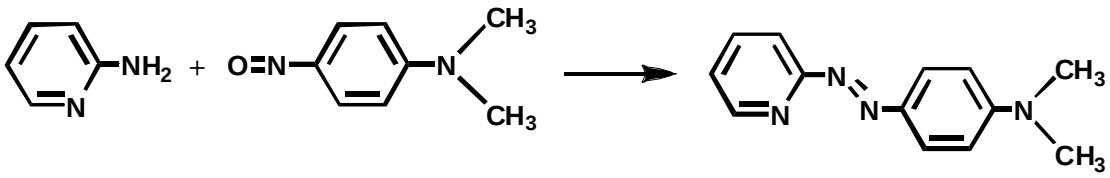

2-aminopyridine *N,N*-dimethyl-1,4-nitrosoaniline 2-(4′-*N,N*dimethyaminophenyl Azopyridine (dmazpy) (eq.1)

The yield of dmazpy ligand is 56.24%. The solubility of dmazpy was tested in various kind of organic solvents as shown in Table 1. Except water, dmazpy are completely soluble in all organic solvents.

Table 1. Solubility of 2-(4′-*N,N*-dimethylaminophenylazo)pyridine(dmazpy)ligand.

solvent	**solubility**
hexane	+++
toluene	+++
dichoromethane	+++
chlorofrom	+++
benzene	+++
ethylacetate	+++
acetone	+++
acetonitrile	+++
dimethylformamide (DMF)	+++
dimethylsulfoxide (DMSO)	+++
ethanol	+++
methanol	+++
Water	+

The symbol of solubility, +++ represents the completely soluble of ligand 0.0010 g in 3 mL of solvents.

Characterization of 2-(4′-*N,N*-dimethylaminophenylazo)pyridine(dmazpy) ligand. The structure and chemistry of the dmazpy ligand was investigated by using these techniques:

- Proton Nuclear Magnetic Resonance spectroscopy
- Infrared spectroscopy
- UV-Visible absorption spectroscopy
- Cyclic Voltammetry

3.1.1 Proton Nuclear Magnetic Resonance spectrometry (^{1}H-NMR spectroscopy)

The Nuclear Magnetic Resonance spectroscopy is a technique to support the structure of ligand. The chemical shift (δ, ppm) and J-coupling (Hz) of dmazpy ligand is reported in part per million (ppm) witch appeared downfield from tetramethylsilane (TMS, $(CH_3)_4Si$) (δTMS 0 ppm in $CDCl_3$) solution. The type of protons in dmazpy ligand is divided in to 7 groups as shown in Figure 28.

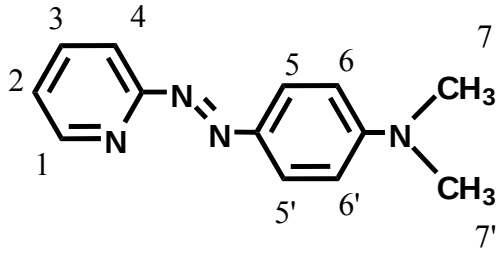

Figure 28 Structure of dmazpy ligand with protons numbering system.

Table 2. ^{1}H- NMR spectroscopic data of the dmazpy ligand

H- position	J-coupling (Hz)	δ (ppm)	Amounts of H	peak
1	5.7, 1.2	8.67	1	dd
4	12, 1.8	8.01	1	dd
2	7.5, 1.8	7.82	1	dt
5	8.1	7.76	2	d
3	7.7, 1.2	7.28	1	dt
6	9.0	6.75	2	d
7	-	3.10	6	s

d = doublet dd = doublet of doublet dt = doublet of triplet s = singlet

The types of protons in 2-(4′-*N,N*′-dimethylaminophenylazo)pyridine ligand are divided in to 7 groups . The detail of each signal can be described below.

The proton-1 is on pyridine located next to pyridine nitrogen atom which gives doublet of doublet signal (dd) at the most downfield. The proton signal is splited by the proton-2 (J = 5.7 Hz) and by the proton-3 (J = 1.2 Hz).

The proton-2 located next to the proton-1. The signal of this proton is doublet of triplet (dt) peak. The splitting of the triplet peak (J = 7.5-7.8) is observed for coupling with proton-1 and proton-3. Then each of triplet peak is splited to doublet peak (J = 1.8 Hz) from long range coupling with proton-4.

The proton-3 is the proton which is opposite to pyridine nitrogen. The proton is less effected from nitrogen atom than that of the proton-2 thus the chemical shift value is less than that of the proton-2. The signal of this proton also doublet of triplet peak. It is splited by the proton-2 and 4 (J = 7.7 Hz) and by the proton-1 (J = 1.2 Hz)

The proton-4 located next to the proton -3 and it is effected from nitrogen of azo function. The signals appear at downfield position more than that of proton-2 and 3. The signal is doublet of doublet. It is splited by proton -3 (J=12 Hz) and by the proton -2 (J = 1.8 Hz)

The proton-5 and 5′ are two equivalent protons on phenyl ring located closed to azo nitrogen. The rotation of phenyl ring leads the proton-5 signal appeared at the upper field than that of the proton-4. The proton-5 interacts with proton 6 and gives the doublet peak with J-coupling 8.1 Hz.

The proton-6 and 6′ are two equivalent protons located next to the proton-5. The signal is also doublet of doublet peak which is splited by proton -5 (J=9.0 Hz).

The proton-7 are the methyl protons (-CH_3). The signal shows singlet peak of 6 protons .

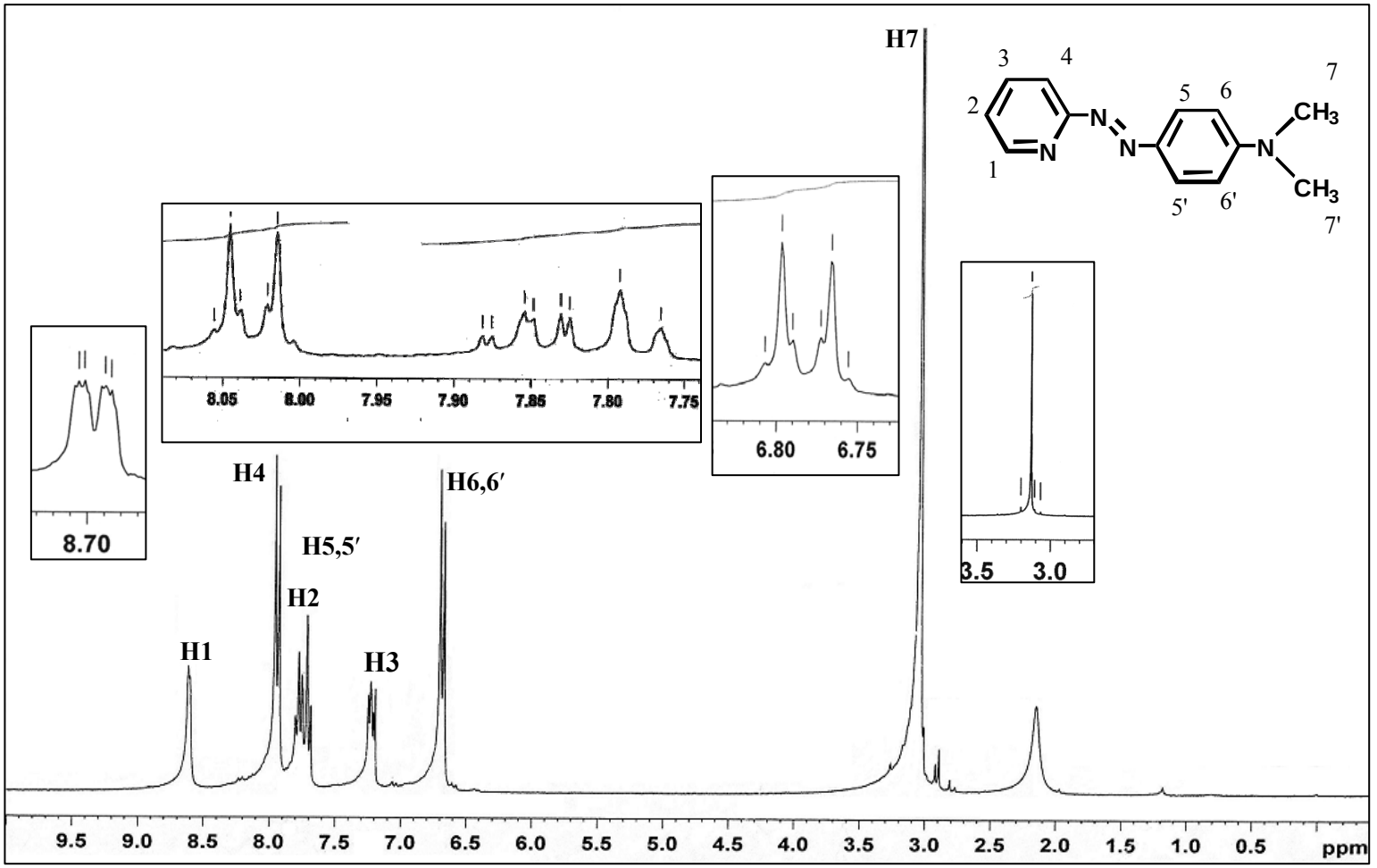

Figure 29 ^{1}H- NMR spectrum of 2-(4′-*N,N*-dimethylaminophenylazo)pyridine (dmazpy)

3.1.2 Fourier transform infrared spectroscopy (FTIR spctroscopy)

Infrared spectroscopy is a main technique to study functional groups of the synthesized compounds. Infrared spectra were recorded in KBr pellet in the range of 4000- 400 cm^{-1} region. The infrared spectroscopic data of the dmazpy ligand is shown in Table 3.

Teble 3. Infrared spectroscopic data of the 2-(4′-*N,N*-dimethyl aminophynyl-azo pyridine (dmazpy) ligand

Vibration mode	**Frequencies (cm^{-1})**
sp^2 C-H stretching	3080(s)
N=N stretching	1399(s)
C=C stretching	1603(s) 1499(m)
C=N	1524 (s)
C-H bending of para disubstituted benzene	816(m)

s = strong, m = medium w = weak

The FTIR spectrum of dmazpy ligand shows some important bands around 1600-500 cm^{-1}. It is characterized by a strong band of sp^2 C-H stretching at 3080 cm^{-1}, N=N stretching at 1399 cm^{-1}, C=C streching at 1603 and 1449 cm^{-1}, C=N stretching at 1524 cm^{-1}, and C-H bending of para disubstituted benzene at 816 cm^{-1}. There exists a weak band of C=C stretching at 1460 cm^{1}. The most important peak is N=N stretching which is used for considering the π–acidity property in azo complexes. The N=N stretching of dmazpy ligand shows the intense peak at 1399 cm^{-1}. Meanwhile, the N=N stretching of a similar compound like 2-(phenylazo) pyridine(azpy) Figure 31 shows this band at 1420 cm^{-1} (Krause and Krause,1980) which is stronger than that of dmazpy. This result indicates that methylaniline substituent -$N(CH_3)_2$ makes the N=N bond to be weaker due to the delocalize of electrons from substituent group to the antibonding orbital of azo moiety.

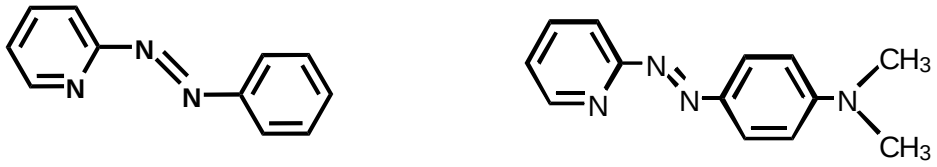

Figure 30 Structure of 2-(phenylazo)pyridine (azpy) ligand and 2-(4′-*N,N*-dimethyl-aminophenylazo)pyridine (dmazpy) ligand

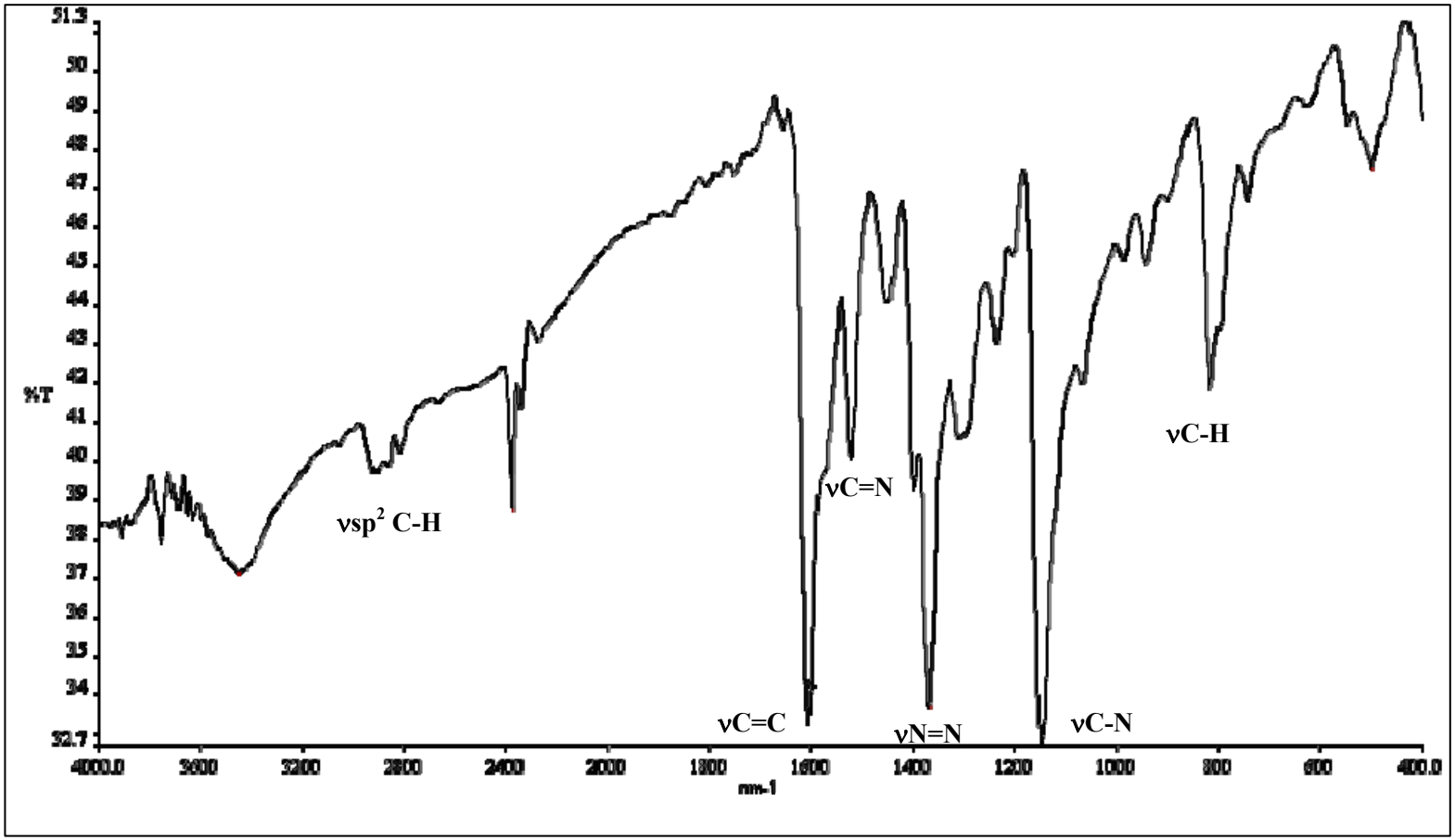

Figure 31 IR spectrum of 2-(4′-*N,N*-dimethylaminophenylazo)pyridine(dmazpy)

3.1.3 UV- Visible absorption spectrophotometry

UV-Visible absorption spectroscopy is a technique to study the electronic transitions of compound. The electronic absorption spectra of the dmazpy compound in four solvents were recorded in the range of 200-800 nm (Figure 32). The spectral data are given in Table 4.

Table 4. Absorption data in UV- Visible range of 2-(4′-*N,N*- dimethylamino-phenylazo)pyridine ligand (dmazpy)

solvent	**[a]polarity of solvent**	**dmazpy**	
		λ_{max} (nm)	**ε ($M^{-1}cm^{-1}$)**
hexane	0.1	398	1.89×10^{-4}
dichloromethane	3.5	427	2.54×10^{-4}
acetonitrile	5.8	423	2.79×10^{-4}
ethanol	5.2	431	1.60×10^{-4}

[a]data taken from Polarity Index of Burdict & Jackson laboratory, INC. Michigan, USA.

The absorption spectra in visible region show the maximum wavelenghs of absorption (λ_{max}) of the ligand in the range of 400-500 nm with high molar extinction coefficient : ε (>10,000 $M^{-1}cm^{-1}$) which is allowed transition of $\pi \rightarrow \pi^*$. The maximum wavelenghs of absorption spectra are dependent on the polar of solvents. The λ_{max} gives rise to red shifting with high polar solvent because the π^*energy levels are stabilized. Then the energy gap between ground state and excited state becomes closer. The transition energy from $\pi \rightarrow \pi^*$ decreases.

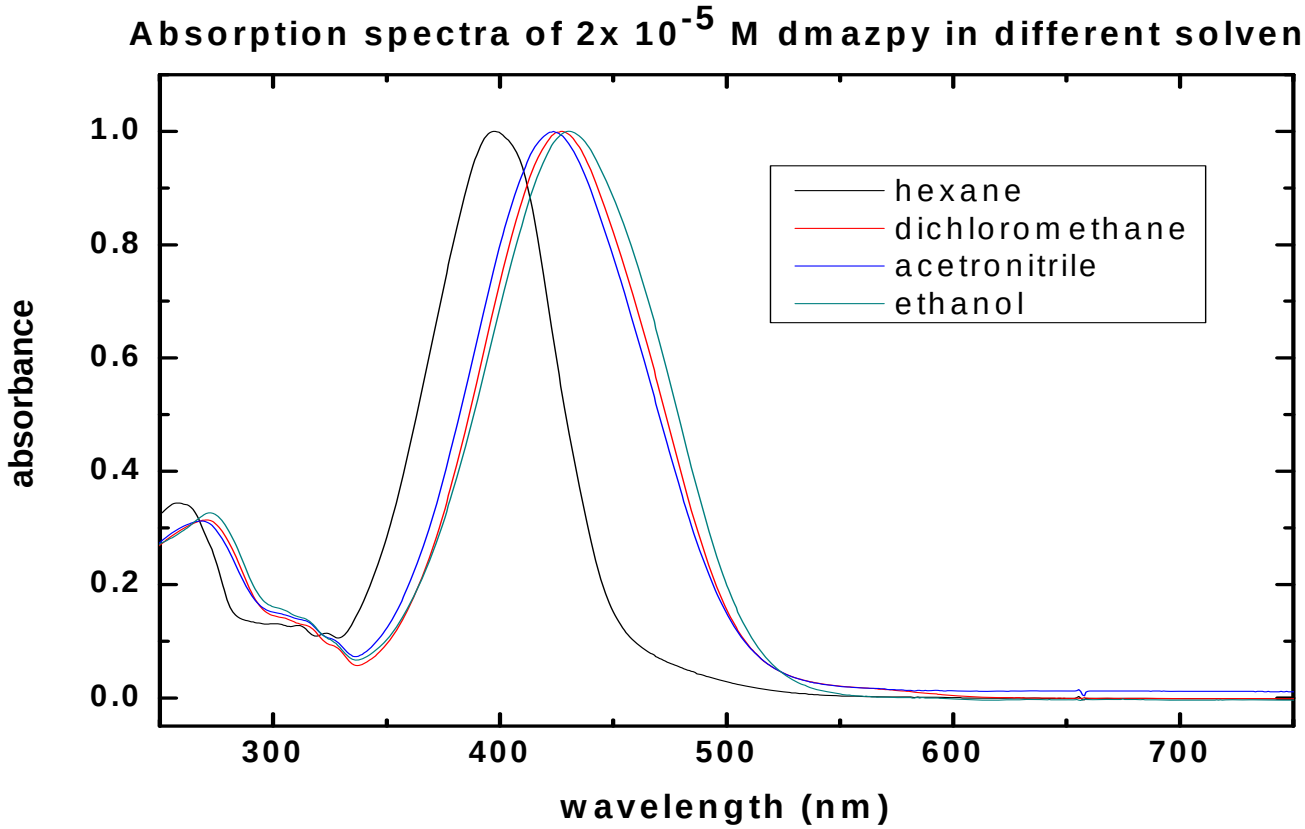

Figure 32 Absorption spectra of 2-(4′-*N,N*-dimethylaminophenylazo)pyridine (dmazpy) in different solvents.

3.1.4 Cyclic Voltammetry of 2-(4′-*N*,*N*-dimethylaminophenylazo) pyridine (dmazpy)

Electrochemical properties of the ligand was studied by cyclic voltammetry using a glassy carbon as a working electrode. The votammogram was examined in acetonitrile using 0.1 M tetrabutylammonuim hexafluorophosphate (TBAH) as a supporting electrolyte at the scan rate of 50 mVs^{-1}. Voltammetric data are given in Table 5 and Figure 33. The voltammogram shows four peaks where two peaks of those are in the reductive potential range (negative potential) and other two are in oxidative potential range (positive potential). The potentials were compared with the ferrocene couple (0.44 V in acetonitrile).

Table 5. Cyclic Voltammetric data of dmazpy in 0.1 M TBAH acetonitrile at scan rate 50 mV/s using Ferrocene/Ferrocenium (Fc/Fc^{+}) as an internal standard

compounds	$E_{1/2}$ (V) (ΔE_p (V))			
	oxidation		reduction	
	I	II	I	II
Dmazpy	1.25 (0.12)	0.95 (0.14)	-0.97(0.22)	-1.17(0.14)

$E_{1/2}$ = $(E_{pa}+E_{pc})/2$, where E_{pa} and E_{pc} are anodic and cathodic peak potentials, respectively; $\Delta E_p = E_{pa}-E_{pc}$.

Oxidation range

The possible potential range in the studied system was able to scan from 0 to 1.8 V at scan rate 50 mV/s. The dmazpy shows two signals in this potential range. One is quasi-reversible couples (II) at $E_{1/2}$ of 1.25 V and another one is irreversible peak (I) at $E_{1/2}$ of 1.31 V. Both a signals are corresponding to the electron oxidation of $[NCH_3]/[NCH_3]^{+}$ similar to the observation in 2-(4′-*N*,*N*-diethylamino-phenylazo)pyridine(deazpy) (Yoopensuk, 2013).

reduction range

In the potential range 0 to-1.8 V at scan rate 50 mV/s in acetonitrile, The dmazpy shows one quasi-reversible couple peak (I) at Ep_c = -0.97 V and one irreversible couple peak (II) at Ep_c = -1.17 V. It is believed that the reduction peak corresponds to the reduction of the azo function, as shown in the equation 2.

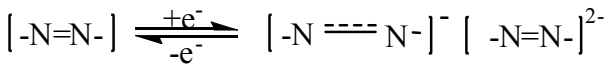

(eq.2)

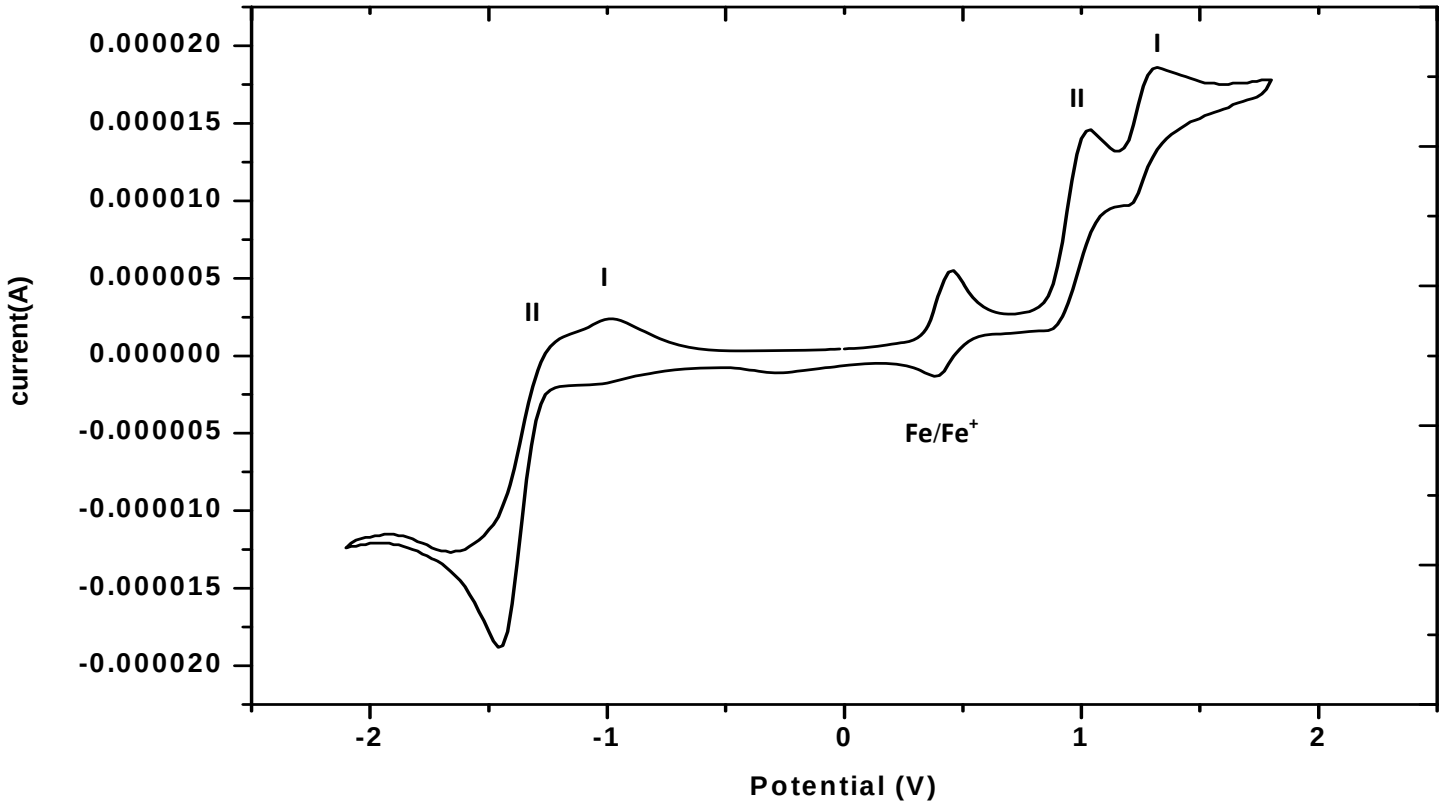

Figure 33 Cyclic voltammogram of 2-(4′-*N,N*-dimethylaminophenylazo)pyridine(dmazpy) in 0.1 M TBAH CH_3CN at scan rate 50 mV/s.

3.2 Synthesis and characterization of dichloro 2-4′-*N,N*- Dimethylamino phenylazo) pyridine Zinc (II) complex

Synthesis of [Zn(dmazpy)Cl_2] complex

Synthesis and characterization of the novel complex of the dmazpy ligand with Zn^{2+} has been carried out. In a typical one-pot synthesis, $ZnCl_2$ (0.30 mmol, 0.041 g) was dissolved in CH_3CN (20 mL) and synthesized dmazpy (0.30 mmol, 0.086 g) ligand was added. The reaction mixture was refluxed at 75 ^oC for 4 h. the solution turned from orange to be pinkish-purple. After the reaction, The mixture was filtered through a sintered glass. Then the solution was left for overnight. The resulting solution was crystallized and recrystallized in dichloromethane: methanol (2:1) mixture at room temperature**.**

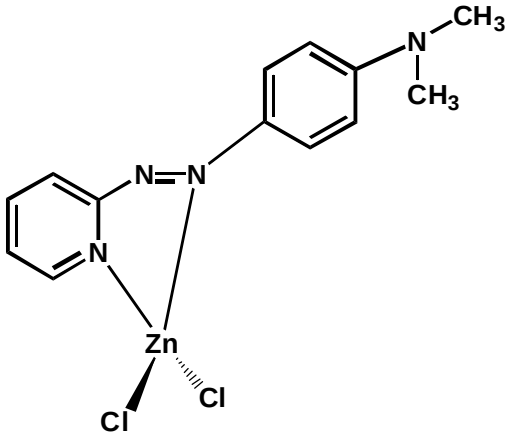

Figure 34 The structure of [Zn(dmazpy)Cl_2].

Characterization of [Zn(dmazpy)Cl_2] complex. The chemistry of the [Zn(dmazpy)Cl_2] was investigated by using the following techniques

- Single crystal X-ray diffraction

- Proton Nuclear Magnetic Resonance spectroscopy

- Infrared spectroscopy

- UV-Visible absorption spectrophotoscopy

3.2.1 X- ray structure of $Zn(dmazpy)Cl_2$

Azo-imine ligands and their transition metal complexes have attracted much interest owing to their potential on biological activities (Velders *et al*., 2000; Holtze *et al*.,2000), as well as their possible application as a catalyst in epoxidation reaction (Barf *et al.*, 1995). However, most of the results were obtained for Ru^{II} complexes, whereas studies on Zn(II) ion are still quite rare. Herein the crystal structure of the [2,(4'-*N,N*-dimethylaminophenylazo)pyridine] dichlorozinc(II) is reported. The Zn(II) atom is coordinated in a distorted tetrahedral geometry by two Cl atoms and two N atoms from dmazpy chelating ligand (Figure 35) . The crystal data is shown in Table 6. Some selected bond distances and bond angles are exhibited in Table 7. The Zn-Cl distances are 2.1860(8) and 2.1888(7) Å for Zn-Cl1 and Zn-Cl2, respectively which are a bit shorter to the corresponding distances reported for other related compounds:$ZnCl_2$(5-Amino-6,8-dichloro-2,3-bis(2-pyridyl)quinoxaline) 2.056-2.062 Å (An *et. al*., 2002) and $ZnCl_2$(phthalazine) 2.223-2.229 Å (Celik *et. al.*, 2004). The distances between Zn-N(pyridine, N1) and Zn-N(azo, N3) are 2.040(2) and 2.090(2) Å, respectively. The angles of Cl-Zn-Cl and N(py)-Zn-N(azo) are 117.06(3)^o and 77.49(8) ^{o}, respectively while the Cl-Zn-N angles are in the range 109.47(6) - 120.09(6) ^{o} which are comparable to other related Zn(II) complexes : $ZnCl_2$(5,7-dimethyl-1,2,4-triazolo[1,5-a]pyrimidine)$_2$ 102.09-117.54^o (Salas *et al*., 1994), $ZnCl_2$(5-Amino-6,8-dichloro-2,3-bis(2-pyridyl)quinoxaline) 106.32-113.73^o (An *et al.*, 2002) and $ZnCl_2$(purine)$_2$, 99.9-113.7^o (Laity and Taylor, 1995). In the crystal structure, individual molecules are associated via weak C-H···Cl interactions between hydrogen atom of pyridine ring at the para position with N(pyridine) and the Cl atom of an adjacent molecule (C2—H2···Cl2^i) as shown in Figure 38. The distance of C2···Cl2^i is 3.535(3) Å; I : x−3/2, −y−1/2, z−1/2 . In addition, the molecules are linked by C-H···π interaction between methyl substituent and pyridine ring (Figure 39), C12—H12C···Cg4^{ii}, generating 2D sheet parallel *ab* plane [C12···Cg4^{ii} = 3.784(4) Å; ii : −x, −y, −z]. Both interactions are summarized in Table 8. Nevertheless, there is another by product from the reaction of 1:1 stoichiometry between $ZnCl_2$ and dmazpy ligand which is the ionic complex of $[ZnCl_4][dmazpyH_2]$. This complex structure has been published (Leesakul *et al*.,2012). The structure is commonly observed in other

related compounds e.g. 4-tert-Butyl-2,6-bis[imidazolium-1-yl) methyl]phenol tetrachloro zincate(II) (Xu *et al*., 2005), bis-(quinolinium)tetrachloro zincatedehydrate (Valdés-Martínez *et al*., 2005) and p-Phenylene diammonium tetra-chlorozincate(II) (Bringley *et al*., 2006). The mean value of the Zn—Cl bond distance of $ZnCl_4^{2-}$ anion is 2.266 (8) Å which is generally observed [2.268 (4) Å] (Harrison, 2005). The Cl—Zn—Cl bond angles in Figure. 40 deviate from 109.5° only slightly [108.19 (3)°-111.53 (3)°]. The cationic species $(dmazpyH_2)^{2+}$ is doubly protonated on the pyridine N1 and azo N2 due to their higher electron density. The N atom of the pyridine ring of the cation adopts a *cis*-orientation with respect to the azo moiety (—N2═N3—) which is in contrast to the *trans*-geometry of the free dmazpy ligand (Leesakul *et al*., 2010). However, it is similar to an observation in a related crystal structure of 2-(4-hydroxyphenylazo)pyridine (3:1) tetrafluoroborate (Panneerselvam *et al*., 2000). Nevertheless, only single a protonation on the azo N3 was found. In the title compound, the dihedral angle of mean plane of pyridine-azo-phenyl rings is 2.38 (15)°.The N═N distance of the $(dmazpyH_2)^{2+}$ is 1.313 (3) Å which is obviously longer than that of the free dmazpy ligand, 1.257 (16) Å. It may be caused by the protonation on the N atom of azo group which decreases the azo bond strength in comparison withthe related free dmazpy ligand. It is worth noting that the two Cl atoms of $[Zn—Cl_4]^{2-}$are linked to the protonated pyridine H1A and the protonated N-azo H2A via H-bonding, with an N1···Cl1 distance of 3.173 (3) Å and an N2···Cl3 distance of 3.322 (3) Å, respectively. (Figure. 41 and Table 9). In the crystal structure, the intermolecular π-π stacking interactions (Figure. 42) occur between adjacent pyridine (C*g*1) and phenyl rings (*Cg*2). The centroid-centroid distances, *Cg*1···*Cg*2, in the stacks which are parallel to the aaxis are 3.6270 (18) Å and 3.8685 (18) Å respectively.

Table 6. Crystallographic data of the [Zn(dmazpy)Cl_2] complex.

Empirical formula	Zn C_{13} H_{14} C_{l2} N_4
Formula weight	362.55
Temperature	293(2) K
Wavelength	0.71073 Å
Crystal system	Monoclinic
Space group	$P2_1/n$
Unit cell dimensions	a = 7.7184(3) Å
	b = 13.6251(6) Å
	c = 14.7582(6) Å
	$\alpha = 90^o$
	$\beta = 95.3710(10)^o$
	$\gamma = 90^o$
Volume	1545.22(11) $Å^3$
Z	4
Density (calculated)	1.558 Mg/m^3
Absorption coefficient	1.929 mm^{-1}
Goodness-of-fit on F^2	1.064
Final R indices [$I>2\sigma(I)$]	$R1$ = 0.0302, $wR2$ = 0.0767
R indices (all data)	$R1$ = 0.0376, $wR2$ = 0.0801

Table 7. Selected bond lengths (Å) and angles (^{o}) for the [Zn(dmazpy)Cl_2] complex

Zn(1)-N(1)	2.040(2)	Zn(1)-N(3)	2.090(2)
Zn(1)-Cl(1)	2.1860(8)	Zn(1)-Cl(2)	2.1888(7)
N(1)-C(5)	1.326(3)	N(1)-C(1)	1.346(3)
N(2)-N(3)	1.288(3)	N(2)-C(5)	1.409(3)
N(3)-C(6)	1.380(3)		

Angles

N(1)-Zn(1)-N(3)	77.49(8)	N(1)-Zn(1)-Cl(1)	111.55(6)
N(3)-Zn(1)-Cl(1)	109.47(6)	N(1)-Zn(1)-Cl(2)	114.83(6)
N(3)-Zn(1)-Cl(2)	120.09(6)	Cl(1)-Zn(1)-Cl(2)	117.06(3)
C(5)-N(1)-C(1)	119.2(2)	C(5)-N(1)-Zn(1)	112.18(16)
C(1)-N(1)-Zn(1)	128.48(19)	N(3)-N(2)-C(5)	112.8(2)
N(2)-N(3)-C(6)	117.4(2)	N(2)-N(3)-Zn(1)	116.18(16)
C(6)-N(3)-Zn(1)	126.04(16)		

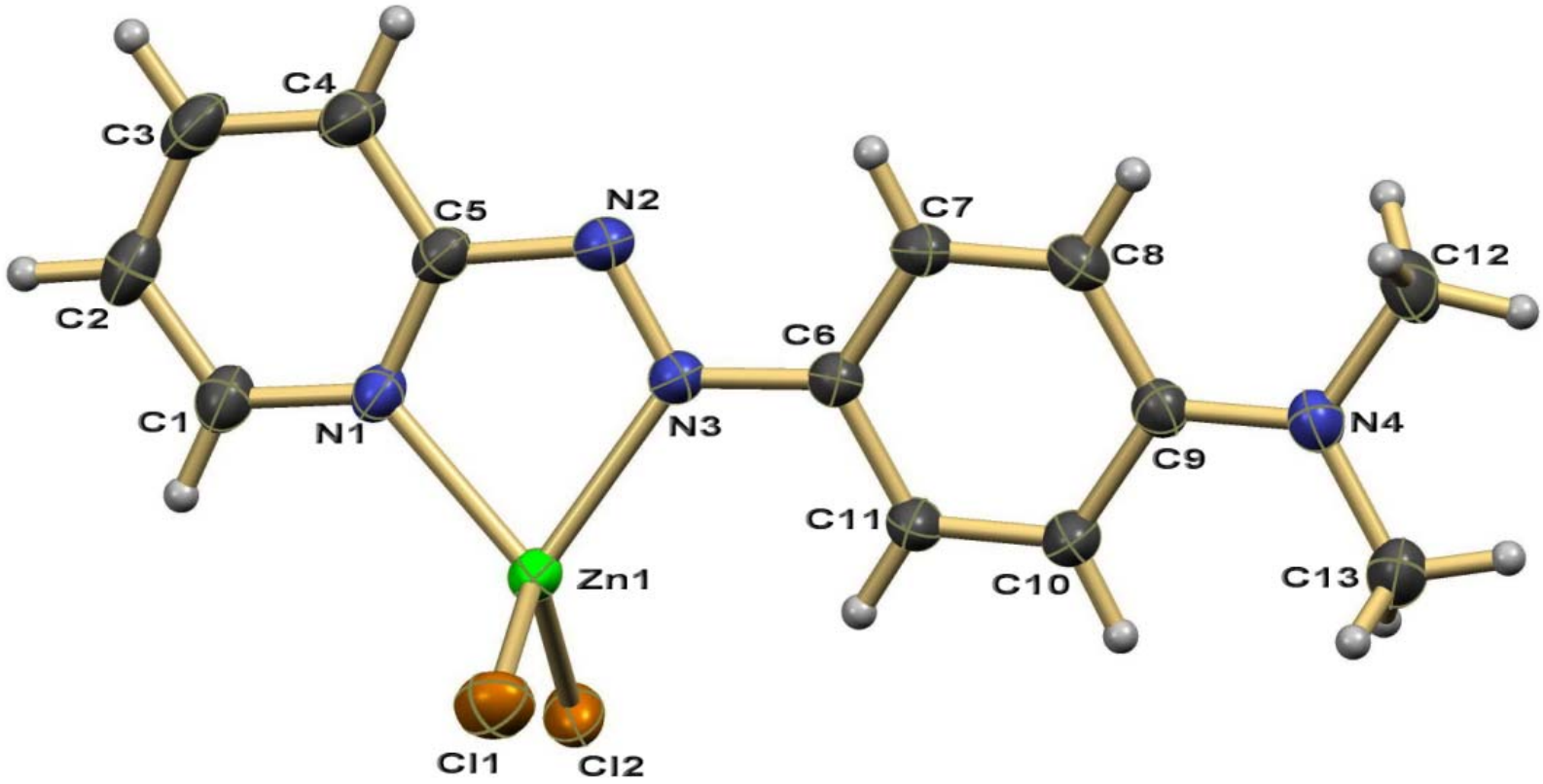

Figure 35 Molecular structure of [Zn(dmazpy)Cl_2] complex

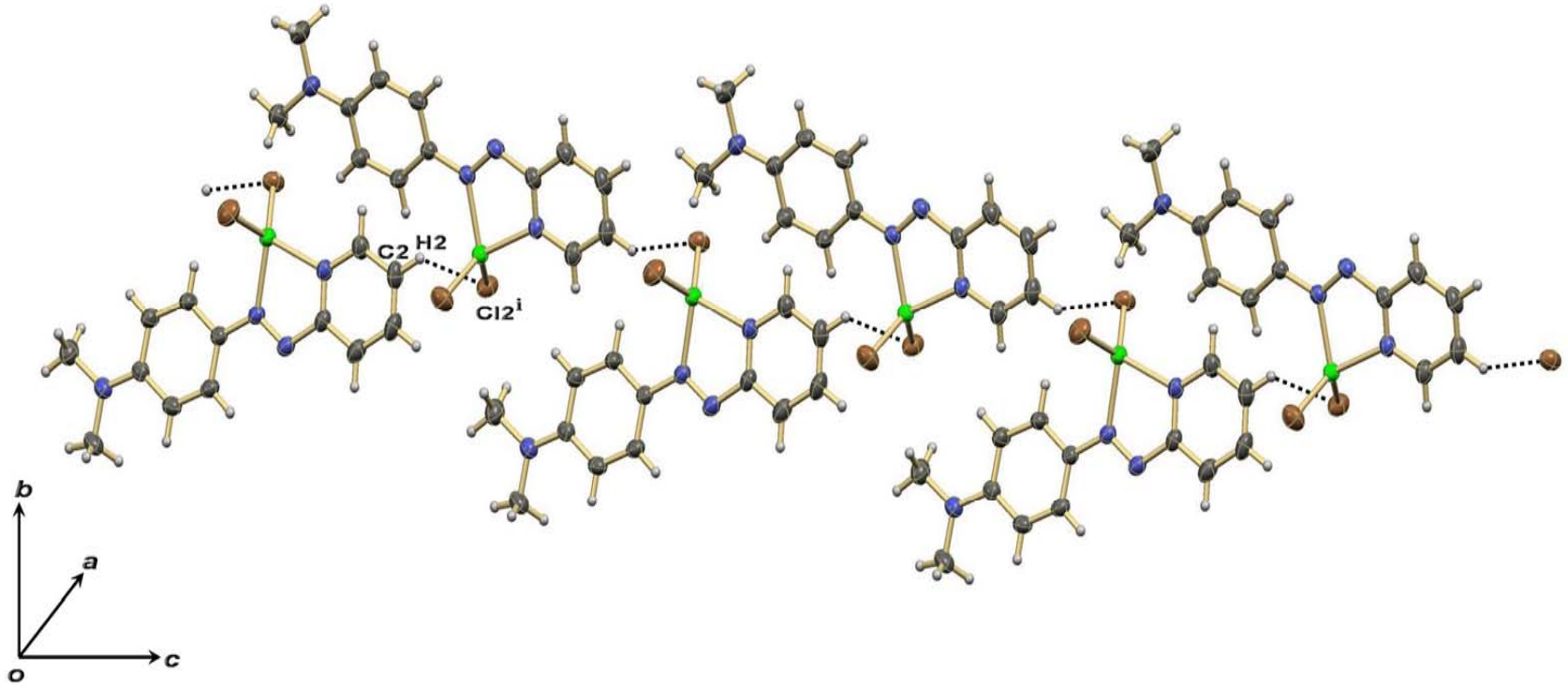

Figure 36 The weak intermolecular interactions of C-H-Cl between the adjacent molecules.

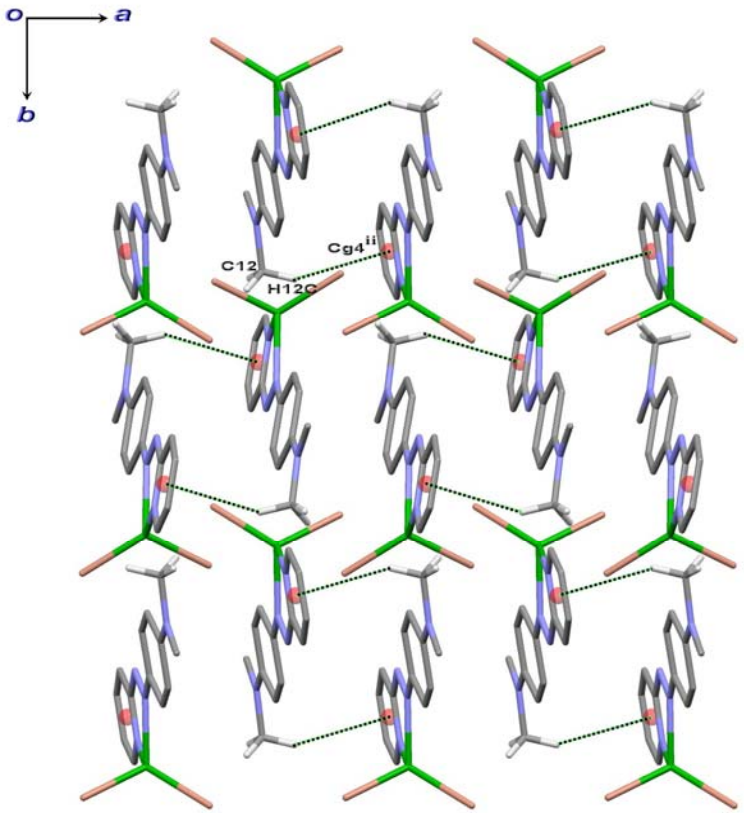

Figure 37 The π-π interactions between molecules in crystal packing.

Table 8. Atomic coordinates (1×10^4) and equivalent isotropic displacement parameters ($Å^2 \times 10^3$) for[Zn(dmazpy)Cl_2]. U(eq) is defined as one third of the trace of the orthogonalized U^{ij} tensor.

	x	y	z	U(eq)
Zn(1)	2513(1)	2379(1)	952(1)	50(1)
Cl(1)	117(1)	3044(1)	323(1)	81(1)
Cl(2)	4921(1)	3214(1)	889(1)	66(1)
N(1)	2173(3)	1803(2)	2198(1)	51(1)
N(2)	2085(3)	316(2)	1353(1)	54(1)
C(5)	1924(3)	840(2)	2164(2)	52(1)

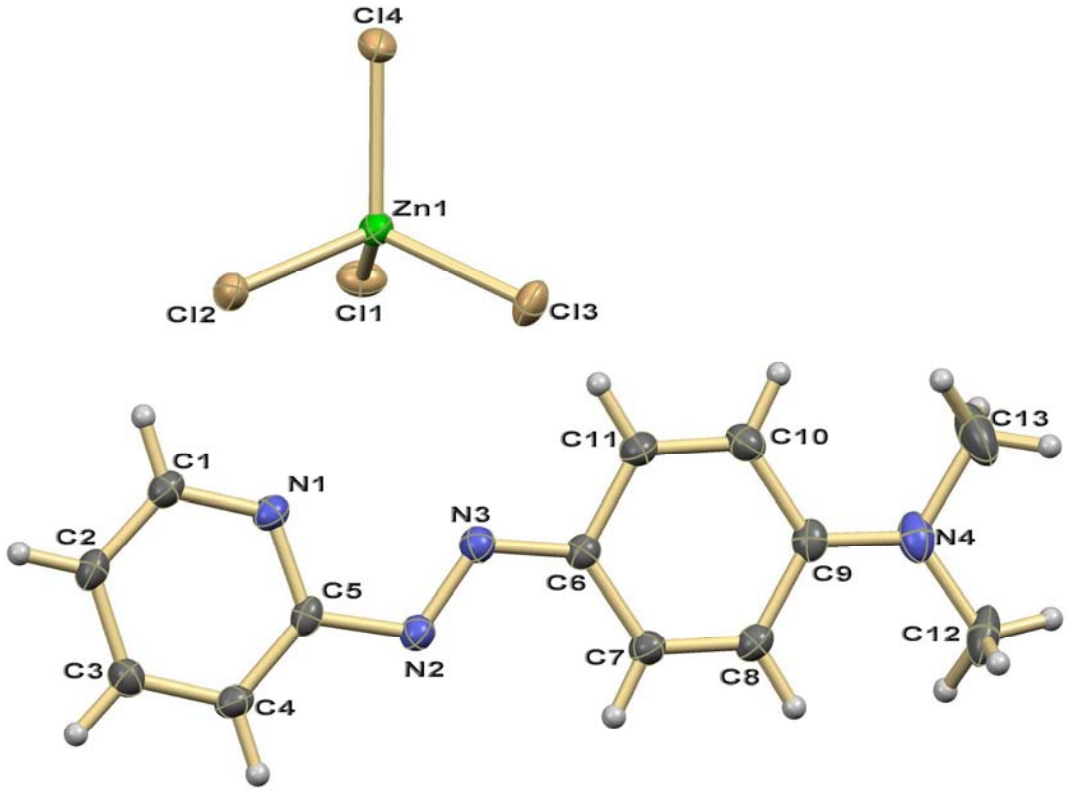

Figure 38 Molecular structure of $[(dmazpyH_2)^{2+}(ZnCl_4)^{2-}]$ complex**.**

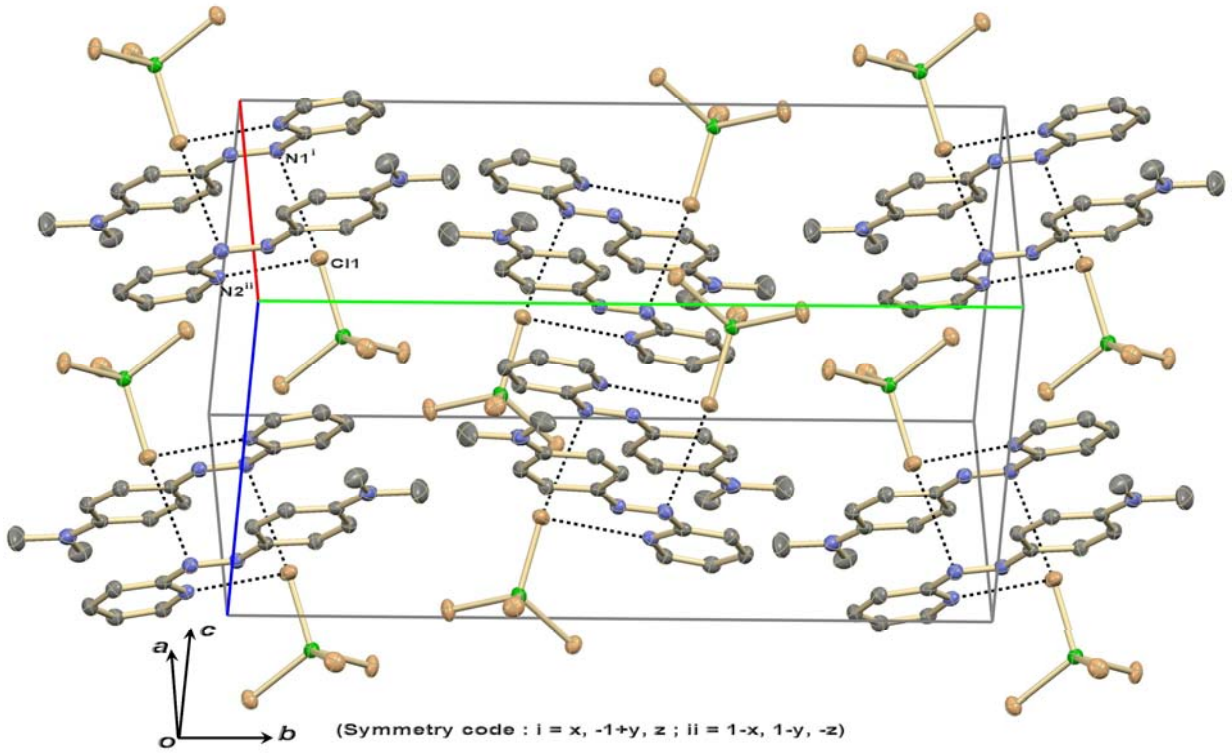

Figure 39 Hydrogen bonding interactions of $[(dmazpyH_2)^{2+}(ZnCl_4)^{2-}]$ complex**.**

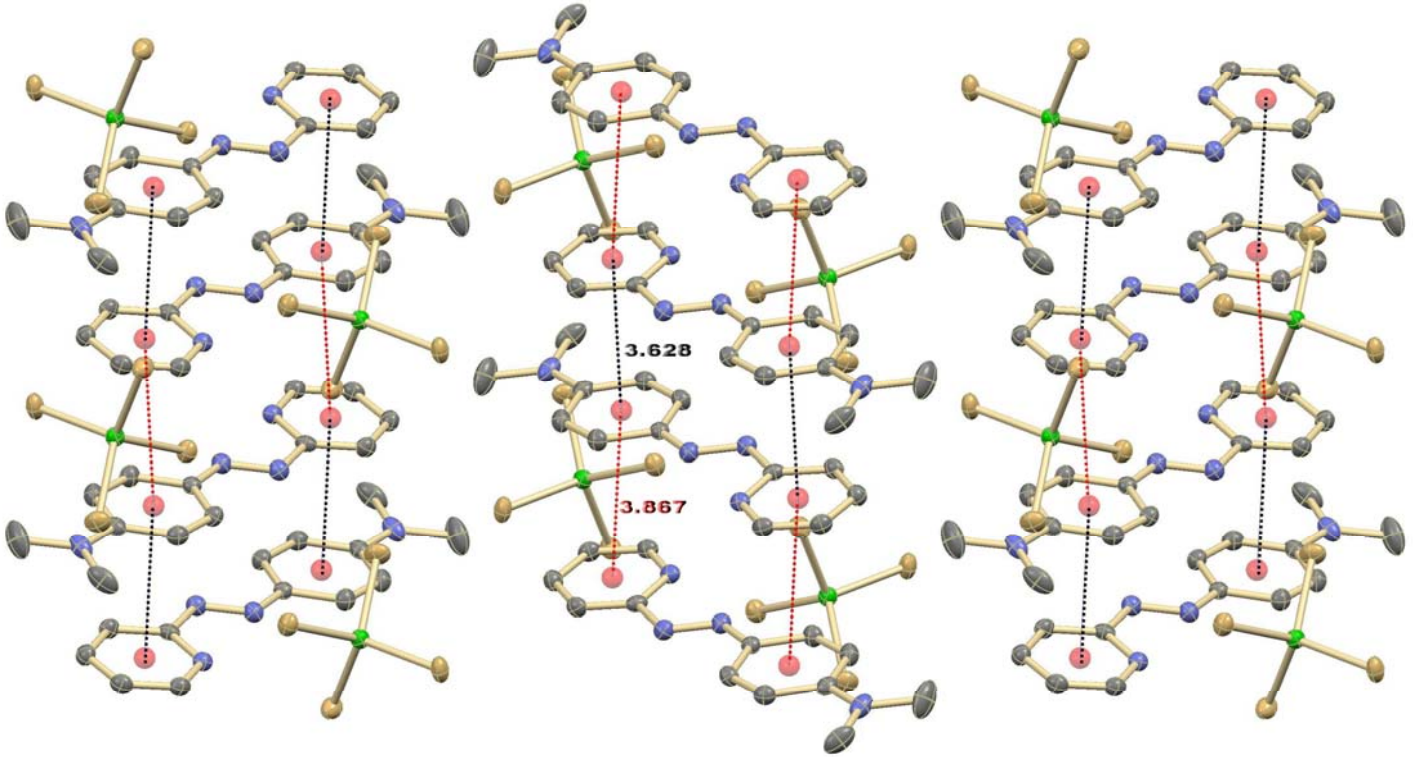

Figure 40 The π···π stacking between phenyl and pyridine rings of $[(dmazpyH_2)^{2+}\ (ZnCl_4)^{2-}]$ complex**.**

Table 9. Hydrogen-bond geometry (A˚,º).

D—H---A	D—H	H--- A	D---A	D—H---A
N1—H1A---N3	0.90(2)	2.21(3)	2.595 (3)	106 (2)
N2—H2A---Cl3	0.89 (2)	2.45(2)	3.322 (3)	165 (3)
N1—H1A---Cl1	0.89 (2)	2.37 (2)	3.173 (3)	150 (3)

3.2.2 Proton Nuclear Magnetic Resonance spectrometry

The ^{1}H NMR spectrum of Zn(dmazpy)Cl_2 is similar to the spectrum obtained from free ligand. However, the chemical shifts of this case are higher than that of free ligand as usual.

The types of protons in Zn(dmazpy)Cl_2 complex are divided into 7 groups. The proton numbering system was shown in Figure 41. ^{1}H NMR data are shown in Table 10. The ^{1}H NMR results support the structures of complex. The spectrum is as shown in Figure 42.

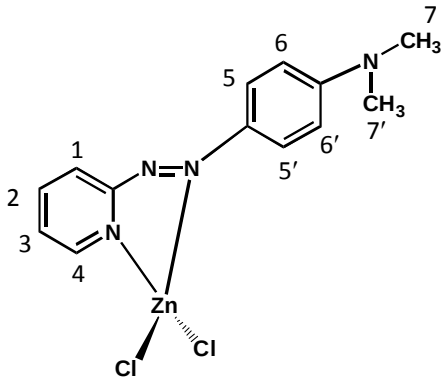

Figure 41 The types of protons in Zn(dmazpy)Cl_2

Teble 10. ^{1}H- NMR spectroscopic data of the [Zn(dmazpy)Cl_2] complex

H–position	Free ligand(dmazpy)			Complex(Zn-dmazpy)		
	δ(ppm)	Amont of H	peak	δ(ppm)	Amont of H	peak
1	8.68	1	dd	8.65	1	dd
4	8.22	1	dd	8.22	1	dd
2	7.83	1	td	8.11	1	td
5	7.76	2	d	7.98	2	d
3	7.29	1	td	7.55	1	td
6	6.75	2	d	6.85	2	d
7	3.10	6	s	3.32	6	s

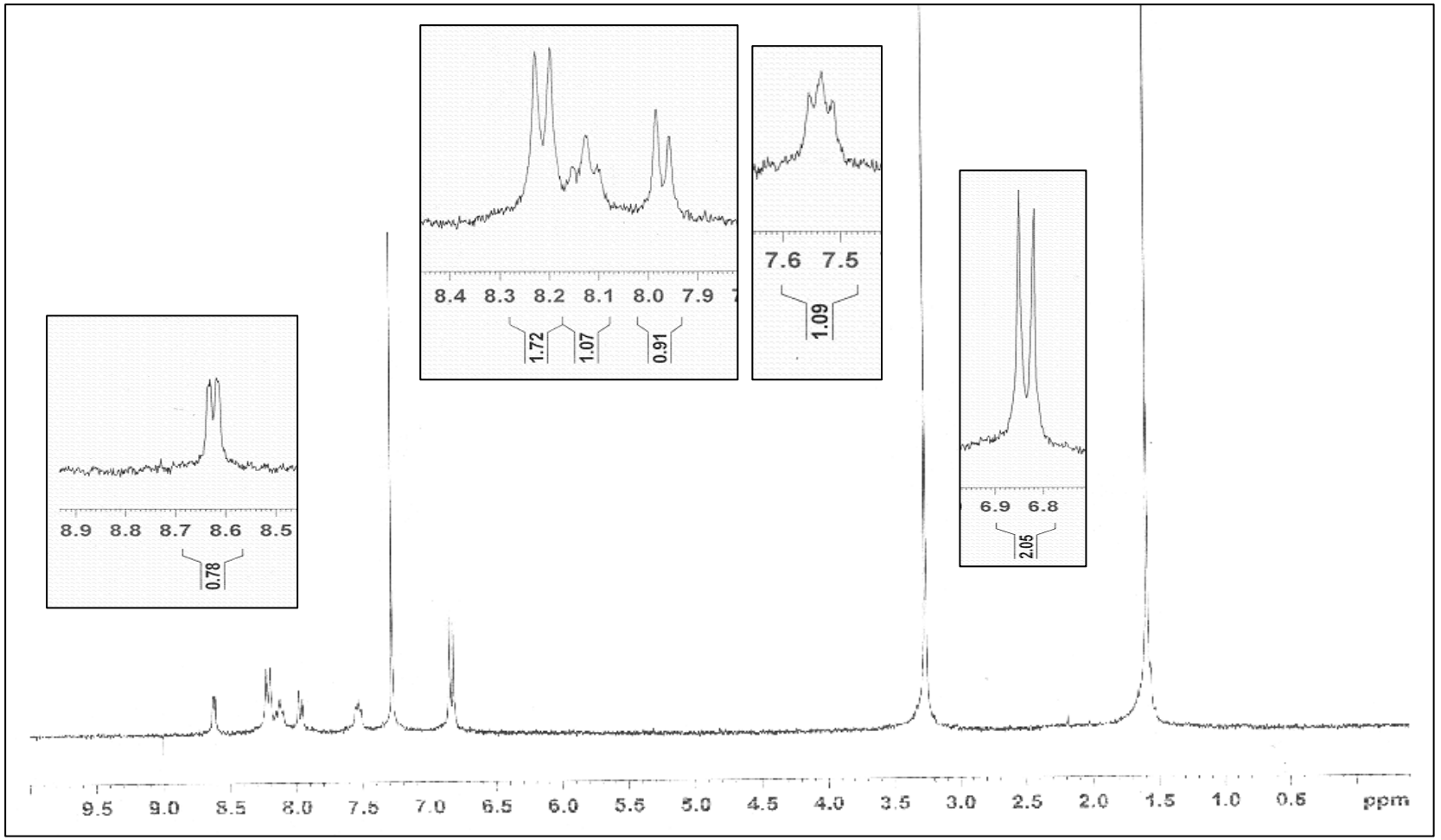

Figure 42 ^{1}H- NMR spectrum of [Zn(dmazpy)Cl_2] in $CDCl_3$**.**

3.2.3 Infrared spectroscopy (FTIR spctroscopy)

Infrared spectroscopy is a technique to study the functional groups of the compound. Infrared spectrum of [Zn(dmazpy)Cl_2] sample was prepared by KBr pellet and recorded in the range of 4000- 400 cm^{-1}. The infrared spectroscopic data of the [Zn(dmazpy)Cl_2] complex is shown in Table 11. The IR spectrum of [Zn(dmazpy)Cl_2] complex is exhibited in Figure 43.

Teble 11. Infrared spectroscopic data of the [Zn(dmazpy)Cl_2] complex

Vibration mode	**Frequencies (cm^{-1})**
N=N stretching	1258(s)
C=N stretching	1624(s)
C=C stretching	1549(s)
C-H bending	796(m)

The Infrared (IR) spectrometric result supports that the dmazpy bound with Zn^{2+}. The vibrational frequencies of the complex appeared to be different from those observed in the free ligand. Nevertheless, the focusing vibrational mode is the νN=N stretching. It has been found that the N=N stretching occurs at 1258 cm^{-1} lower frequency than that of the free dmazpy ligand (1399(s)). On complexation, the νN=N wave number is decreased with respect to the free ligand, is an indication that the N atom of dmazpy ligand coordinates with Zn^{2+}.

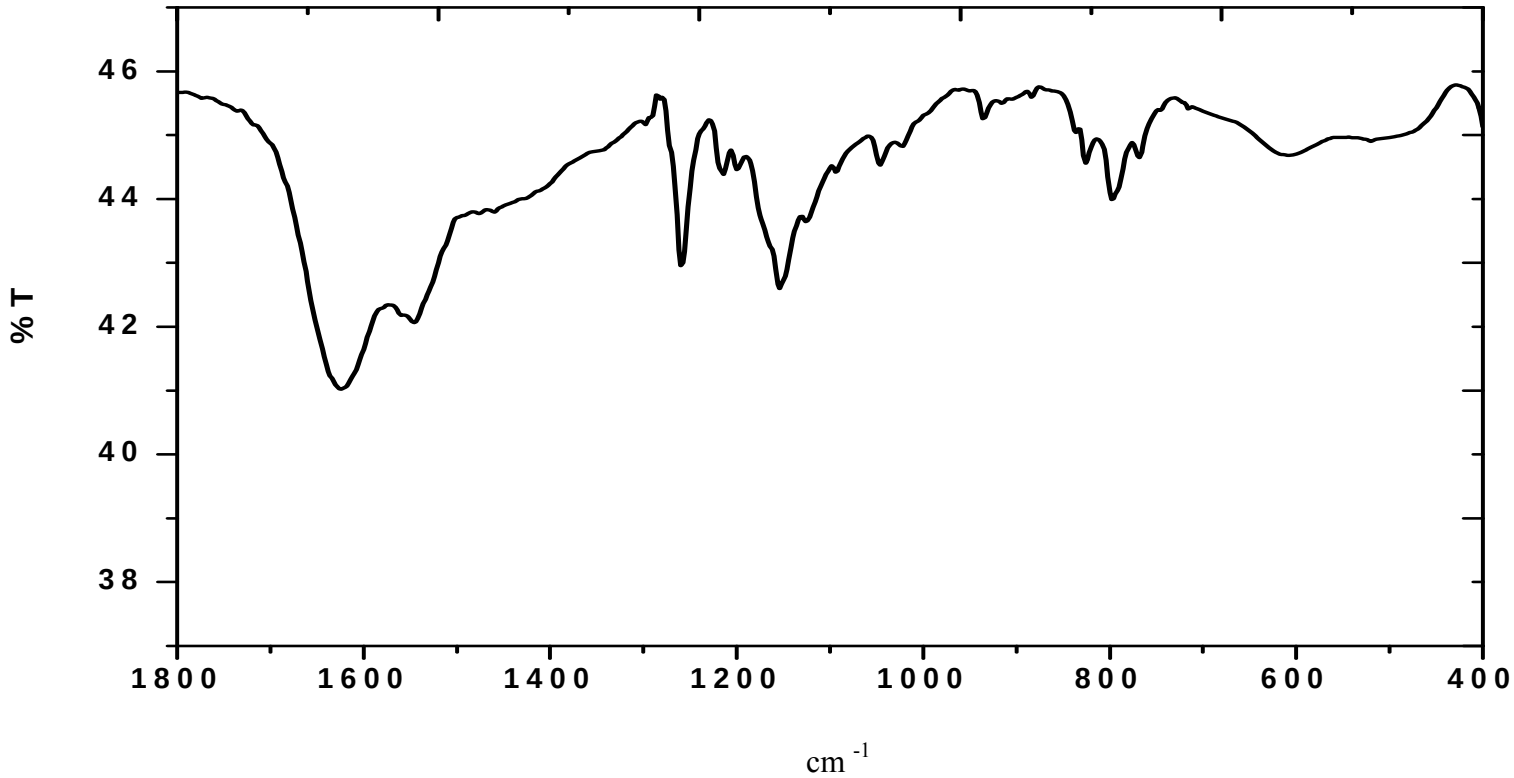

Figure 43 IR spectrum of [Zn(dmazpy)Cl_2] complex**.**

3.2.4 UV-Visible absorption spectrophotometry

UV-Visible absorption spectroscopy is a technique to study the electronic transitions of the compound. The UV-vis data shows the absorption band in visible region with the λ_{max} absorption of complex at 552 nm with high molar extinction coefficient (10,600 $M^{-1}cm^{-1}$). The absorption spectrum of the $[Zn(dmazpy)Cl_2]$ complex in methanol is shown in Figure 44.

From the figure 44, there are two absorption bands at 430 nm and 552 nm, respectively. The band at 430 nm belongs to the adsorption band of dmazpy itself which might be possible that the ligand is not totally eliminated. However, the band at 552 nm comes from the complex of $[Zn(dmazpy)Cl_2]$.

3.2.5 Luminescence spectrometry

Luminescence spectrum of $[Zn(dmazpy)Cl_2]$ was measured by exciting the molecule at 550 nm and the spectrum was scanned from 560 to 800 nm, A weak emission band is exhibited with the maximum wavelength at 620 nm, as shown in the Figure 45. The emission band was tested whether whether it is an emission band caused form luminescence which does not are from scattering by varying the excitation wavelengths.

It can be confirmed that the emission bands are not affected by changing the excitation wavelength (Figure 46).

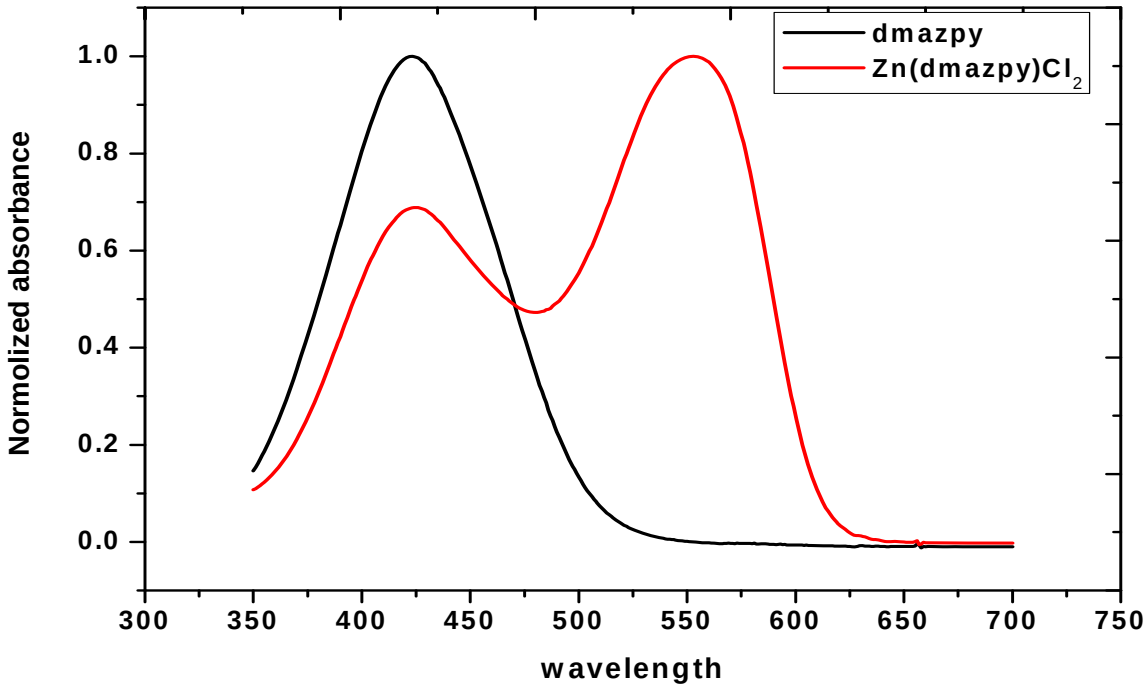

Figure 44 Normalized absorption spectrum of 4 x 10^{-5} M dmazpy ligand and [$Zn(dmazpy)Cl_2$] complex in acetronitile.

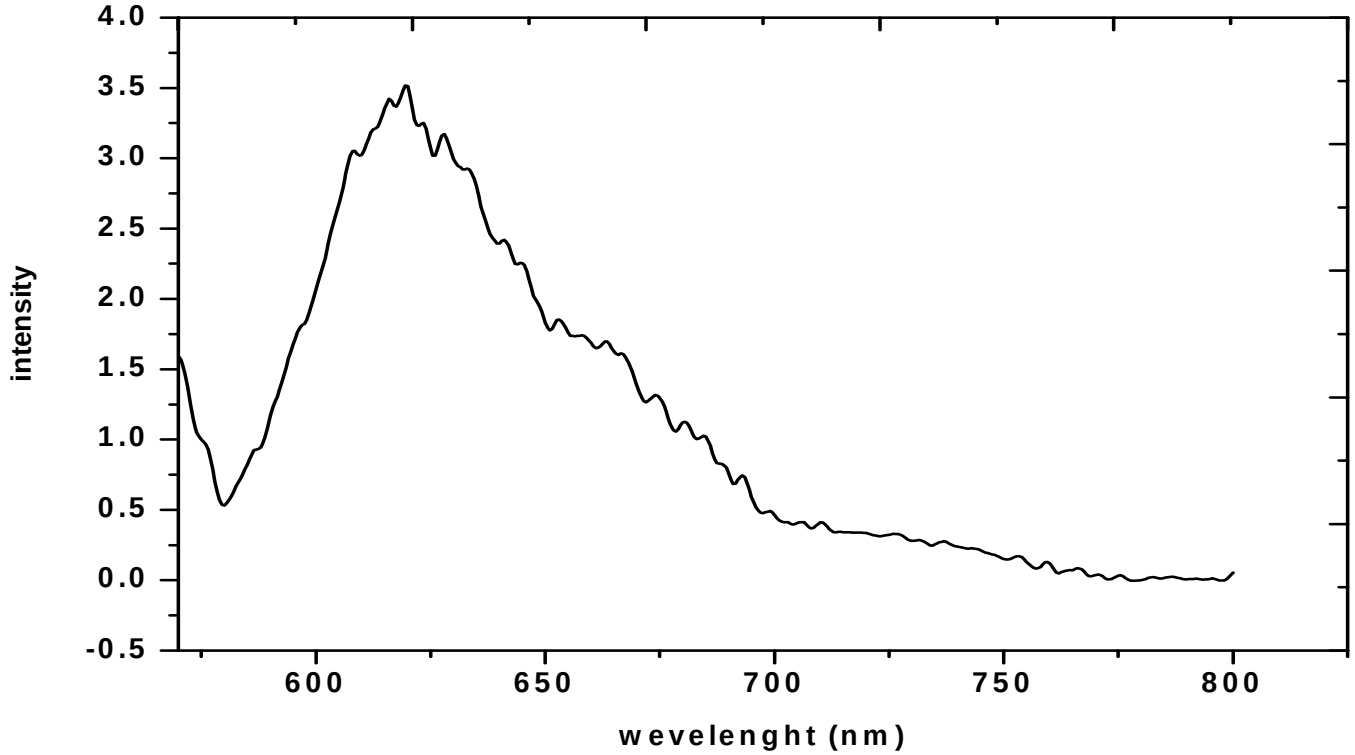

Figure 45 Emistion spectra of [Zn(dmazpy)Cl_2] in CH_3CN.

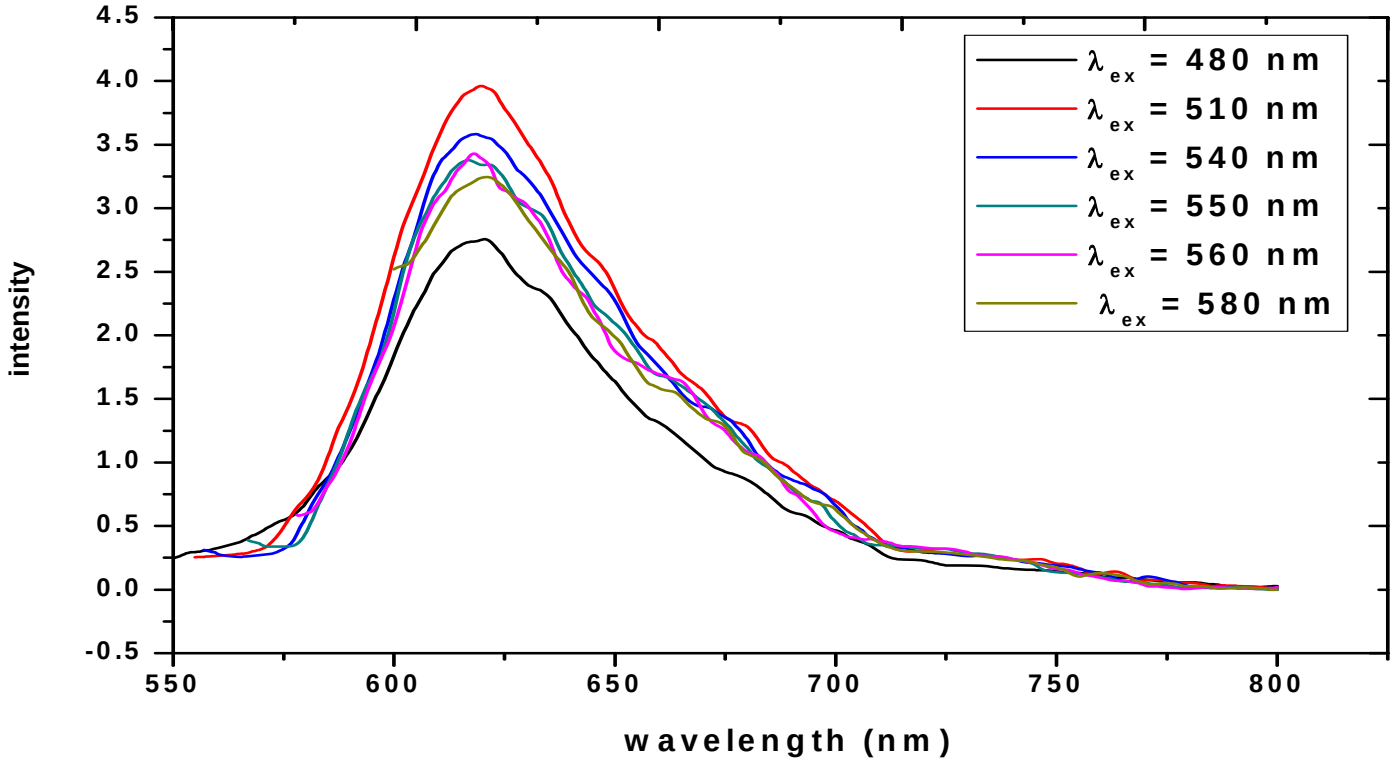

Figure 46 Emistion spectra of [Zn(dmazpy)Cl_2] in CH_3CN from various excitation wavelength.

3.3 Synthesis and characterization of [Ru(dmazpy)(*p*-cymene) Cl]Cl

Synthesis of [Ru(dmazpy)(*p*-cymene)Cl]Cl

Ru-*p*-cymene dimer (306 mg, 0.5 mmol) was added to a THF solution (8 mL) containing dmazpy ligand (226 mg, 1.0 mmol). The color of the mixture immediately turned from red to green. The reaction mixture was stirred at room temperature for 2 h. The precipitate was filtered off, washed with THF and filtered off again to remove unreacted dmazpy. The residue was dissolved by CH_2Cl_2 (5 mL) and then precipitated with diethyl ether (10 mL) giving the green solid with 63 % yield. The solubility data [Ru(dmazpy)(*p*-cymene)Cl]Cl are summarized in Table 12. The complex is completely soluble in all studied organic solvents.

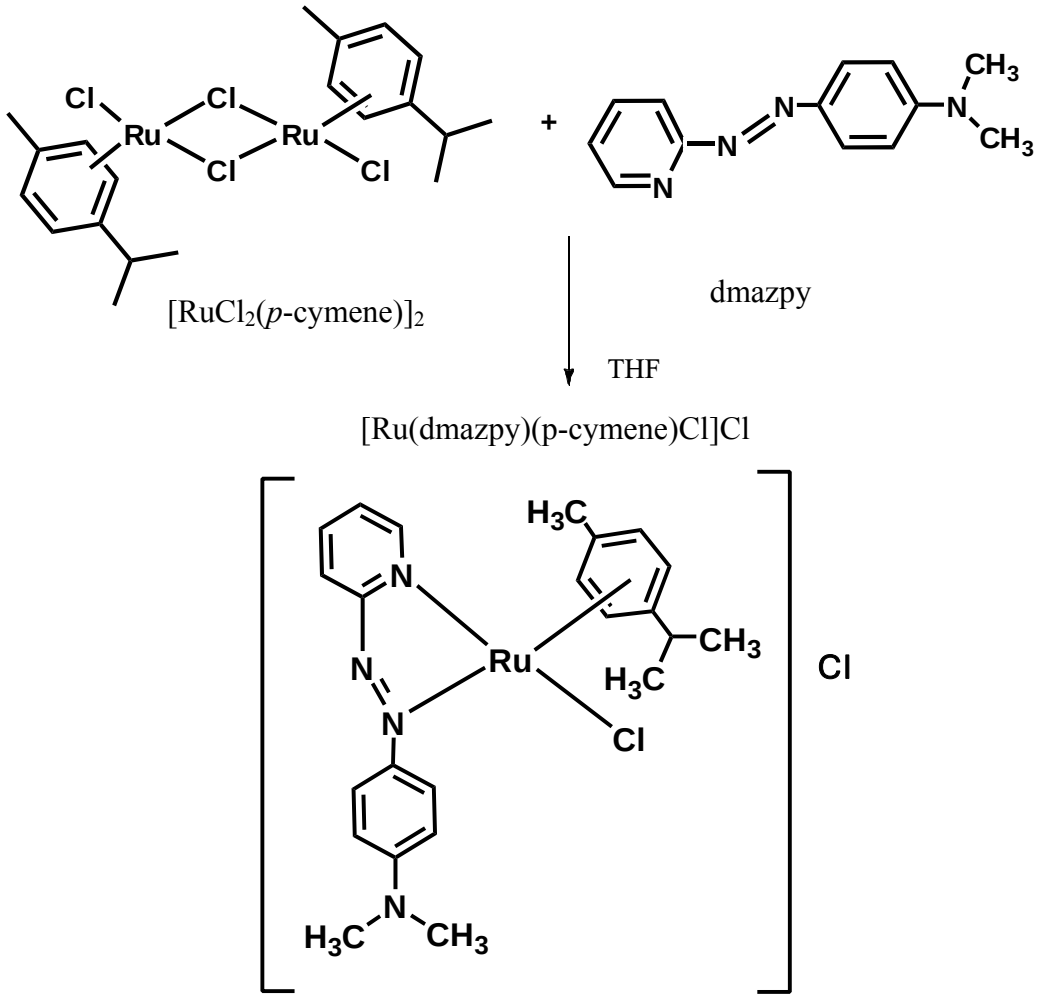

Figure 47 The synthesis procedure of [Ru(dmazpy)(*p*-cymene)Cl]Cl

Table 12. Solubility of [Ru(dmazpy)(*p*-cymene)Cl]Cl

solvent	**solubility**
hexane	+++
toluene	+++
dichoromethane	+++
chlorofrom	+++
benzene	+++
ethylacetate	+++
acetone	+++
acetonitrile	+++
dimethylformamide (DMF)	+++
dimethylsulfoxide (DMSO)	+++
ethanol	+++
methanol	+++
water	+++

The symbol of solubility, +++ represents the completely soluble of complex 0.0010 g in 3 mL of solvents.

Characterization of [Ru(dmazpy)(*p*-cymene)Cl]Cl complex.

The chemistry of the [Ru(dmazpy)(*p*-cymene)Cl]Cl complex was investigated by using these techniques.

- Neclear Megnetic Resonance spectrometry
- Infrared spectrometry
- Elemental analysis
- Fast-atom bombardment (FAB) mass spectrometry
- UV-Visible absorption spectrophotometry
- Cyclic Voltammetry

3.3.1 Nuclear Magnetic Resonance spectroscopy

Nuclear Magnetic Resonance (NMR) spectroscopy is a technique to determine the molecular structure of a studied compound. The structure of [Ru(dmazpy)(*p*-cymene) Cl]Cl complex was investigated by using 1D and 2D NMR spectroscopic techniques (^{1}H NMR, ^{1}H-^{1}H COSY NMR, ^{13}C NMR, DEPT NMR ,^{1}H-^{13}C HMQC NMR and ^{13}C -^{13}C HMBC NMR). The NMR spectra of the complex were recorded in CD_3OD on Bruker 300 MHz. The tetramethylsilane (TMS) was used as the internal standard.

The ^{1}H NMR results of [Ru(dmazpy)(p-cymene)Cl]Cl complex show 2 sets of ligand signals from the dmazpy and *p*-cymene. The proton signals belonging to the dmazpy ligand are exhibited for 7 signals arising from 14 protons, whereas the signals from the *p*-cymene part shows 8 signals from 14 protons. The structure of the [Ru(dmazpy)(*p*-cymene)Cl]Cl complex with proton numbering is shown in Figure 48. The symbol of ′ is referred to the equivalent proton. The ^{1}H-NMR spectrum of the [Ru(dmazpy)(*p*-cymene)Cl]Cl complex is displayed in Figure 49. The assignment of individual proton resonances have been assigned using ^{1}H-^{1}H COSY NMR spectroscopy Figure50. The ^{1}H-NMR data of the complex are collected in Table 13.

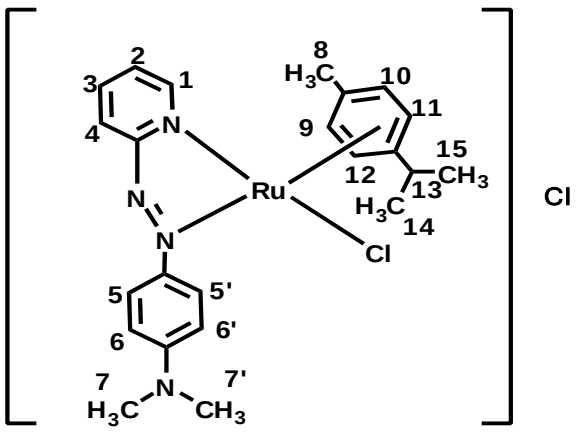

Figure 48 The structure of [Ru(dmazpy)(*p*-cymene)Cl]Cl complex with proton numbering system.

Table 13. ^{1}H-NMR data and ^{1}H-^{1}H COSY of [Ru(dmazpy)(*p*-cymene)Cl]Cl in MeOD-d_4 solvent.

H -position	δ_H (ppm)	J-coupling (Hz)	Signal character	amounts of H	^{1}H-^{1}H COSY
1	9.21	4.8	d	1H	H-2
2	7.53	7.35, 1.5	dt	1H	H-1, H-3
3	8.11	3.0	t	1H	H-2
4	8.22	6.9	d	1H	H-3
5,5′	8.15	6.0	d	2H	H-6
6,6′	6.96	5.2	d	2H	H-5
7,7′	3.22	-	s	6H	-
8	2.23	-	s	3H	-
9	5.74	6.6	d	1H	H-12
10	5.83	6.3	d	1H	H-11
11	5.91	6.0	d	1H	H-10
12	6.07	6.3	d	1H	H-9
13	2.34	-	m	1H	H-14
14	0.92	6.9	d	1H	H-13
15	0.86	6.9	d	1H	H-13

d = doublet dt = doublet of triplet t = triplet s = singlet

The ^{1}H-NMR signals of [Ru(dmazpy)(*p*-cymene)Cl]Cl appeared for 15 signals. The detail of each signal can be described below.

The proton-1 is on pyridine located next to pyridine nitrogen atom which gives signal at most downfield. The proton signal is splitted by the proton-2 (J = 4.8 Hz). Therefore, the signal shows as a doublet (d) peak.

The proton-2 located next to the proton-1. The signal of this proton is doublet of triplet (dt) peak. The splitting of the triplet peak (J = 4.2) is observed form the coupling of this proton with proton-1 and proton-3. Then each of triplet peak is splitted to doublet signal (J = 1.5 Hz) from long range coupling with proton-4.

The proton-3 is the proton which is opposite to pyridine nitrogen. The proton is less effected from nitrogen atom than that of the proton-2 thus the chemical shift value is lower than that of the proton-2. The signal of this proton also shows doublet of triplet peaks. It is splitted by the proton-2 and 4 (J=3 Hz) and long range coupling by the proton-1 (J = 1.5 Hz).

The proton-4 located next to the proton-3 and it is affected from nitrogen of azo function. The signal occurs at downfield position more than proton-2 and 3. It shows at upfield position than that of proton-1. The signal is doublet of doublet peaks. It is splitted by proton-3 (J=6 Hz) and by the proton-2 (J = 1.2 Hz), respectively.

The proton-5 and 5′ are two equivalent protons on phenyl ring located closed to azo nitrogen. The proton-5 signal appears at upfield position than that of proton-4. The proton-5 interacts with proton 6 and gives the doublet peak with J-coupling 6 Hz.

The proton-6 are two equivalent protons located next to the proton-5. The signal is similar to the signal from 5,5′ proton which is also doublet of doublet peaks. The signal is splitted by proton -5 (J=5.7 Hz)

The proton-7 and 7′ are the methyl protons (-CH_3). The signal is singlet peak of 6 protons .

The proton-8 are the methyl protons (-CH_3) substituent on the benzene ring of *p*-cymene part. The signal is also singlet peak of 3 protons.

The proton-9 is the proton of the benzene ring. The signal of this proton is also doublet peaks coupling with the proton-12 (J = 6.6 Hz).

The proton-10 is the proton which is opposite to the proton-9 in benzene ring. The signal of this proton is a doublet peak. It is splitted by the proton-11 (J = 6.3 Hz).

The proton-11 is the proton located on benzene ring which is opposite to the proton -9. The signal of this proton also the doublet peaks. It is splitted by the proton-10 (J = 6.6 Hz).

The proton-12 is the proton on the benzene ring of *p*-cymene. The signal of this proton is a doublet peak. It causes from the coupling with the proton-9 (J = 6.3 Hz).

The proton-13 signal is multiplet peaks. It is splitted by the proton-14 and proton -15.

The proton-14 are the methyl protons ($-CH_3$) of the substituent in *p*-cymene. The signal is a doublet peak. It is splitted by the proton-13. (J = 6.9 Hz).

The proton-15 signal is similar to the proton-14. It is methyl protons of *p*-cymene. The ^{1}H-NMR another signal is a doublet peak. It is splitted by the proton-13. (J = 6.9 Hz).

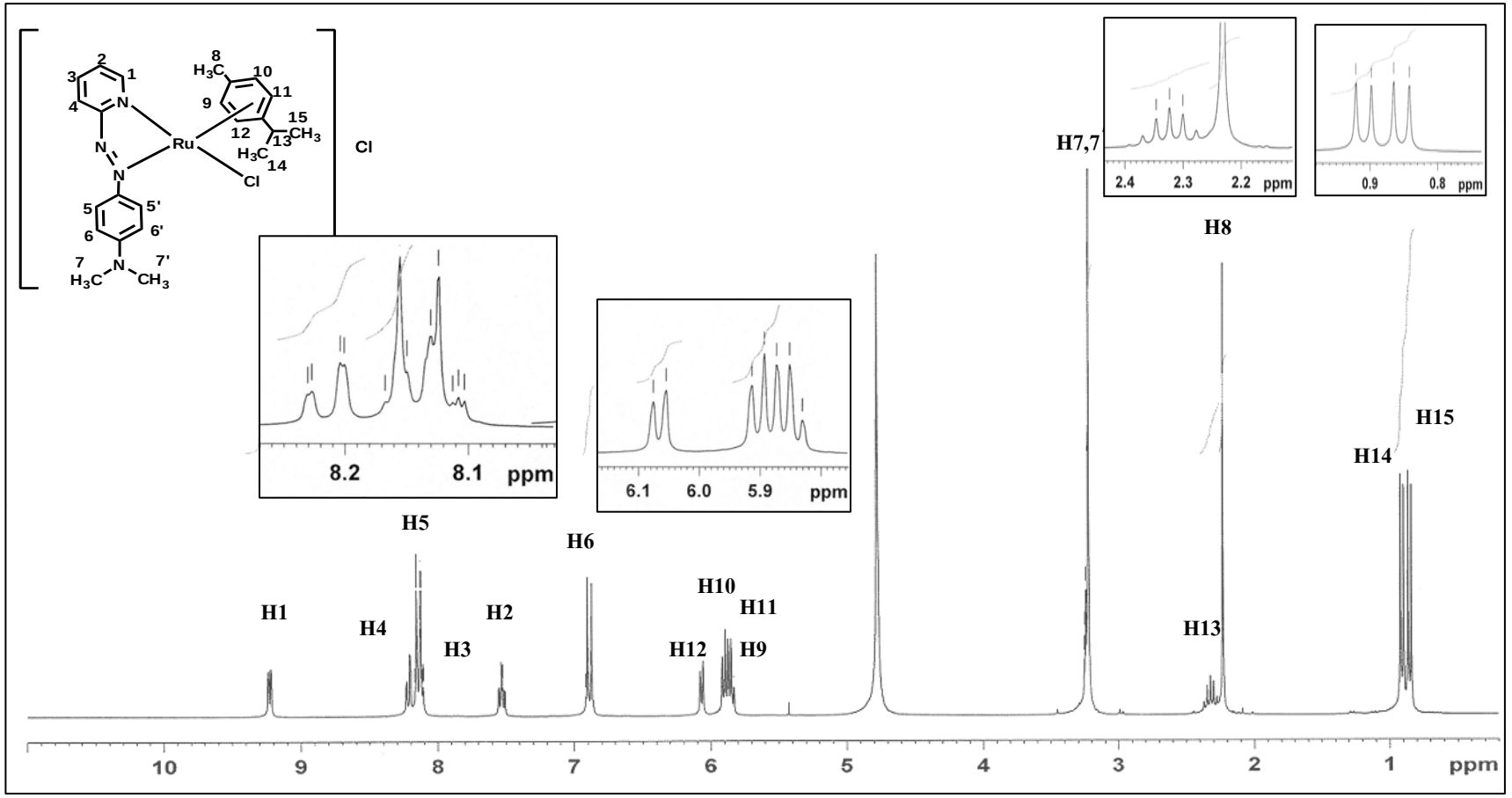

Figure 49 [1]H NMR spectrum of [Ru(dmazpy)(*p*-cymene)Cl]Cl in (methanol-*d4*) (300 MHz)

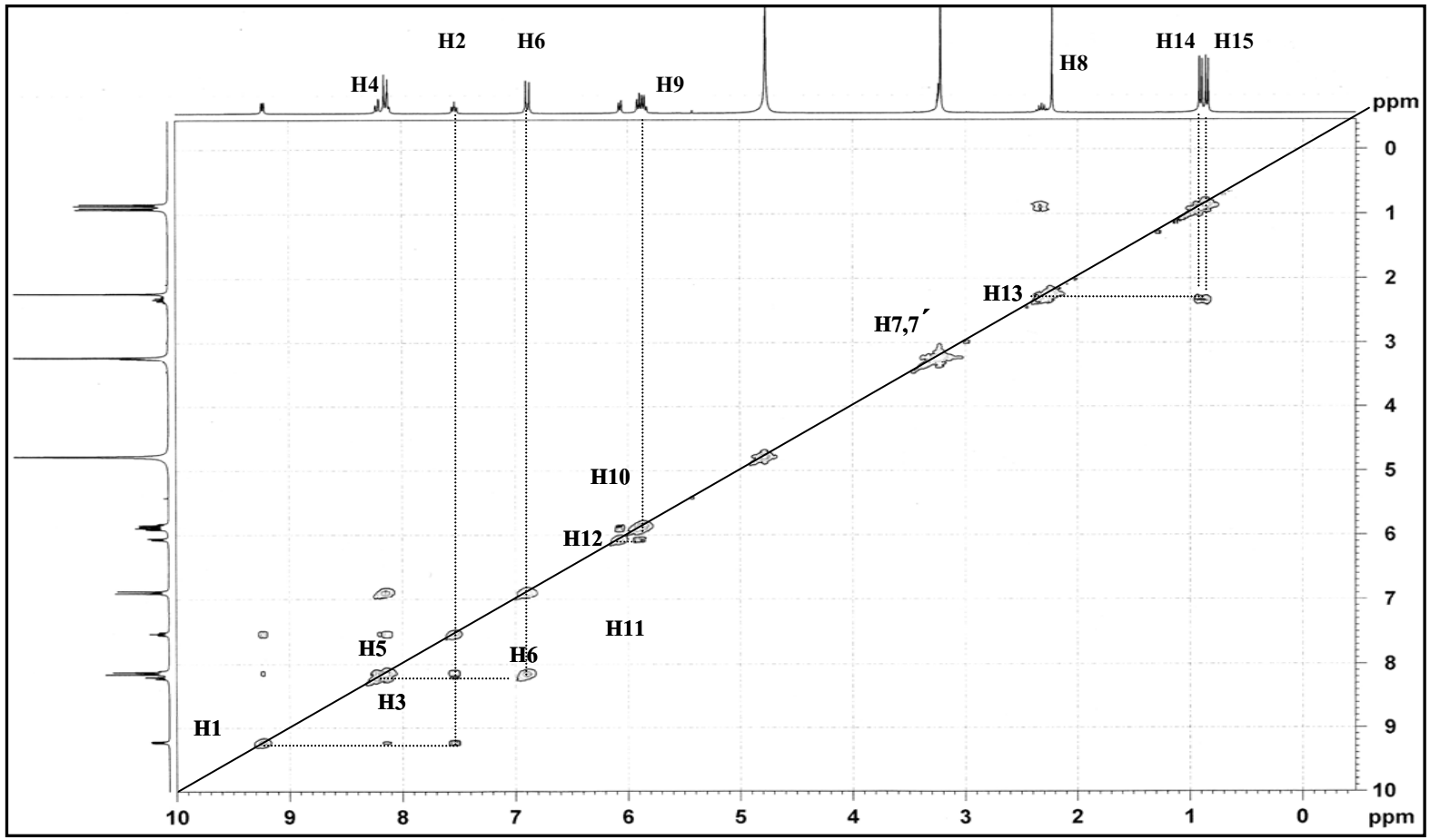

Figure 50 ^{1}H- ^{1}H COSY NMR spectrum of [Ru(dmazpy)(*p*-cymene)Cl]Cl in (methanol-d_4) (300 MHz)

^{13}C- NMR spectroscopy

The ^{13}C NMR of [Ru(dmazpy)(*p*-cymene)Cl]Cl complex shows 20 signals of carbon corresponding to the expected structure. The carbon numbering of the structure is shown in Figure 51. It consists of 5 quaternary carbon (C) signals, 13 methyne carbon signals (CH) and methyl carbon (CH_3) for 5 signals. The symbol of ′ is refers to the equivalent carbon. The ^{13}C-NMR spectra of the [Ru(dmazpy)(*p*-cymene)Cl]Cl complex is displayed in Figure 52. The assignment of the type of carbon has been assigned using DEPT 90 NMR, DEPT 135 NMR by DEPT 90 NMR assignment of the methyl carbon (CH) and DEPT 135 assignment of all types of carbons Figure 53 and 55, respectively. The ^{13}C-NMR data of the complex are collected in Table 14.

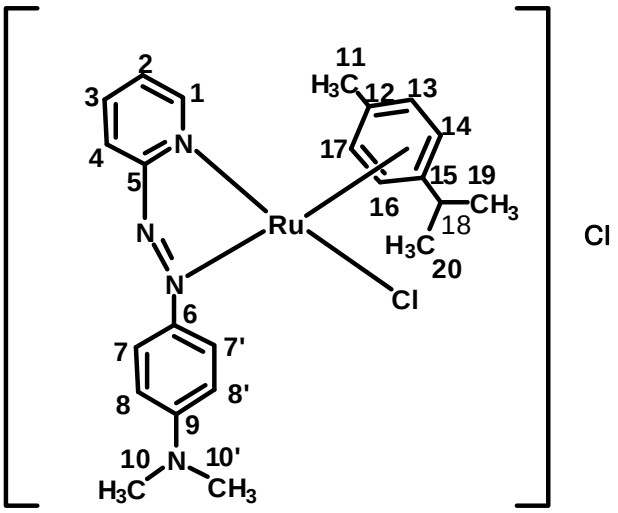

Figure 51 The structure of [Ru(dmazpy)(*p*-cymene)Cl]Cl complex with carbon numbering system.

Table 14. Chemical shifts of ^{13}C NMR data according of types of carbons [Ru(dmazpy)(*p*-cymene)Cl]Cl.

Typs of carbon	chemical shift (ppm)
Quaternary carbon (C)	δc 106.78, δc 108.34, δc 146.11, δc 155.75 and δc 164.11
methane carbon (CH)	δc 153.46, δc 140.81, δc 128.59 (x2), δc 124.93, δc 111.84 (x2), δc 89.12, δc 89.71, δc 87.44, δc 87.11 and δc 31.00
methyl carbon (CH_3)	δc 39.44(x2), δc 20.84, δc 20.77, and δc 17.77

Table 15. ^{1}H-^{13}C HMQC DEPT 90 DEPT 135 and HMBC NMR data of [Ru(dmazpy)(*p*-cymene)Cl]Cl in MeOD-d_4 solvent.

C-position	δ_H (ppm)	^{13}C HMQC (δ_C,ppm)	DEPT 90	DEPT 135	HMBC
1	9.21	153.46(CH)	153.46		C-2, C-3, C-5
2	7.53	125.20(CH)	125.20		C-1, C-4, C-5
3	8.11	140.81(CH)	140.81		C-2, C-5
4	8.22	124.39(CH)	124.39		C-1, C-2, C-5
5	-	164.11(C)	-		-
6	-	155.75(C)	-		-
7,7′	8.15	128.59(CH)	128.59 (x2)		C-6, C-9
8,8′	6.96	111.84(CH)	111.84 (x2)		C-9
9	-	146.96(C)	-		-
10,10′	3.22	39.44(CH_3)	-	39.44 (x2)	-
			-		
11	2.23	17.77 (CH_3)	-	17.77	C-12,C-13
12	-	108.34(C)	-		-
13	5.91	87.11(CH)	-		C-13, C-15
14	5.74	89.70(CH)	89.96		C-12, C-15
15	-	106.78(C)	-		-
16	5.83	89.12(CH)	89.26		C-12, C-15
17	6.07	87.44 (CH)	87.71		C-13
18	2.34	31.00(CH)	31.02		C-14, C-15
19	0.86	20.77(CH_3)	-	20.77	C-18, C-20
20	0.92	20.83(CH_3)	-	20.84	C-18, C-19

In order to confirm the relationship between carbon and proton ^{13}C-^{1}H position, the ^{1}H-^{13}C HMQC NMR was used whereas, the HMBC NMR was applied to confirm the relationship between the carbon-carbon (^{13}C -^{13}C).

The proton-1 (δ_H = 9.21 ppm) relates with the chemical shift of carbon at 153.46 ppm nearly the chemical shift of carbon at 125.20 (C2) 140.81 (C3) and 164.11 (C5) ppm.

The proton-2 (δ_H = 7.52 ppm) relates with the chemical shift of carbon at 125.20 ppm nearly the chemical shift of carbon at 124.39 (C4) 153.46 (C1) and 164.16 (C5) ppm.

The proton-3 (δ_H = 8.11 ppm) relates with chemical shift of carbon at 140.81 ppm nearly the chemical shift of carbon at 125.20 (C2) and 164.16 (C5) ppm.

The proton-4 (δ_H = 8.22 ppm) relates with chemical shift of carbon at 124.39 ppm closed to the chemical shift of carbon at 153.46 (C1) 125.20 (C2) and 164.11 (C5) ppm.

The proton-5 and 5 ′ (δ_H = 8.15 ppm) relates with chemical shift of carbon at 128.59 ppm closed to the chemical shift of carbon at 155.75 (C6) and 146.96 (C9) ppm.

The proton-6 and 6′ (δ_H = 6.96 ppm) relates with chemical shift of carbon at 111.84 ppm closed to the chemical shift carbon at 146.96 (C9) ppm.

The proton-7 and 7′ (δ_H = 3.22 ppm) relate with chemical shift of carbon at 39.44 ppm.

The proton-8 (δ_H = 2.23 ppm) relates with chemical shift of carbon at 17.77 ppm nearly the chemical shift of carbon at 108.34 (C12) and 87.11 (C13) ppm.

The proton-9 (δ_H = 6.07 ppm) relates with chemical shift of carbon at 87.44 ppm nearly the chemical shift of carbon at 106.78 (C15) ppm.

The proton-10 (δ_H = 5.91 ppm) relates with chemical shift of carbon at 87.11 ppm located closed to the chemical shift of carbon at 108.34 (C12) and 87.71 (C14) ppm.

The proton-11 (δ_H = 5.74 ppm) relates with chemical shift of carbon at 89.71 ppm located closed to chemical shift of carbon at 17.77 (C11) and 106.48 (C16) ppm.

The proton-12 (δ_H = 5.83 ppm) relates with chemical shift of carbon at 89.12 ppm nearly the chemical shift of carbon at 108.34 (C12) and 106.78 (C15) ppm.

The proton-13 (δ_H = 2.34 ppm) relates with chemical shift of carbon at 31.00 ppm located closed to chemical shift of carbon at 89.71 (C14) and 106.78 (C15) 89.12 (C16) ppm.

The proton-14 (δ_H = 0.92 ppm) relates with chemical shift of carbon at 20.77 ppm nearly the chemical shift of carbon at 31.00 (C18) and 20.84 (C20) ppm.

The proton-15 (δ_H = 0.86 ppm) relates with chemical shift of carbon at 20.84 ppm located closed to the chemical shift of carbon at 31.00 (C18) and 20.77 (C19) ppm.

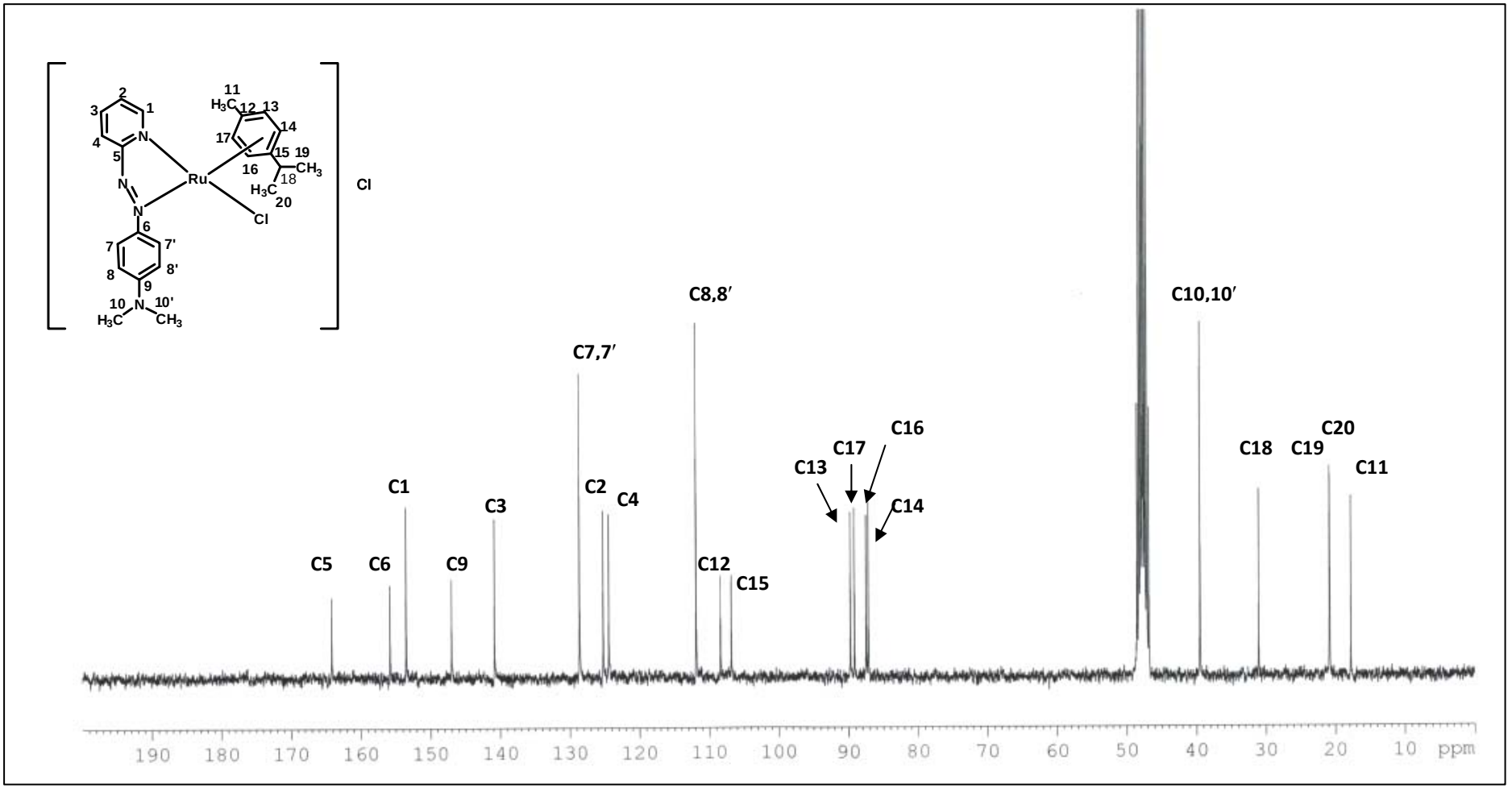

Figure 52 ^{13}C NMR spectrum of [Ru(dmazpy)(*p*-cymene)Cl]Cl in (methanol-d_4) (300 MHz).

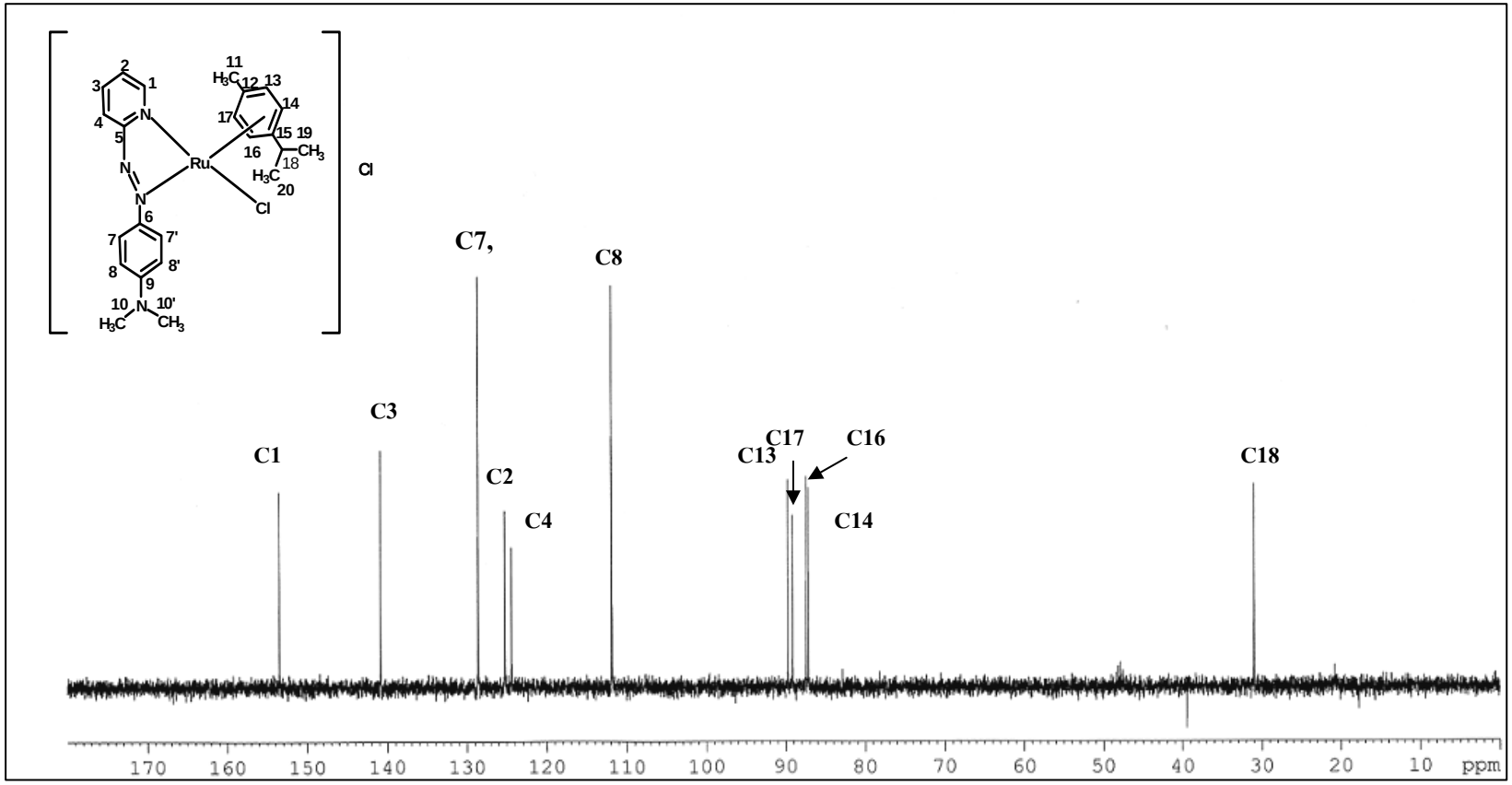

Figure 53 DEPT 90 ^{13}C NMR spectrum of [Ru(dmazpy)(*p*-cymene)Cl]Cl in (methanol-d_4) (300 MHz)

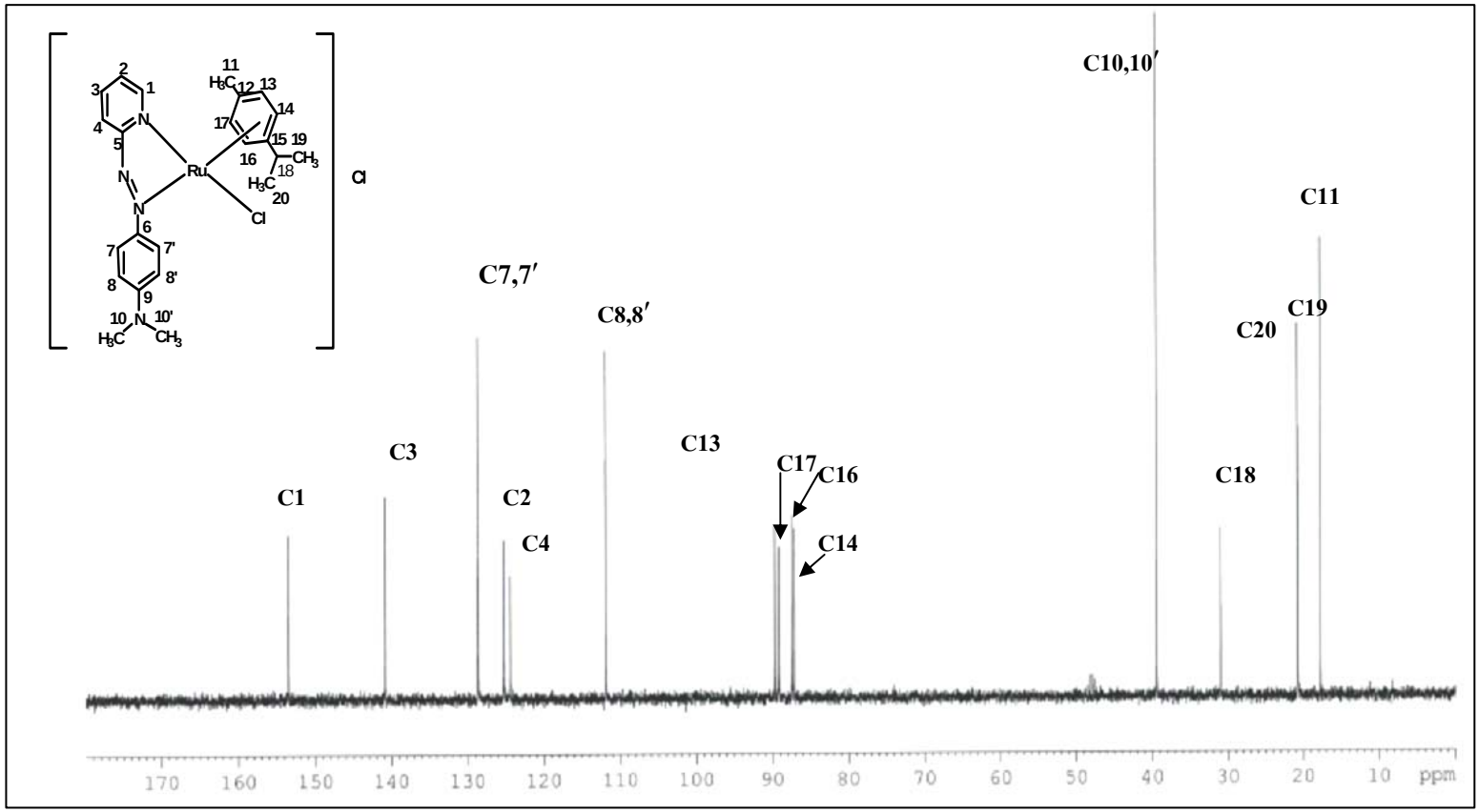

Figure 54 DEPT 135 ^{13}C NMR spectrum of [Ru(dmazpy)(*p*-cymene)Cl]Cl in (methanol-d_4) (300 MHz)

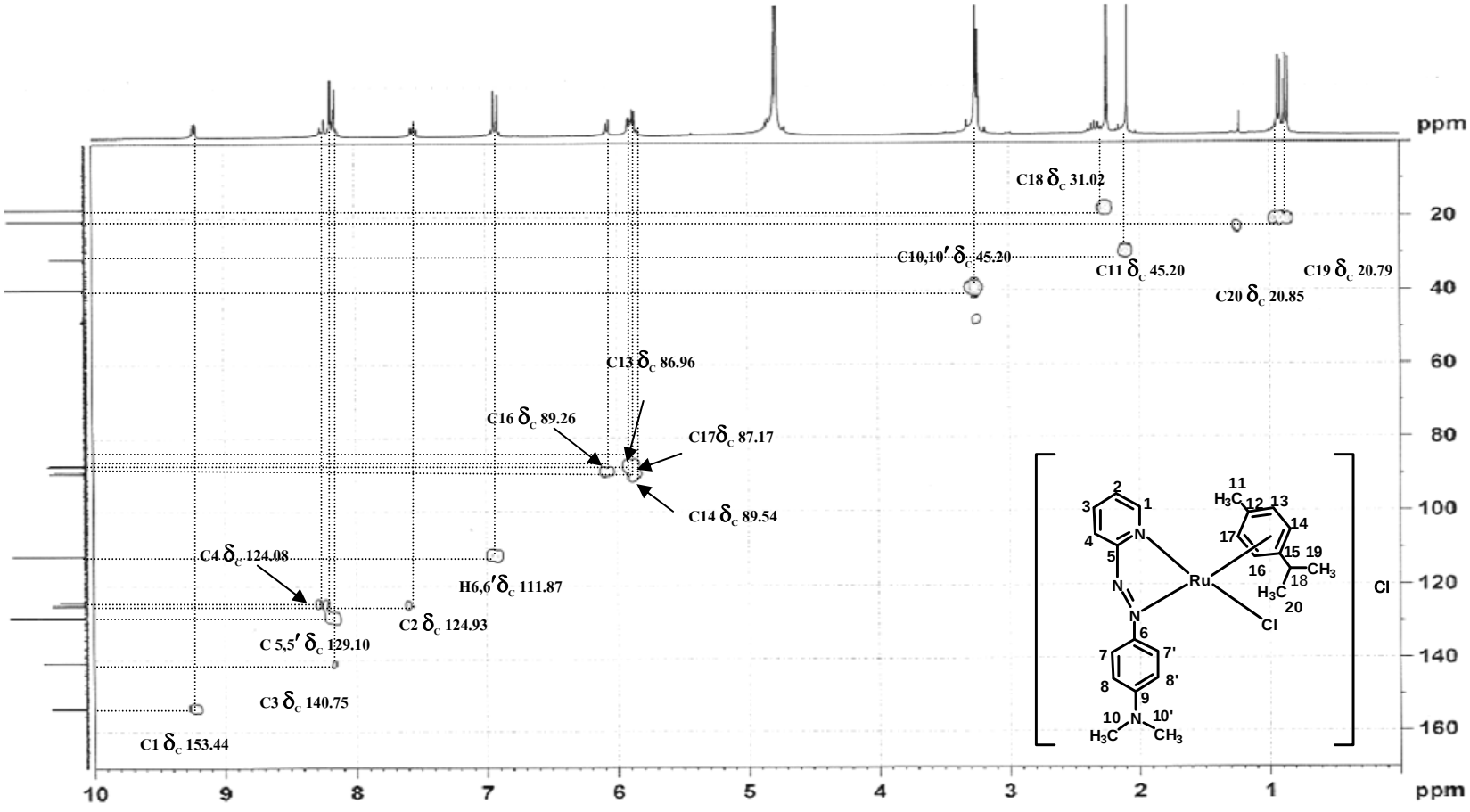

Figure 55 HMQC NMR spectrum of [Ru(dmazpy)(*p*-cymene)Cl]Cl in (methanol-d_4) (300 MHz)

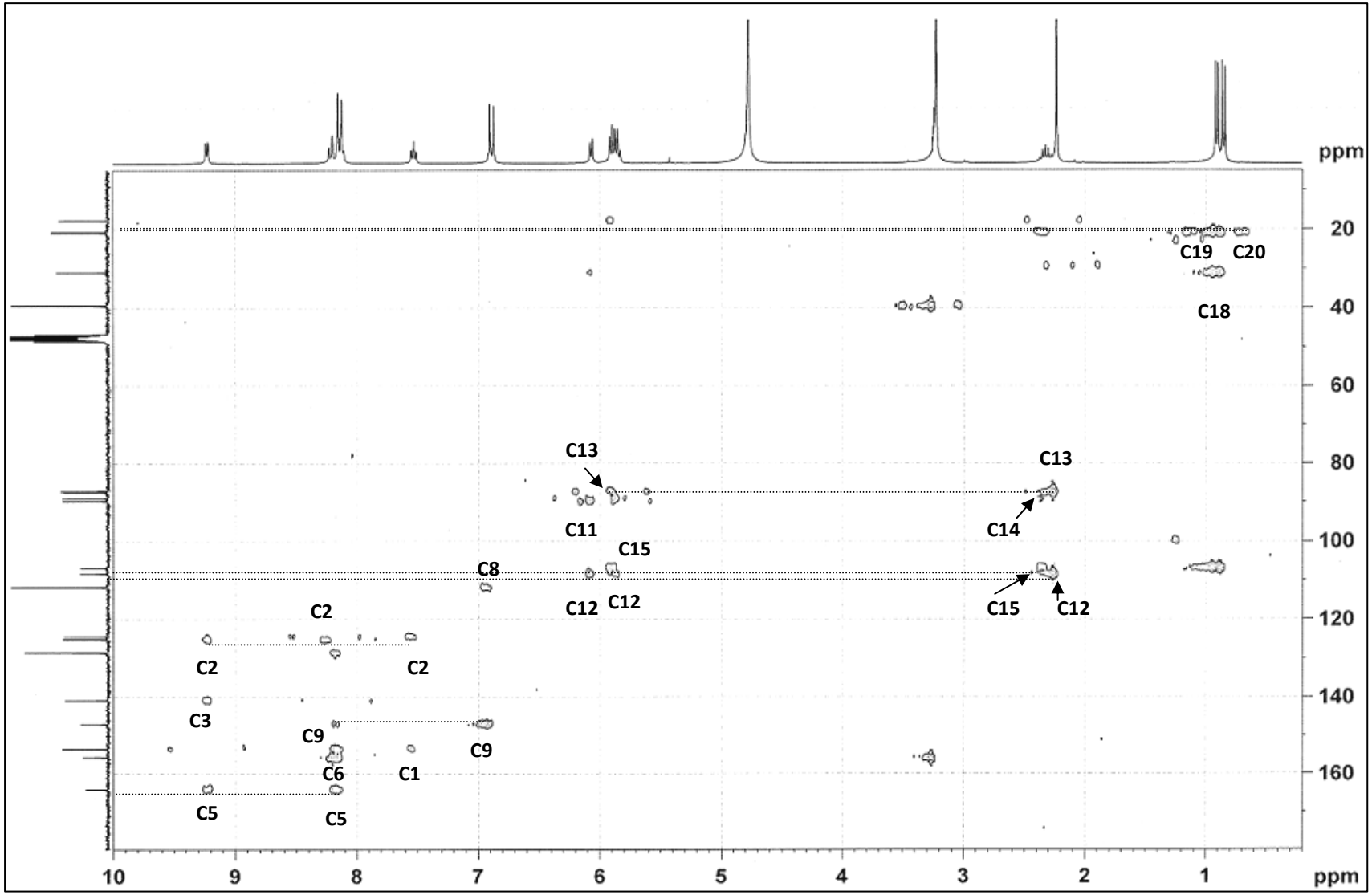

Figure 56 HMBC NMR spectrum of [Ru(dmazpy)(*p*-cymene)Cl]Cl in (methanol-d_4) (300 MHz)

3.3.2 Infrared spectroscopy

Infrared spectroscopy is a technique to study the functional groups of compounds. Infrared spectra were collected by using KBr pellets in the range of 4000-400 cm^{-1}. The important vibrational frequencies are C=C, C=N and N=N stretching modes and C-H bending in monosubstituted benzene**.** The infrared spectrum of [Ru(dmazpy)(*p*-cymene)Cl]Cl complex is shown in Figure 57 and summarized data was listed in Table 16.

Table 16. IR data of [Ru(dmazpy)(p-cymene)ClCl complex

Vibrational modes	**frequencies (cm^{-1})**
sp^2 C-H stretching	2967(s)
C=N stretching	1598(s)
C=C streching	1448(w)
N=N stretching	1294(s)
C-H bending of para disubstituted benzene	833(m), 526(m)

s = strong, m = medium w = weak

The infrared spectrum of [Ru(dmazpy)(*p*-cymene)ClCl complex shows the important peaks at 1598 cm^{-1} and 1448 cm^{-1}, corresponding to C= N and C= C stretching in the pyridine ring of the ligand, respectively. The sharp band at 1294 cm^{-1} is assigned to the N=N stretching. It has been found that the N=N stretching occurs at the lower frequency than that of the free ligand (1399(s)). It causes from the electron backbonding from Ru (II) to π^* orbital of ligand. Therefore the azo (N=N) bond order of the complex becomes weaker.

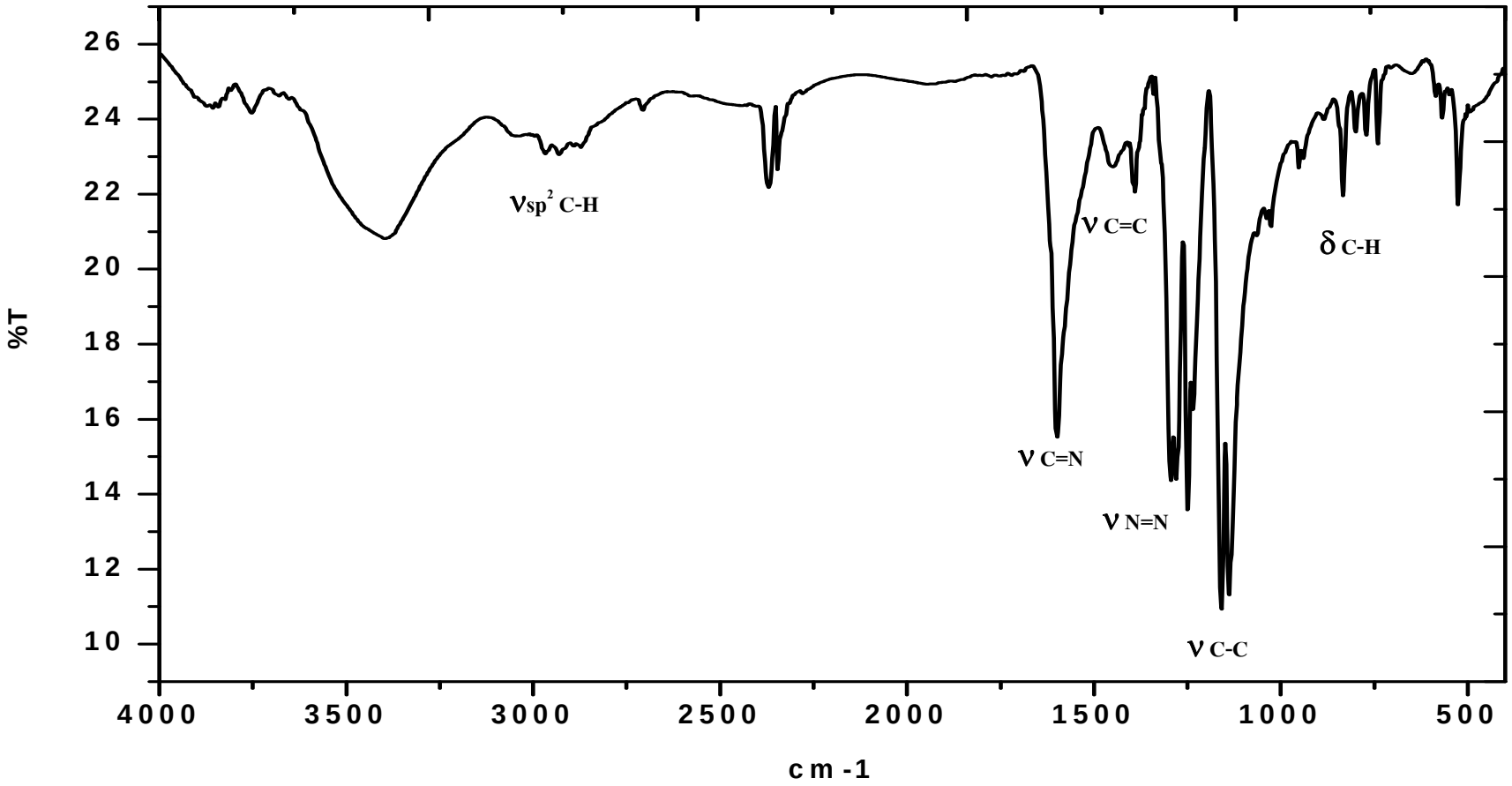

Figure 57 IR spectrum of [Ru(dmazpy)(*p*-cymene)Cl]Cl**.**

3.3.3 Elemental analysis

Elemental analysis is a technique to study the composition of elements in a compound. It is shown that the analytical data of the compounds correspond to the calculated values. The elemental analysis data are listed in Table 17.

Table 17. Elemental analysis data of [Ru(dmazpy)(*p*-cymene)Cl]Cl + $2H_2O$ complex

Mw of the $RuC_{23}H_{32}N_4O_2Cl_2$ = 568.24

investigate	% Element (SD)		
	%N	% C	% H
Calc.	9.58 (0.23)	48.57 (0.42)	5.63 (0.37)
Found	9.62 (0.11)	48.15 (0.49)	5.50 ($6.07x10^{-2}$)

Elemental analysis of C, N and H by theoretical calculations are compared with the experimental values. It has been found that the amount of carbon nitrogen and hydrogen are good agreement. The complex is moistured. Water is not completely eliminated. The best results of calculated values of existing 2 molecules of water agreement with the experimentally found comparison with other amount of water molecules as shown below

[Ru(dmazpy)(p-cymene)Cl]Cl Mw.= 532.24

% C = 51.89

% N = 10.53

% H = 5.26

[Ru(dmazpy)(p-cymene)Cl]Cl + H_2O Mw.= 550.24

%C = 50.20

%N = 10.18

%H = 5.45

[Ru(dmazpy)(p-cymene)Cl]Cl + $2H_2O$ Mw.= 568.24

%C = 48.57

%N = 9.85

%H = 5.63

[Ru(dmazpy)(p-cymene)Cl]Cl + $3H_2O$ Mw.= 586.24

%C = 47.12

%N = 9.55

%H = 5.79

3.3.4 Electrospray mass spectroscopy (ES-MS)

The ES mass spectrometry is a technique to study the mass of molecular ions of the studied compound. Mass spectrum of [Ru(dmazpy (*p*-cymene)Cl]Cl complex is shown in Figure 61 and the summarized data are listed in Table 18. The molecular weight of the [Ru(dmazpy)(*p*-cymene)Cl]Cl complex is 532.24 g/mol. The most intense peak is the m/z 497, which give 100% relative abundance. The molecular ion is assigned to $[Ru(dmazpy)(p\text{-cymene})Cl]^+$ caused by the lossing of Cl^- counter ion. Another intense peak is at m/z 499 which give 80% relative abundance is assigned to the molecular ion of $[Ru(dmazpy+2H^+)(p\text{-cymene})Cl]$ and the in tense peak at m/z 496 which give 70% relative abundance is assigned to the molecular ion of the $[Ru(dmazpy\text{-}H^+)(p\text{-cymene})Cl]$. The followings are the schemes of the fragmentation of (Ru(dmazpy))(*p*-cymene)Cl]Cl at different relative abundant percentages.

Table 18. Mass spectroscopic data of [Ru(dmazpy)(*p*-cymene)Cl]Cl (represented with M leter)

m/z	Stoichiometry	Equivalent species	Rel. abun
497.0	[Ru(dmazpy)(*p*-cymene)Cl]	M-Cl	100%
499.0	$[Ru(dmazpy+2H^+)(p\text{-cymene})Cl]$	$[M\text{-}Cl] + 2H^+$	80%
496.1	$[Rudmazpy\text{-}H^+)(p\text{-cymene})Cl]$	[M-H-Cl]	70%

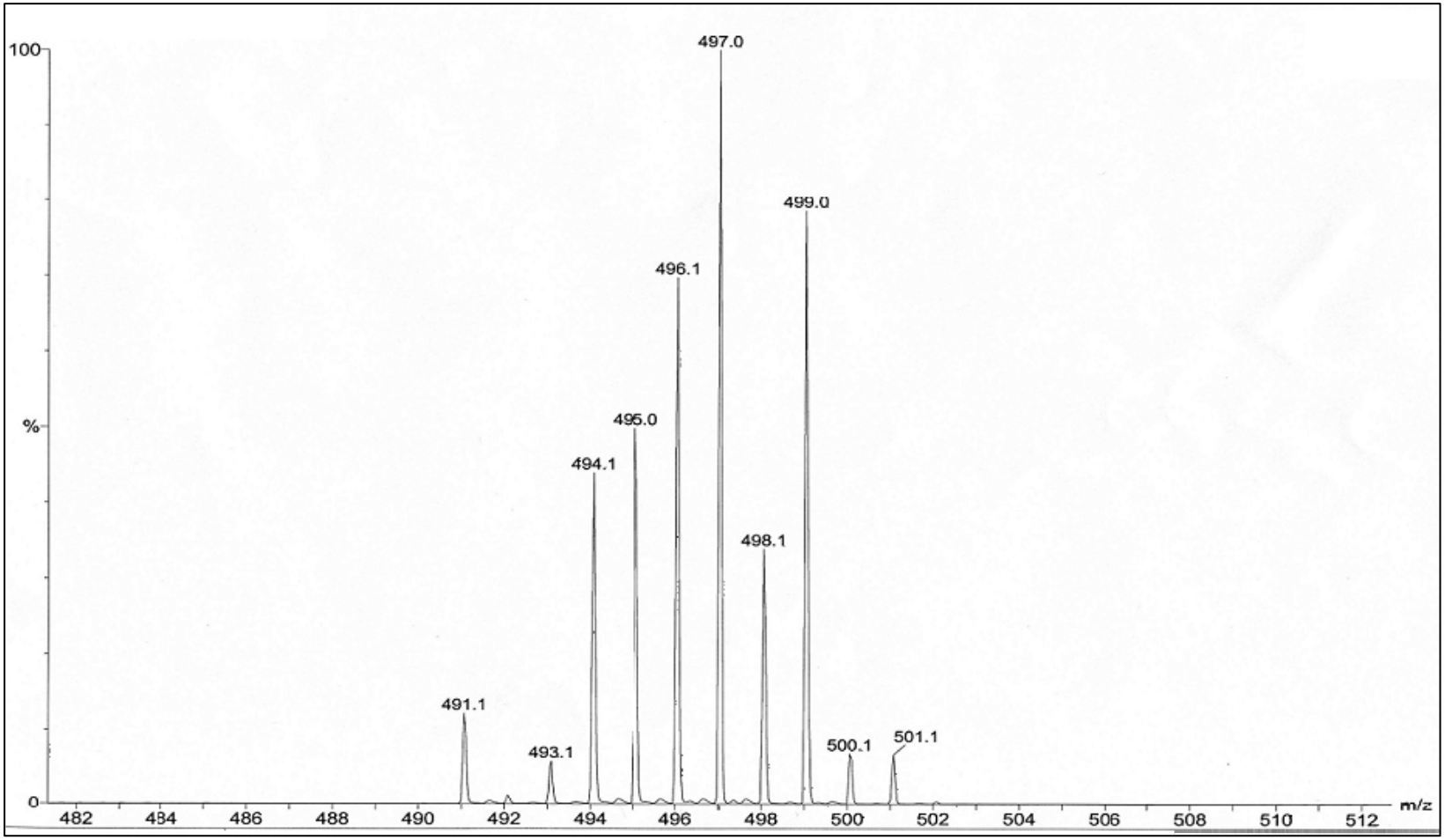

Figure 58 ES-MS spectrum of [Ru(dmazpy)(*p*-cymene)Cl]Cl.

3.3.5 UV- Visible absorption spectrophotometry

The electronic absorption spectrum of the [Ru(dmazpy)(*p*-cymene) Cl]Cl complex in acetonitrile solvent was recorded in the range of 200-800 nm. The absorption spectrum of the complex is shown in Figure 59. The absorption band in UV region is an intra ligand $\pi \rightarrow \pi^*$ allowed transition while the absorption band at λ_{max} 586 nm in visible region is assigned to metal to ligand charge transfer (MLCT). The complex is absorbed in range 580-620 nm light renders a substance blue. (Tawat *et al*., 2007)

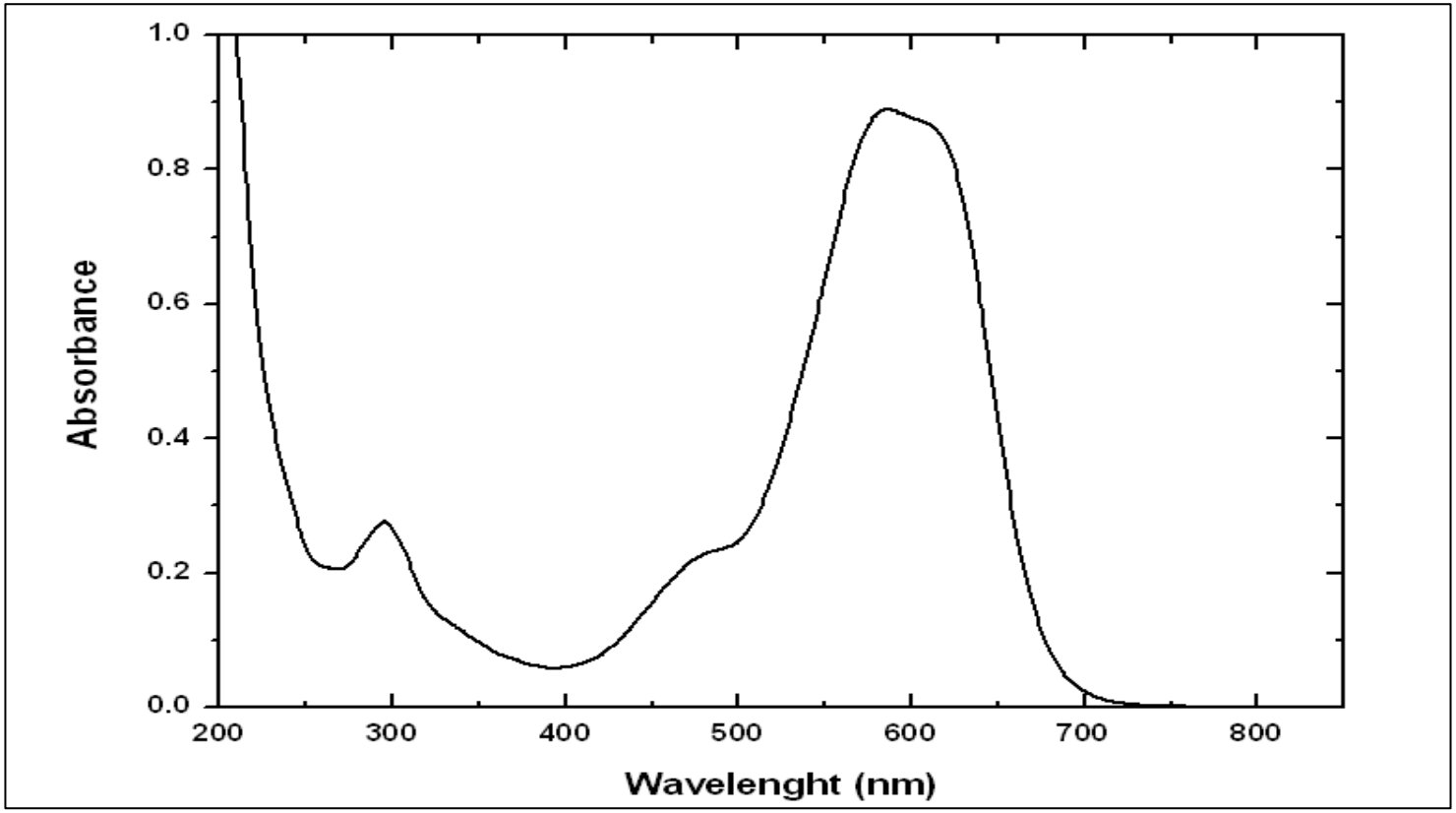

Figure 59 Absorption spectrum of $3x10^{-5}$ M [Ru(dmazpy)(*p*-cymene)Cl]Cl in CH_3CN.

3.3.6 Cyclic Voltammetry

The electrochemical activity of the [Ru(dmazpy)(*p*-cymene)Cl]Cl complex was studied by cyclic voltammetry at a glassy carbon working electrode. It was examined in acetonitrile using 0.1 M tetrabutylammonuim hexafluorophosphate (TBAH) as a supporting electrolyte. The cyclic voltammograms were mainly measured at the scan rate of 50 mVs^{-1}. Voltammetric data are given in Table 19 and the voltammograms are shown in Figure 63. At scan rate 50 mVs^{-1}, voltammogram shows four peaks, two peaks of these are in the reduction potential range (negative potential) and other are in the oxidation potential (positive potential). The potentials were compared with the potential of a ferrocene couple (ferrocene couple occur at 0.44 V vs SCE). (Ocakoglu *et al*., 2007)

Table 19. Cyclic voltammetric data of [Ru(dmazpy)(*p*-cymene)Cl]Cl in acetonitrile

compound	$E_{1/2}$ (V) (ΔE_p (V))			
	oxidation		reduction	
	I	II	I	II
complex	1.18 (0.35)	1.7 (0.15)	-0.46 (0.14)	-1.6

$E_{1/2}$ = $(Ep_a+Ep_c)/2$, where Ep_a and Ep_c are anodic and chathodic peak potentials, respectively; $\Delta Ep = Ep_a-Ep_c$;

Oxidation range

In the potential range 0 to -1.8 at scan rate 50 mV/s in acetonitrile, The voltammograms (Figure 64 and 65) show two quasi-reversible 0 to + 1.8 V. couple at $E_{1/2}$ = 1.70 V and 1.18 V which are assigned present tense to the redox of Ru^{2+}/Ru^{3+} and Ru^{3+}/Ru^{4+} respectively wich are related to the report of Shang (Shang *et al*., 2012)

reduction range

In the potential range 0 to -1.8 at scan rate 50 mV/s in acetonitrile. The complex shows one quasi-reversible couple at $E_{1/2}$ = -0.46 V and an irreversible peak at E_{pc} = -1.06 V. It is believed that there are the reduction peaks of azo moiety and and *p*-cymene, respectively (equation 3 >> and 4). It should be noted that azo function is able to accept electron better than that of arene group. That is why the potential of azo part is assigned at less negative potential.

$$\left[\text{-N=N-}\right] \underset{-e^-}{\overset{+e^-}{\rightleftharpoons}} \left[\text{-N ---- N}\right]^- \qquad \text{(eq.3)}$$

$$[\text{Ru(dmazpy)(}p\text{-cymene)Cl}]^+ \xrightarrow{+e^-} [\text{Ru(dmazpy)(}p\text{-cymene)Cl}] \qquad \text{(eq.4)}$$

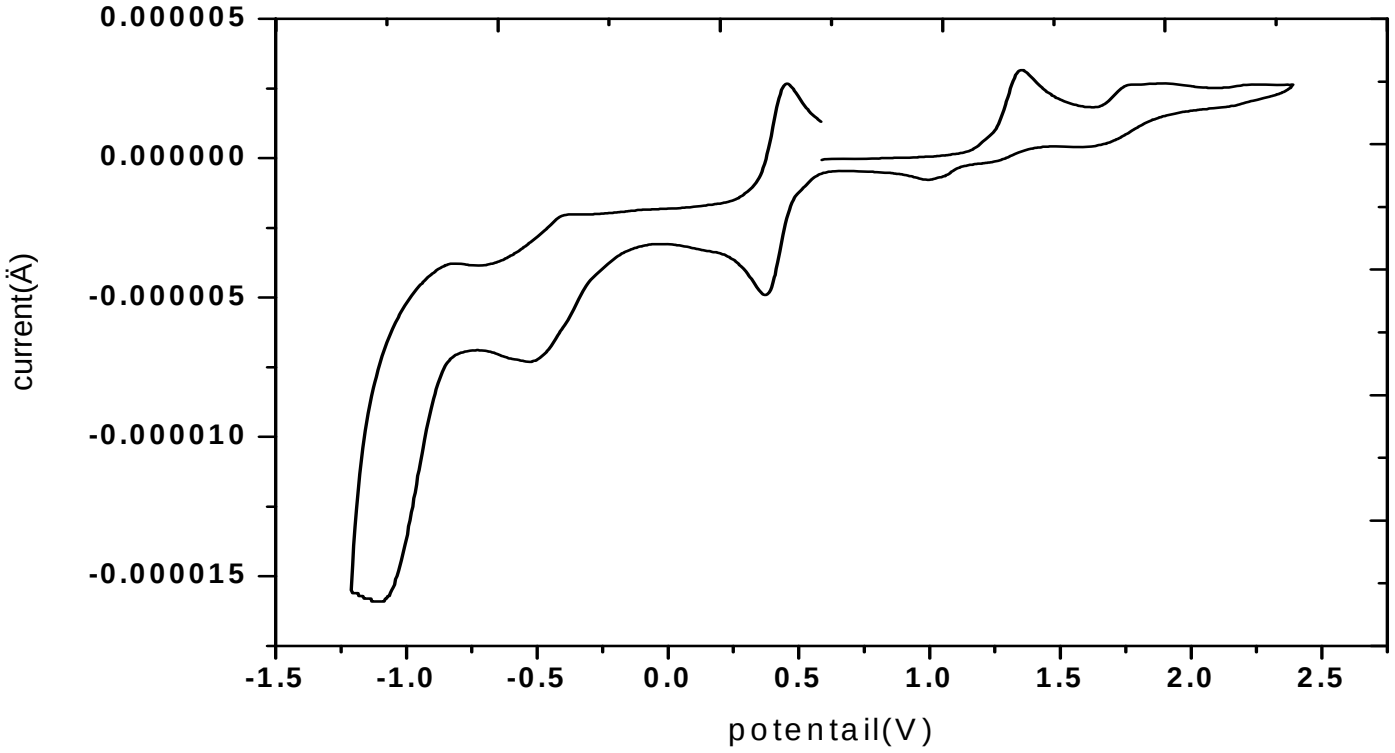

Figure 60 The cyclic voltammograms of [Ru(dmazpy)(*p*-cymene)Cl]Cl in CH_3CN.

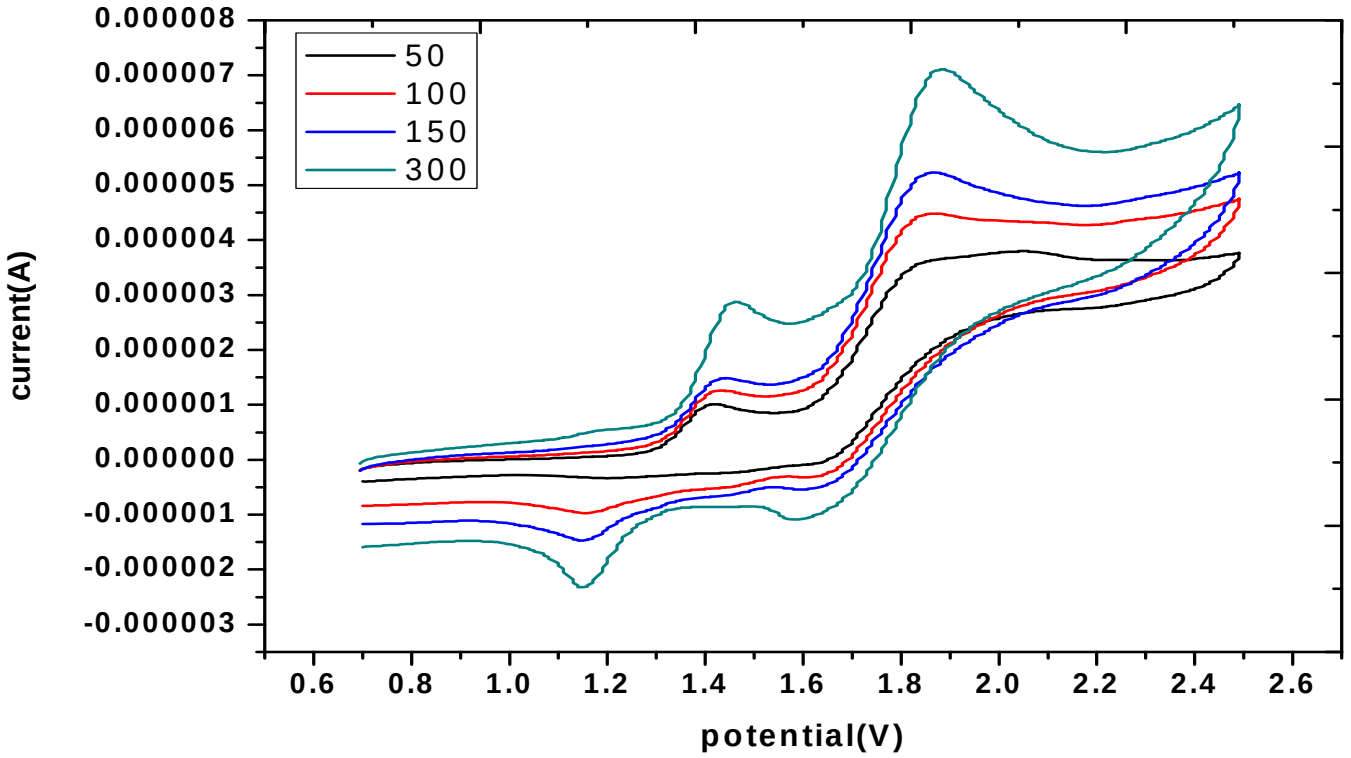

Figure 61 The oxidation cyclic voltammograms of [Ru(dmazpy)(*p*-cymene)Cl]Cl scanned with various scan rate (50, 100,150, 300, mV/s).

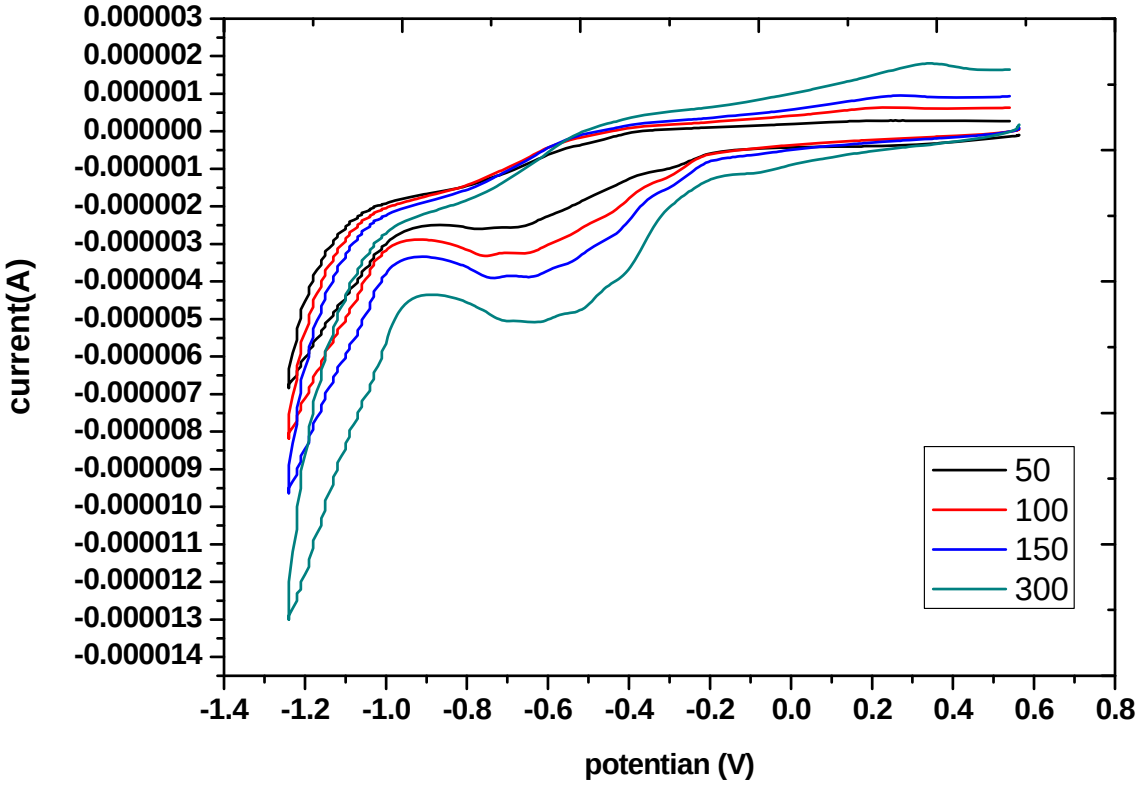

Figure 62 The reduction cyclic voltammograms of [Ru(dmazpy)(*p*-cymene)Cl]Cl scanned with various scan rate (50, 100,150, 300 mV/s).

3.4 Synthesis and characterization of [Ru(dmazpy)(dcbpyH$_2$)(NCS)$_2$]

The [Ru (dmazpy)(dcbpyH$_2$)(SCN)$_2$] complex was synthesized by 2 methods. Method 1: the synthesis pathway was improved from Song and coworker. (Song *et a*., 2009). One pot reaction was shown in Figure 66.

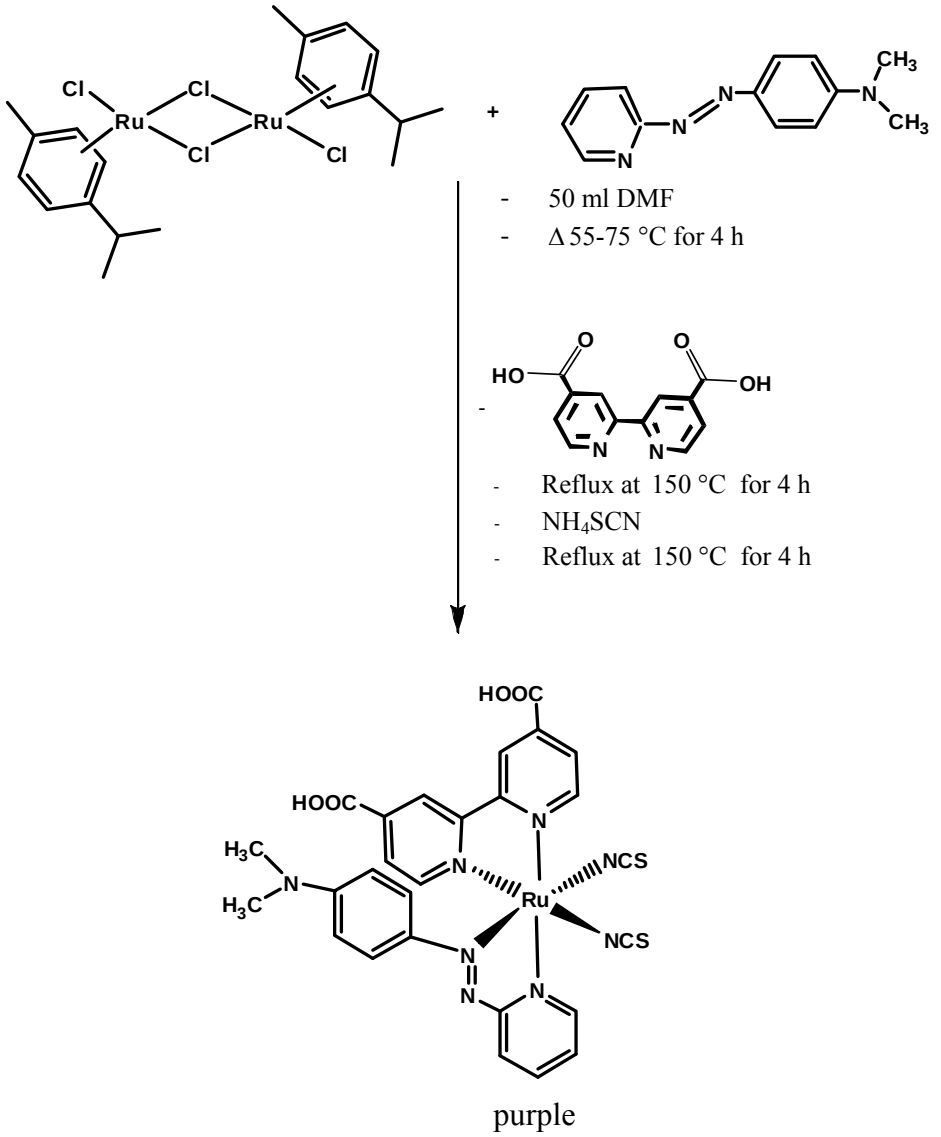

Figure 63 The synthesis pathway of the [Ru(dmazpy)(dcbH$_2$)(SCN)$_2$] complex.

According to one pot synthesis, The purple complex was obtained after the reaction completed. The synthesized complex was primarily tested by TLC. There are two spots with purple and reddish purple. The R_f values of each spot are 0.75 and 0.78, respectively. It is indicated that the complex has not yet been pure absolutely. The complex was purified by column chromatography on silica gel column which was eluted with methanol. The purple band and red purple band were continously eluted. Both bands of the complex were collected and evaporated. After washing the synthesized complex and let it dry at room temperature, the yield of purple complex is 20 mg (6.37%) and that of the reddish purple complex is 47 mg (15%). The complex structure was characterized by ^{1}H NMR spectroscopy. The ^{1}H NMR spectrum indicated that the synthesized complex is not pure. There existed both of water and impurity signals around 3-5 ppm. The resolution of the spectrum is certainly not clear.

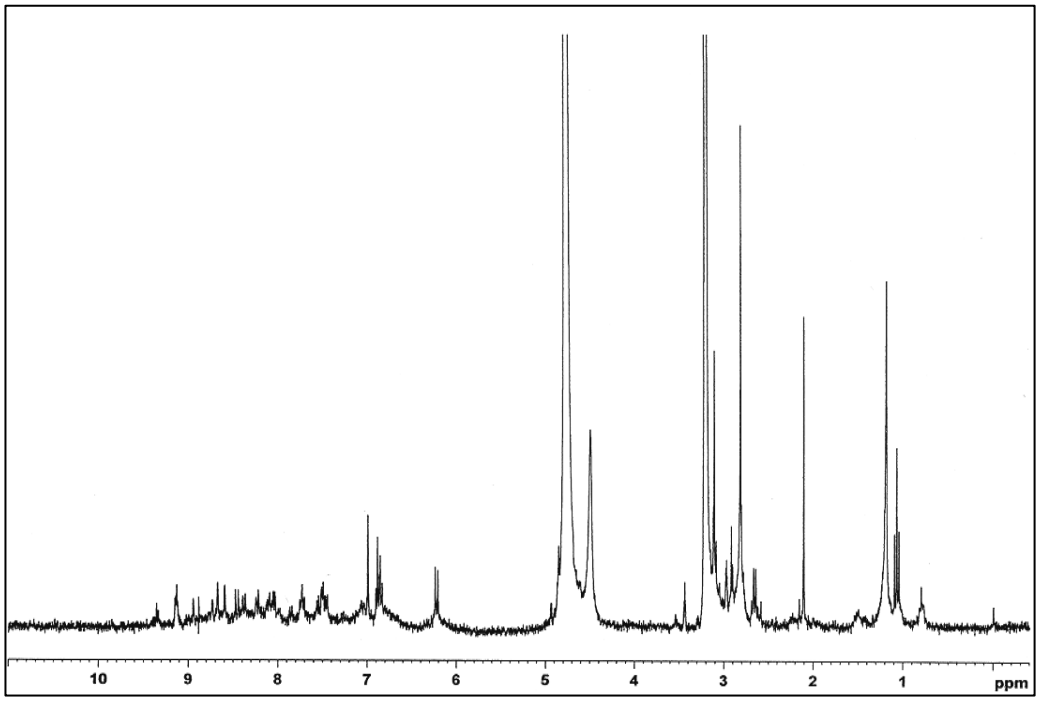

Figure 64 ^{1}H NMR spectrum of [Ru(dmazpy)(dcbpyH$_2$)(NCS)$_2$] in MD$_3$DO-d_6

Then the complex was further purified by column chromatography on LH-20 sephadex column which was eluted with methanol for six times. Many colored bands like pale purple, Bluish-purple and deep purple bands were collected from the purification. The structure of complex was again characterized by ^{1}H NMR spectroscopy. The purple band was the predominant fraction. However, after it was characterized by ^{1}H-NMR spectroscopy, it was found that the obtained complex is still not pure. Since, the intense signal of H_2O the other signals. The second ^{1}H NMR spectrum was compared with the first spectrum. It is found that the second spectrum shows better clear signals in the aromatic region (6-10 ppm). However, the signal of alkyl region (4-2 ppm) are hindered mainly by H_2O signal. The ^{1}H-NMR result is shown in Figure 65.

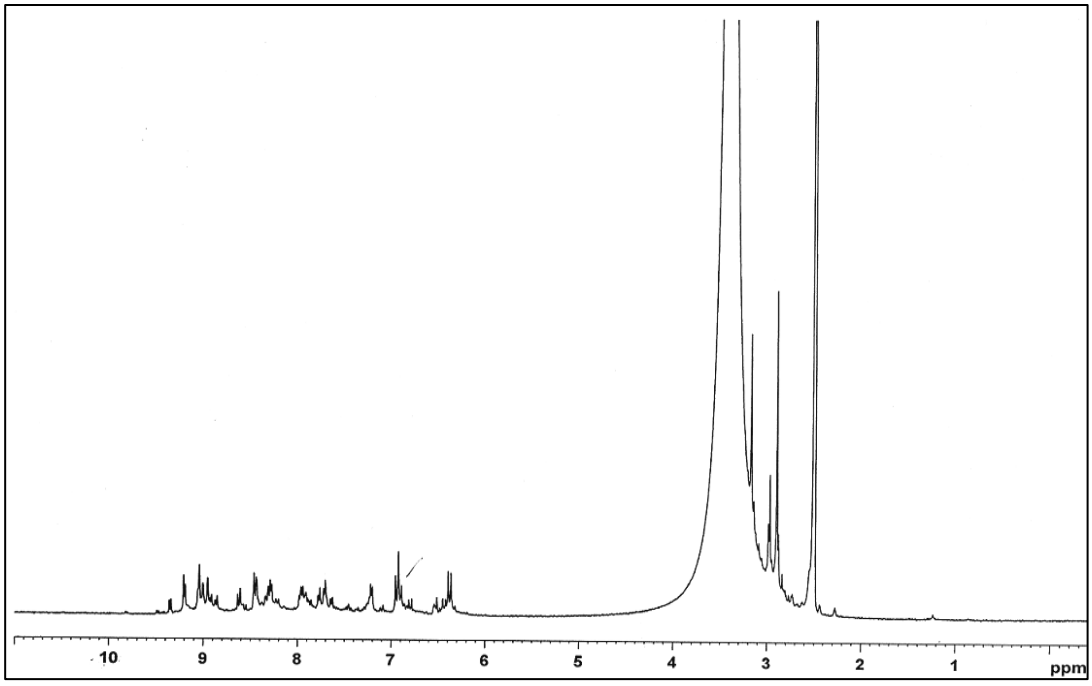

Figure 65 ^{1}H NMR spectrum of [Ru(dmazpy)(dcbpyH_2)$(NCS)_2$] in DMSO-d_6

Afterward the complex was measured FTIR spectrum for determining the difference between the synthesized complex and the free ligand. The functional group of the complex was confirmed by FTIR technique which shown in the Figure 66.

The IR spectrum of the complex gives the important vibrational modes of νN=N of the dmazpy ligand appears at 1386 cm^{-1}, νC-O of the $dcbpyH_2$ ligand occurs at 1594 cm^{-1} and νC=N of NCS ligand is at 2109 cm^{-1}. These vibrational frequencies occur at different frequencies compared with free dmazpy and $dcbH_2$ ligands as shown in the Table 3. Therefore it is believed that the complex was formed.

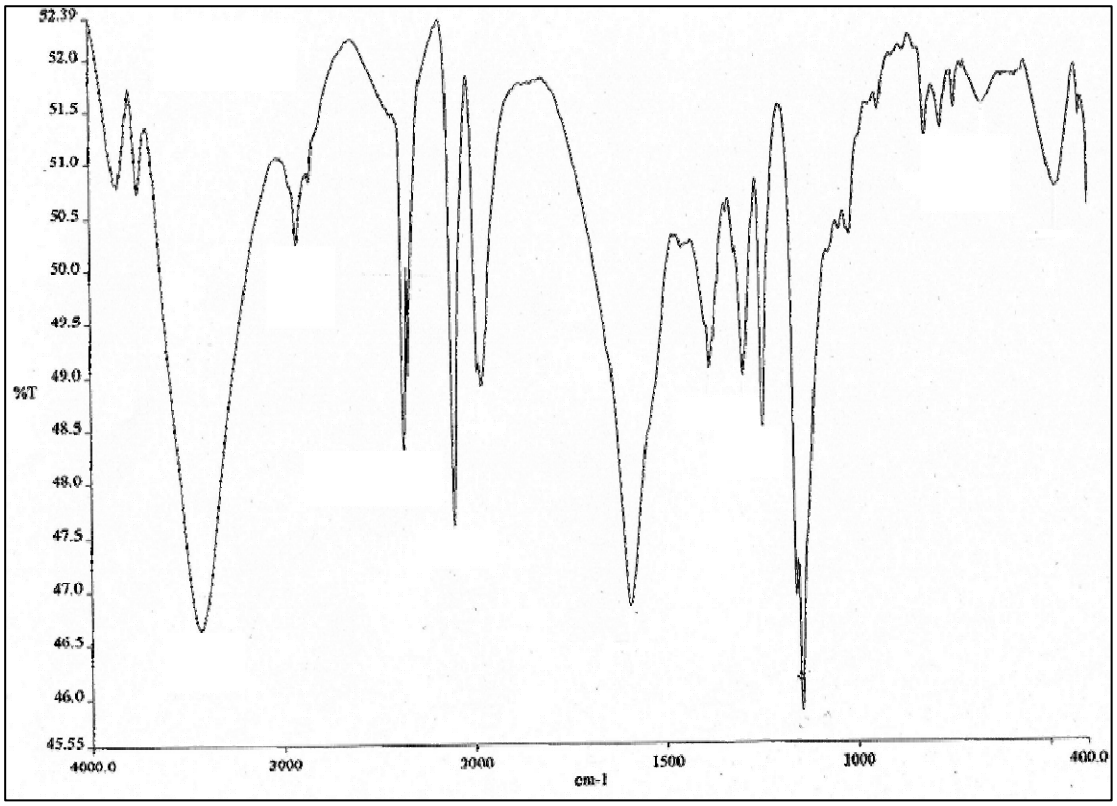

Figure 69 IR spectrum of $[Ru(dmazpy)(dcbpyH_2)(NCS)_2]$

For the photo-physical property, the absorption spectrum of complex in methanol is shown in Figure 70. The lowest metal-to-ligand charge transfer (MLCT) from d-π^* absorption band is at 520 nm (ε = 16825 $M^{-1}cm^{-1}$) and 640 nm (ε =6600 $M^{-1}cm^{-1}$) being as a shoulder band. While the absorption band at 294 nm is assigned to be an intra ligand π-π^* transition of dmazpy.

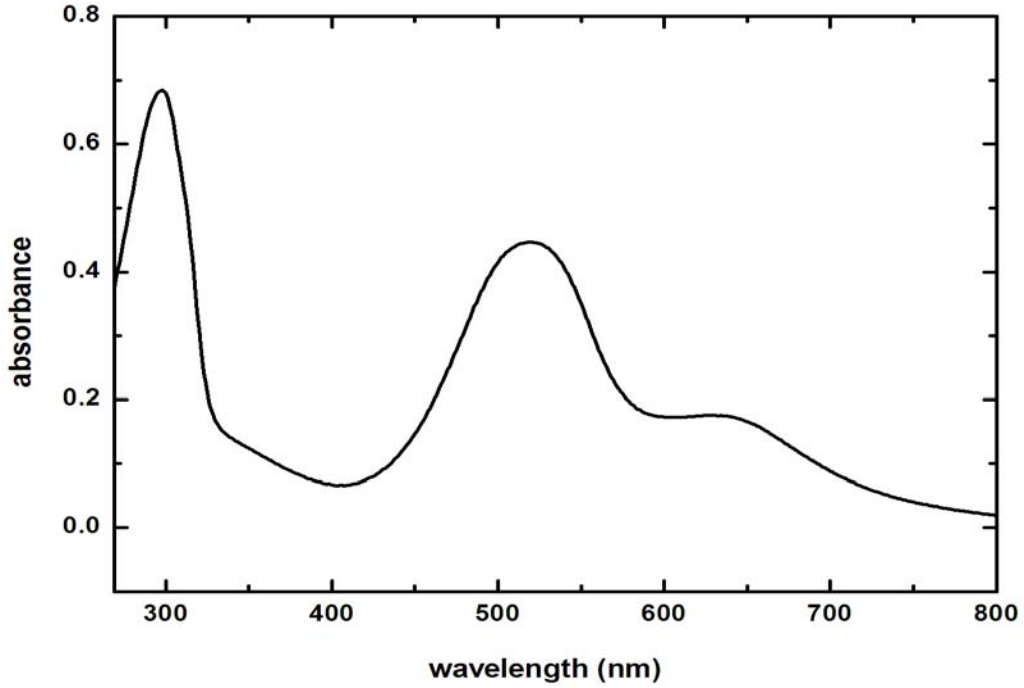

Figure 67 UV-Vis absorption spectrum of [Ru(dmazpy)(dcbpyH_2)$(NCS)_2$] in $3x10^{-4}$ CH_3OH.

The second process of the synthesis of the [Ru(dmazpy)(dcbpyH_2)$(NCS)_2$] complex was improved from Sahin method by using [Ru(dmazpy)(p-cymene)Cl]Cl precursor (Sahin *et al*., 2010). The reaction pathway was shown in Figure 68.

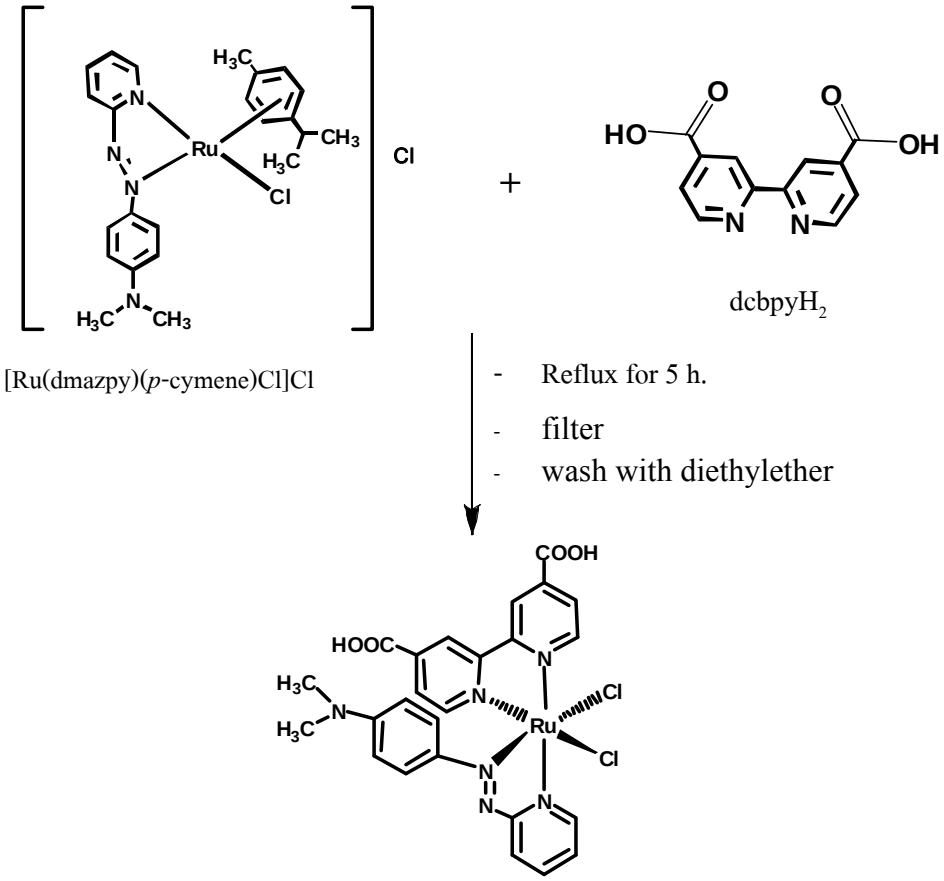

[Ru(dmazpy)(dcbpyH$_2$)Cl$_2$]

Figure 68 The reactions of the [Ru(dmazpy)(dcbpyH$_2$)Cl$_2$] complex.

After the reaction completed, the purple synthesized complex was obtained and it was primary tested by TLC. It shows only one spot with R_f =0.77. Anyway, the ^{1}H NMR result suggested that the structure of synthesized complex was not pure definitely. The complex was purified by column chromatography on LH-20 sephadex column for 3 times which was eluted with methanol. Two colored bands of pale purple, and deep purple were collected from the purification. The purple band was the predominant fraction. However, after it was characterized by ^{1}H-NMR spectroscopy, it was found that the obtained complex is still not pure (Figure 69). One can see that H_2O signal around 2-3 ppm was appeared and hindering, other signals of alkyl group. It has been tried to get rid of the water by adding Na_2SO_4 before measuring ^{1}H NMR. The ^{1}H NMR spectrum shows that the signals of the synthesized complex gets better resolution (Figure 70) but there are still some unexpected signals in the range of 3-4 ppm. Besides, many ^{1}H signals of aromatic region (6-10 ppm) disappeared. It can be discussed that the tested compound might be consisting of our

expected [Ru(dcbpyH$_2$)(dmazpy)(Cl$_2$)] complex and other complexes which are possible either *bis* complex of [Ru(dmazpy)$_2$Cl$_2$] or somethingeles. There might cause from two factors which are:

1. the dcbpyH$_2$ does not coordinate with Ru(II) but dmazpy, a stronger coordinating ligand like dmazpy, is probably replacing instead of dcbpyH$_2$. It yields the *bis* complex in *cis*-form dcbpyH$_2$ of [Ru(dmazpy)$_2$Cl$_2$].

2. The [Ru(dcbpyH$_2$)(dmazpy)(Cl$_2$)] is not stable. It might be changed to other complexes which is unpredictable.

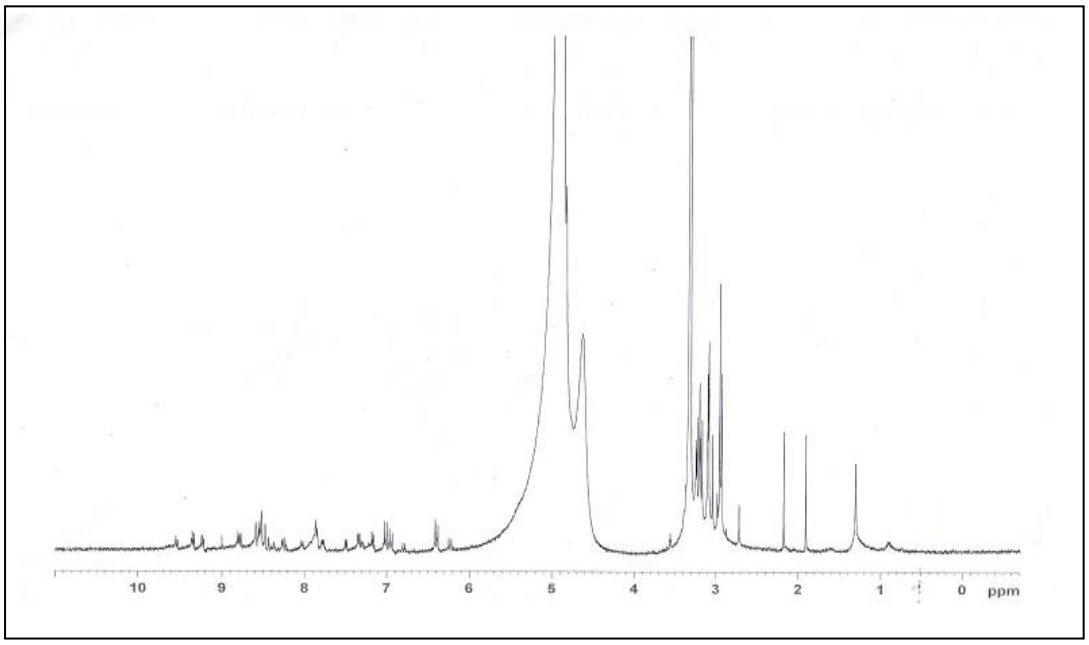

Figure 69 ^{1}H NMR spectrum of the second method of [Ru(dmazpy) (dcbpyH$_2$)(NCS)$_2$] in DMSO-d_6

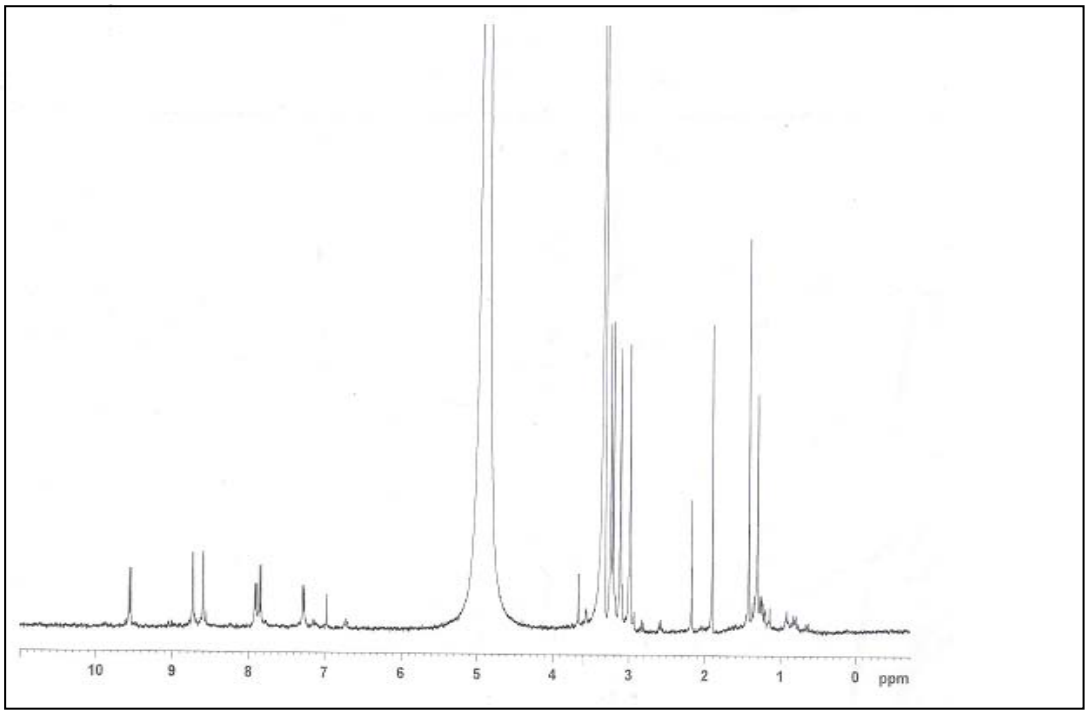

Figure 70 ^{1}H NMR spectrum of futher purify of [Ru(dmazpy)(dcbpyH$_2$)(NCS)$_2$] in DMSO-d_6

However, after measuring the synthesized compound with, the electrospray mass spectrometry which is a technique to confirm the molecular mass of complex. It has been found that the [Ru(dmazpy)(dcbpyH$_2$)Cl$_2$] was certainly obtained. The molecular ions with some fragmentations are corresponding to the molecular weight of the compound. Mass spectrum of [Ru(dmazpy)(dcbpyH$_2$)Cl$_2$] complex is shown in Figure 71. The molecular weight of the [Ru(dmazpy)(dcbpyH$_2$)Cl$_2$] complex is 642.28 g/mol. The most intense peak is at m/z 607.1, which gives 100% relative abundance. The molecular ion is assigned to [Ru(dmazpy)(dcbpyH$_2$)Cl]$^+$ caused by the lossing of Cl$^-$ ion. Another intense peak is at m/z 609.1 which give 60% relative abundance is assigned to the molecular ion of [Ru(dmazpy+2H$^+$)(dcbpyH$_2$)Cl]. The intense peak at m/z 606.1 which give 50% relative abundance is assigned to the molecular ion of the [Ru(dmazpy-H$^+$)(dcbpyH$_2$)Cl]. The summarized data are listed in Table 20. Nevertheless, there exists a tiny impurity at m/z 729 (less than 5% Rel.Abund) which is an unidentified signal.

Table 20. Mass spectroscopic data of [Ru(dmazpy)(dcbpyH$_2$)Cl$_2$] (represented as M)

m/z	Stoichiometry	Equivalent species	Rel. abund
607.1	[Ru(dmazpy)(dcbpyH$_2$)Cl]$^+$	M-Cl	100%
499.0	[Ru(dmazpy+2H$^+$)(dcbpyH$_2$)Cl]	[M-Cl] + 2H$^+$	60%
496.1	[Ru(dmazpy-H$^+$)(dcbpyH$_2$)Cl]	[M-H-Cl]	50%

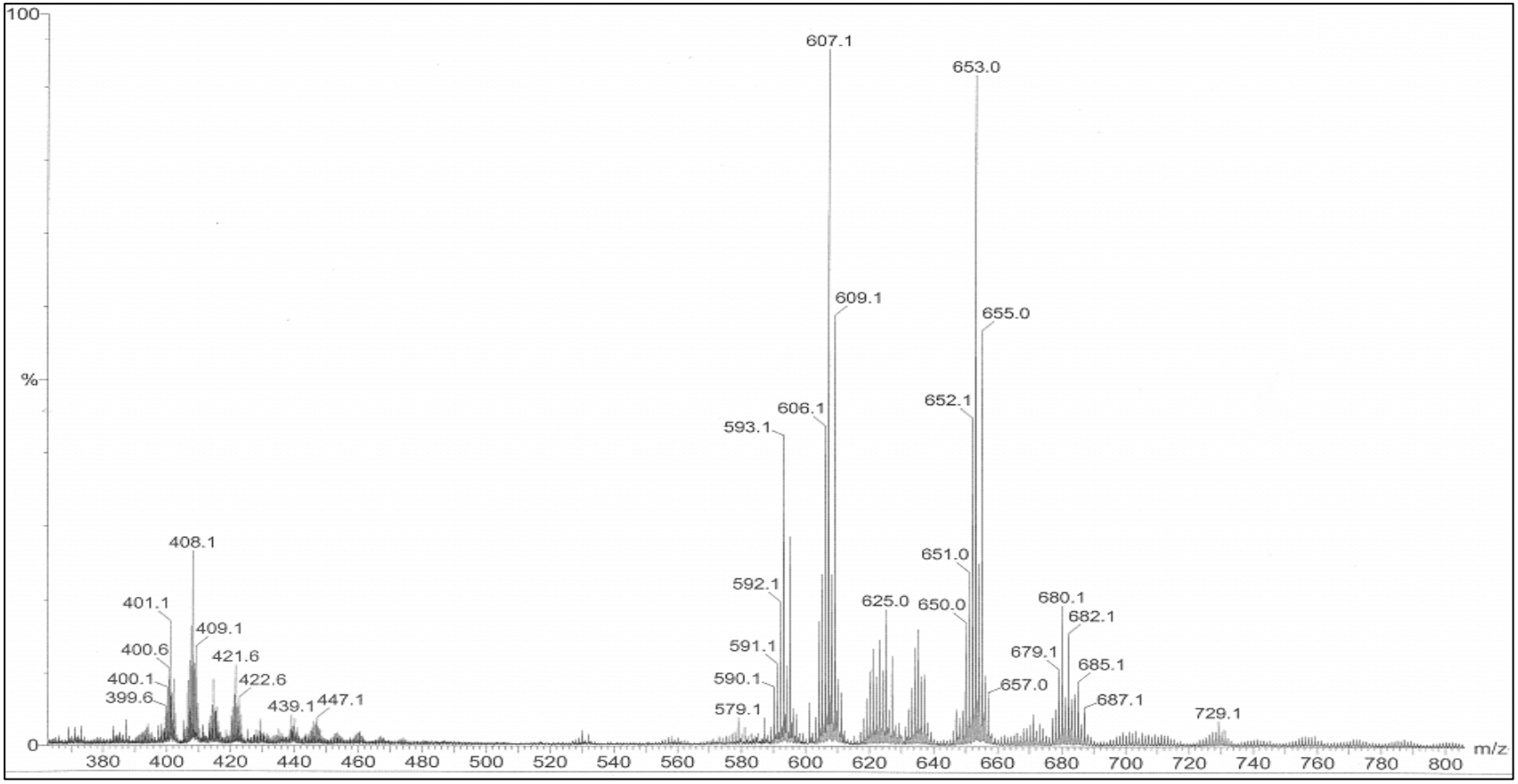

Figure 71 ES-MS spectrum of [Ru(dmazpy)(dcbpyH$_2$)Cl$_2$].

3.5 Synthesis and characterization of $[Ru(dcbpyH_2)_2(dmazpy)](PF_6)_2$

In a typical one-pot synthesis, $RuCl_3.3H_2O$ (0.16 mmol, 0.042 g) was dissolved in DMF (50 mL) and synthesized dmazpy ligand (0.16 mmol, 0.04 g) was added. The reaction mixture was heated at 55-56 ºC under argon for 4 h and then $dcbpyH_2$ (0.032 mmol, 0.08 g) was added. The reaction mixture was refluxed at 155-156 ºC for another 4 h. Excess TBHAP was added to the reaction mixture and heated at 155-156 ºC for 1.5 h. After the reaction, the mixture was then collected on a sintered-glass crucible by suction filtration, washed with acetone and dried in air. The reaction pathway is shown in Figure 72.

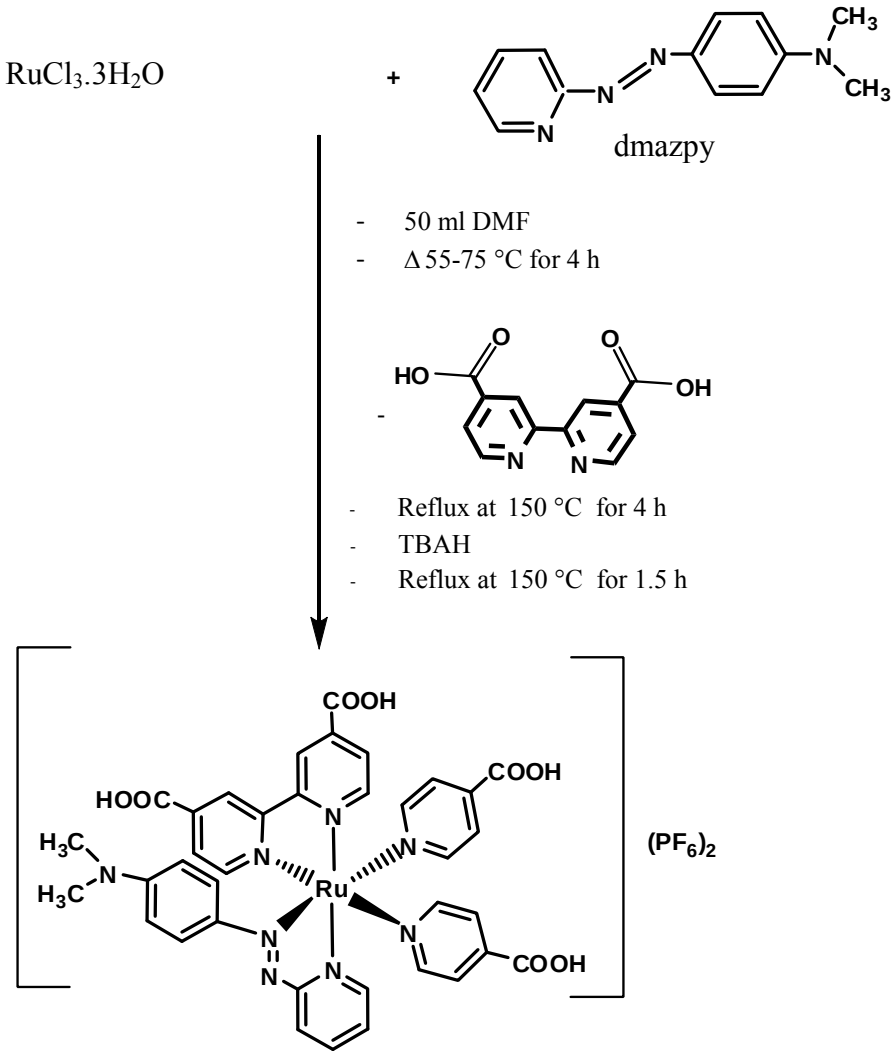

$[Ru(dcbpyH_2)_2(dmazpy)]\ (PF_6]_2$

Figure 72 The reactions of the synthesis of $[Ru(dcbpyH_2)_2(dmazpy)(PF_6)_2$

Characterization of $[Ru(dcbpyH_2)_2(dmazpy)](PF_6)_2$

^{1}H-NMR data were collected in DMSO solvent. The ^{1}H NMR result suggested that the structure of synthesized complex was not pure absolutely. From the structure, the ^{1}H-NMR should exist for 15 signals. However, the measured spectrum showed more signals than expected. There are some signals from impurity occurred at 1-3 ppm..

The $[Ru(dcbpyH_2)_2(dmazpy)](PF_6)_2$ complex was purified by column chromatography on sephadex LH-20 column for 6 times by using methanol as an eluent. The synthesized complex was still not pure completely as recognized from ^{1}H-NMR spectrum in Figure 73. It is because of the carboxylic (-COOH) group in the structure of the complex are quite sensitive to moisture in the air. Beside, it is possible that there are the mixture of the another unexpected complex, $[Ru(dmazpy)_2(dcbpyH_2)]^{2+}$, might be formed because the dmazpy is stroger than the $dcbpyH_2$ ligand. Both isomers are probably not be able to separate from each other by column chromatography.

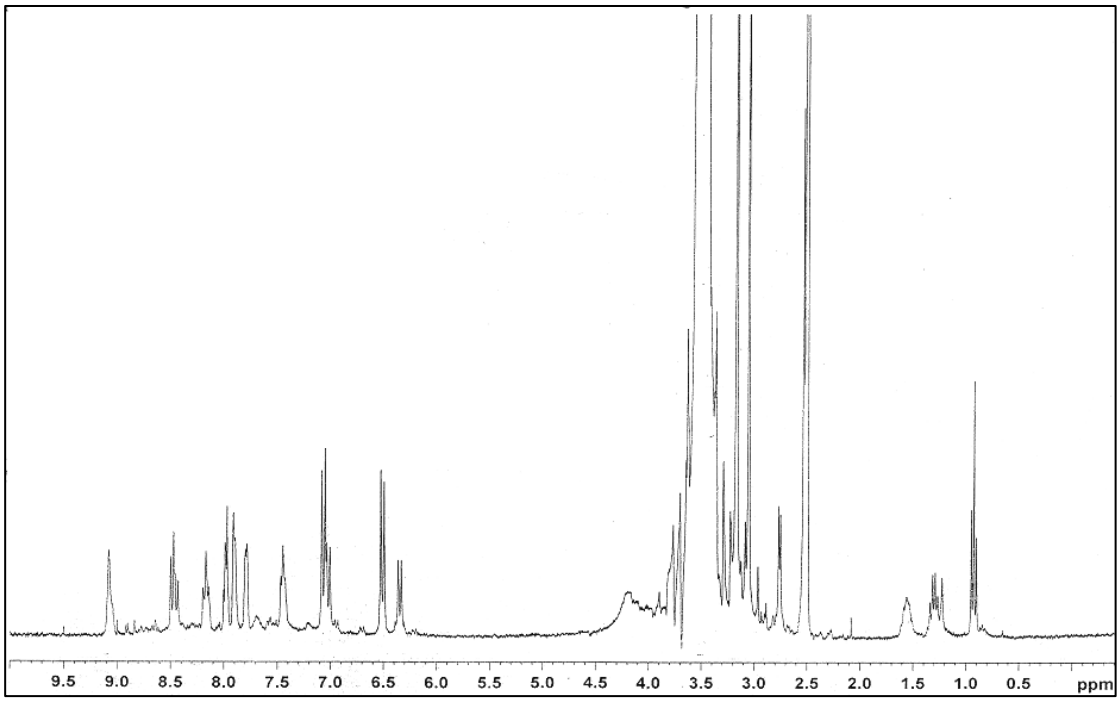

Figure 73 The ^{1}H-NMR spectrum of $[Ru(dcbpyH_2)_2(dmazpy)](PF_6)_2$ in DMSO-d_6

In order to characterize the structure by another technique, IR spectrum was obtained. Infrared spectrum of $[Ru(dcbpyH_2)_2(dmazpy)](PF_6)_2$ was recorded in the range of 4000-400 cm^{-1}. Some important vibrational peaks of the complex were collected in the Table 21.

Table 21. Characteristic peaks of $[Ru(dcbpyH_2)_2(dmazpy)](PF_6)_2$ obtained from the IR spectrum

Vibration mode	**Frequencies (cm^{-1})**
O-H stretching	3422(s, b)
C=O stretching	~1719(s)
N=N stretching	1370(s)
C-O stretching	1291(s)
C-H bending of para disubstituted benzene	766(m)

The Infrared (IR) spectrometric result supports the structure of synthesized complex. It has been found that the N=N stretching occurs at the lower frequency than that of the free ligand (1399(s)), It is due to the electron backbonding from d^6 (RuII) to ligand's π^* orbital of azo moiety giving weaker N=N bond. the azo (N=N) bond order of the complex becomes less. The O-H and C=O stretching modes confirm of the existing of $dcbpyH_2$ ligand in the synthesized complex. The spectrum of $[Ru(dcbpyH_2)_2(dmazpy)](PF_6)_2$ is shown in Figure 74.

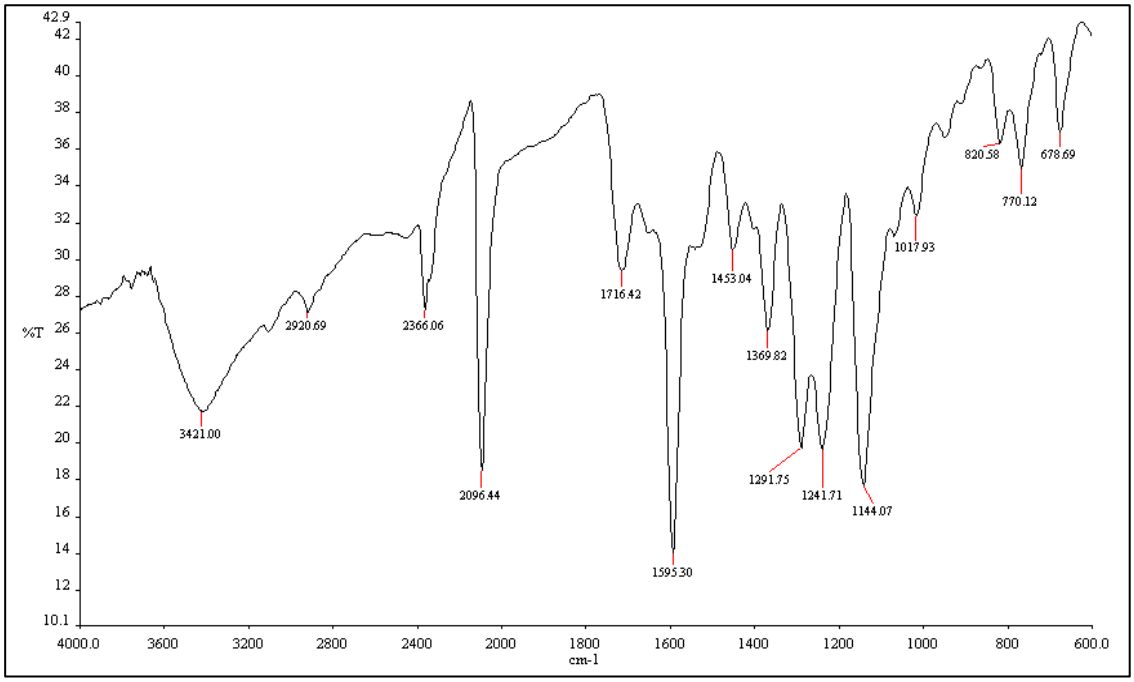

Figure 74 The spectrum of $[Ru(dcbpyH_2)_2(dmazpy)](PF_6)_2$

The electrospray mass spectrum of, $[Ru(dcbpyH_2)_2(dmazpy)](PF_6)_2$ complex is shown in Figure 76. The molecular weight of the $[Ru(dcbpyH_2)_2(dmazpy)](PF_6)_2$ complex is 1,105.4 g/mol. The result from mass spectrum does not show the molecular ions related to the expected complex. Expected fragmentation pathway is shown in scheme 1.

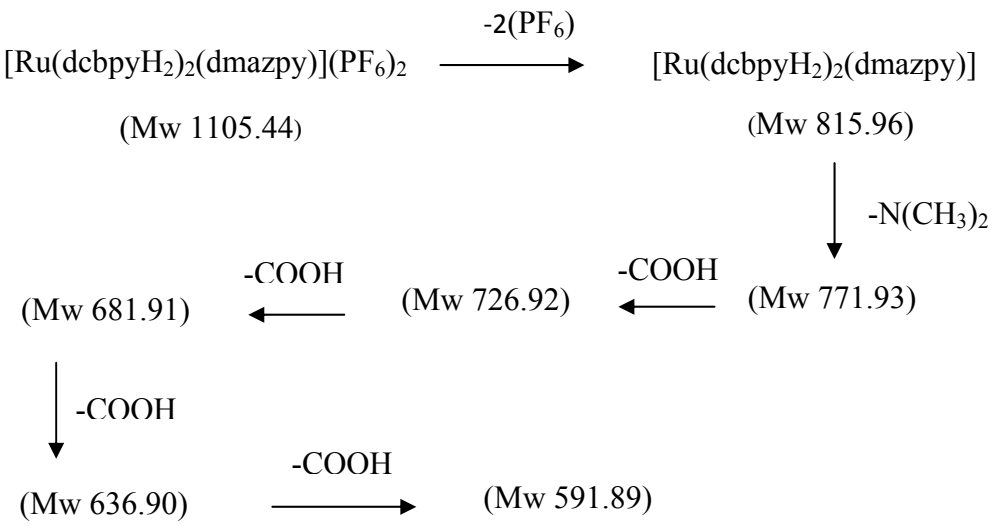

Scheme 1 Expected fragmentation pathway of $[Ru(dcbpyH_2)_2(dmazpy)](PF_6)_2$ for ES-MS

From the obtained spectrum, it is possible that the synthesized complex is $[Ru(dmazpy)_2(dcbpyH_2)](PF_6)_2$ instead of $[Ru(dcbpyH_2)_2(dmazpy)](PF_6)_2$ complex. The m/z 629.1 is correspondind to the molecular ion of $[Ru(dmazpy)_2.2H]^{++}$ species. The most intense peak is the m/z 291.2, which give 70% relative abundance. The molecular ion is assigned to $(PF_6)_2+2H^+$. Another intense peak is at m/z 305.2 which give 35% relative abundance is assigned to the molecular ion of $[(dcbpyH_2)\text{-}4COOH\text{-}3H^+]$ and the in tense peak at m/z 308.2 which give 20% relative abundance is assigned to the molecular ion of the $[(dcbpyH_2)\text{-}4COOH]$. The summarized data are listed in Table 22.

Table 22. Mass spectroscopic data of $[Ru(dcbpyH_2)_2(dmazpy)](PF_6)_2$

m/z	Stoichiometry	Rel. abun
291.2	$(PF_6)_2+2H^+$	70%
305.2	$[(dcbpyH_2)\text{-}4COOH\text{-}3H^+]$	35%
308.2	$[(dcbpyH_2)\text{-}4COOH]$	20%

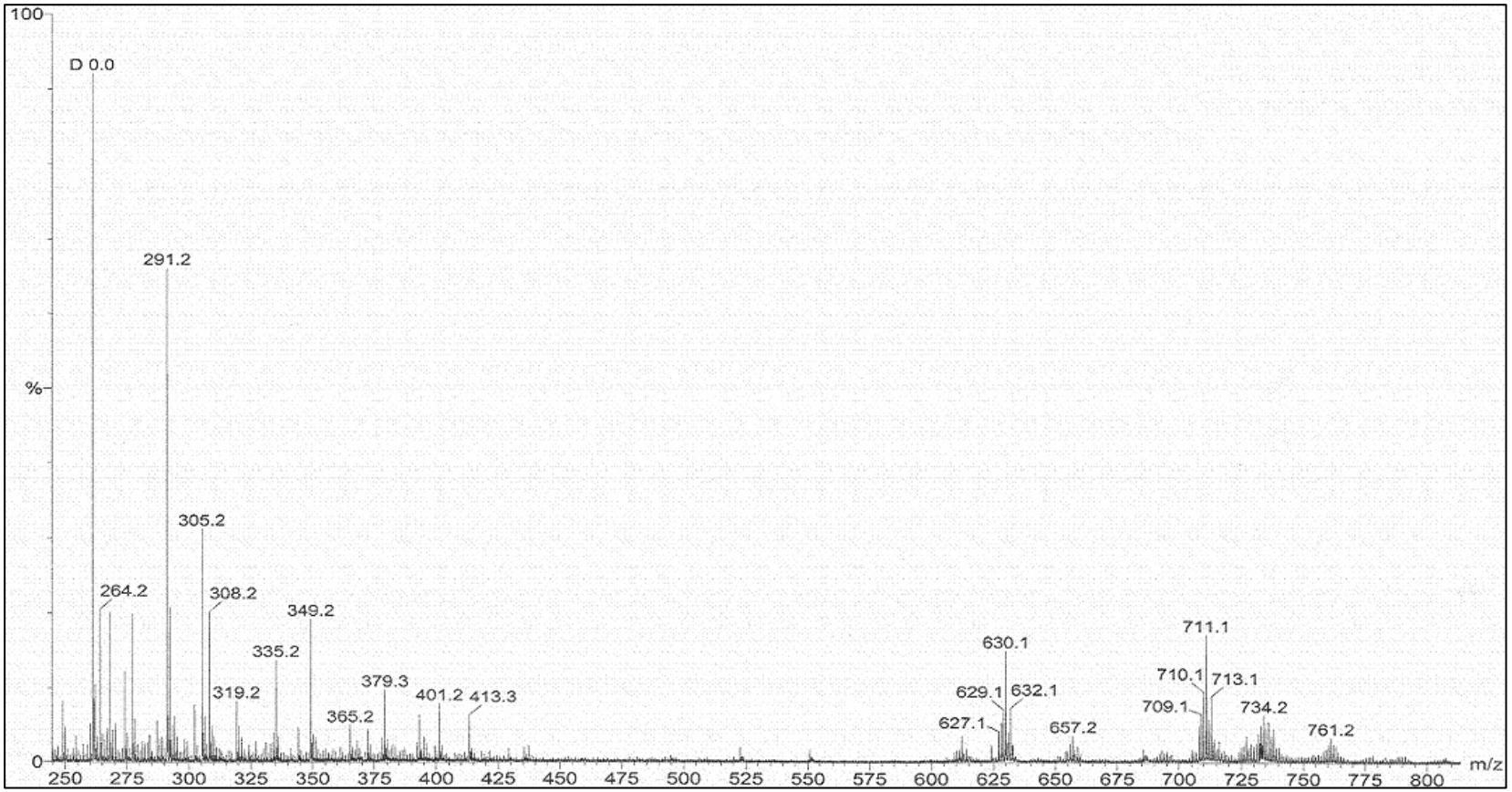

Figure 76 ES-MS spectrum of $[Ru(dcbpyH_2)_2(dmazpy)](PF_6)_2$.

CHAPTER 4
CONLUSION

The azoimine functionalized ligand 2-(4′-*N*,*N*-dimethylamino phenylazo) pyridine (dmazpy) can react with Zn(II) and Ru (II) generating the Zn(dmazpy)Cl_2 and [Ru (*p*-cymene)(dmazpy)Cl]Cl complexes. The Zn(II) complex was a distorted tetrahedral geometry and being as a photoactive substance. It emits a weak luminescence at 620 nm. In addition the by product of $ZnCl_4$.(dmazpy + $2H^+$) ionic complex are formed.

[Ru(*p*-cymene)(dmazpy)Cl]Cl is the precursor which was synthesized and well characterized by spectroscopic techniques. The [Ru(*p*-cymene)(dmazpy)Cl]Cl was later used to synthesize the Ru(dmazpy)(dcbpyH_2)Cl_2 and [Ru(dmazpy)(dcbpyH_2)$_2$](PF_6)$_2$ Complexes. The Ru(dmazpy)(dcbpyH_2)Cl_2 was successfully characterized by ES-MS technique. However, The complex of [Ru(dmazpy)(dcbpyH_2)$_2$](PF_6)$_2$ was not successful from the purification and characterization. However, it is supposed that the [Ru(dmazpy)$_2$(dcbpyH_2)](PF_6)$_2$ was generated in preference.

REFERENCES

An D.-L., Du M., Bu X.-H., Biradha K., Shionoya M. 2002. 5-Amino-6,8-dichloro-2,3-bis(2-pyridyl)quinoxalinedichlorozinc(II). Acta Crystallogr., Sect. E: Struct. Rep. Online. 58, 436.

Anitha C., Sheela C.D., Tharmaraj P., Raja S.J. 2012. Synthesis and characterization of VO(II), Co(II), Ni(II), Cu(II) and Zn(II) complexes of chromone based azo-linked Schiff base ligand. Spectrochim. Acta, Part A. 98, 35-42.

Anitha C., Sheela C.D., Tharmaraj P., Sumathi S. 2012. Spectroscopic studies and biological evaluation of some transition metal complexes of azo Schiff-base ligand derived from (1-phenyl-2,3-dimethyl-4-aminopyrazol-5-one)and5-((4-chlorophenyl)diazenyl)-2 hydroxybenzal -dehyde.Spectro- chim. Acta, Part A. 96, 493-500.

Arslan F. 2007 Synthesis, crystal structure and spectrothermal characterization of zinc(II) salicylato complex with 2,2′-azobispyridine, $[Zn(Hsal)_2 (H_2O)(abpy)].H_2O$. Dyes and Pigments. 75, 521-525.

Barf G.A., Sheldon R.A. 1995. Ruthenium catalyzed epoxidations: mechanistic and synthetic aspects. Molecular Catalysis A: Chemical. 102, 1995.

Bringley J. F. Rajeswaran M. 2006. *p*-Phenylenediammonium tetrachlorozincate(II). Acta Crystallogr., Sect. E: Struct. Rep. Online. 62, 1304-1305.

Byabartta P., Santra P.K., Misra T.K., Sinha C., Kennard C.H.L., Synthesis, spectral characterisation, redox studies of isomeric dichloro-bis-[1-alkyl-2-(naphthyl-(α/β)-azo)imidazole]ruthenium(II). Single crystal X-ray structure of blue-green dichloro-bis-[1-ethyl-2-(naphthylazo) imidazole] ruthenium(II). Polyhedron 20, 905–913.

Celik O., Ide S., Kurt M., Yurdakul S. 2004. Dichlorobis(phthalazine)zinc(II). Acta Crystallogr., Sect. E: Struct. Rep. Online. 60, 1134.

Chen Y., Liu W., Liu B., Zhou X. H., Zou Z. G., Zuo J. L., You X. Z. 2009. Synthesis and charac- terization of new ruthenium(II) complexs containing coupled di(2-pyridyl)and 1,3-dithiole units. Inorg. Chim. Acta. 362, 143-148.

Dharmalingam S., Lee H.-J., Yoon S. 2012. Dichloridobis(2-phenylpyridine-κ*N*) zinc(II). Acta Crystallogr., Sect. E: Struct. Rep. Online. 68, 431–432.

Funaki T., Yanagida M., Onozawa-Komatsuzaki N., Kasuga K., Kawanishi Y., Sugihara H. 2009. A 2-quinolinecarboxylate-substituted ruthenium (II) complex as a new type of sensitizer for dye sensitized solar cell. Inorg. Chim. Acta. 362, 2519-2522.

Grätzel M. 2004. Conversion of sunlight to electric power by nanocrytalline dye-sensitized solar cells. Photochem. Photobiol A: Chem. 164, 3-14.

Grätzel M. 2005. Solar Energy Conversion by Dye-Sensitized Photovoltaic Cells. Inorg. Chim. Acta. 44 (20), 6841–6851.

Gibbons W.M., Shannon P.J., Sun S.-T., Swetlin B.J. 1991. Surface-mediated alignment of nematic liquid crystals with polarized laser light Nature 351, 49–50.

Hansongnern K., Changsaluk U., Wu J-S., Lu T-H. Crystal Structure of the[$Ru(azpy)_2$ (bpy)](PF_6)$_2$ Complex (azpy = 2-(phenylazo)pyridine, bpy = 2,2′-bipyridine). Anal. Sci. 23, 131-132.

Harrison W. T. A. 2005. Ethylenediaminium tetrachlorozincate. Acta Crystallogr., Sect. E: Struct. Rep. Online. 61, 1951-1952.

Ho J. K., Moser H., Kishimoto Y., Hamilton, J. A.1995. Interactions of a very long chain fatty acid with model membranes and serum albumin: implications for the pathogenesis of adrenoleukodystrophy. Clin. Invest. 96, 1455-1463.

Huang W., Lana C-M., Liub Y.-S., Lee P.-H., Chang S.-M., Diau E. W.-G. 2010. Synthesis and Characterization of Novel Heteroleptic Ruthenium Complexes for Dye-Sensitized Solar Cells. Chin. Chem. Soc. 57, 1151-1156.

Jiang K. J., Xia J. B., Masaki N., Noda S., Yanagida S. 2008. Efficient sensitization of nanocrystalline TiO_2 film with high molar extinction coefficient ruthenium complex. Inorg. Chim. Acta. 361, 783- 785.

Kalateh K., Ahmadi R., Amani V. 2010. Dibromido(6-methyl-2,2′-bipyridine κ^2N,N') zinc(II) Acta Crystallogr., Sect. E: Struct. Rep. Online. 66, 1241.

Kay A.; Grätzel M. 1996. Low cost photovoltaic modules based on dye Sensitized nanocrystalline titanium dioxide and carbon powder. Sol. Energ. Mat. Sol. 44, 99-117.

Khalighi A., Ahmadi R., Amani V., Khavasi H.R.2008. Dichlorido(5,5′-dimethyl- 2,2′ -bipyridine-κ^2N,N')zinc(II). Acta Crystallogr., Sect. E: Struct. Rep. Online. 64, 1211–1212.

Kuang D., Klein C., Snaith H. J., Humphry-Baker R., Zakeeruddin S.M., Grätzel M. 2008. A new ion Coordinating ruthenium sensitizer for mesoscopic dye sensitized solar cells. Inorg. Chim. Acta. 361, 699-706.

Lagref J.-J., Nazeeruddin Md. K., Grätzel M. 2008. Artificial photosynthesis based on dye-sensitized Nanocrytalline TiO_2 solar cells. Inorg. Chim. Acta. 361, 735-745.

Laity H.L., Taylor M.R. 1995. Dichlorobis(purine)zinc(II). Acta Crystallogr., Sect. E: Struct. Rep. Online. 51, 1791-1793.

Lee T. Y., Alegaonkar P.S., Yoo J.-B. 2007. Fabrication of dye sensitized solar cell using coated cabon naanotubes. Thin Solid Films. 515, 5131-5135.

Leesakul N., Pakawatchai C., Saithong S., Tantirungrotechai Y., Kwanplod K. 2011. Dichloridobis{*N,N*-diethyl-4-[(pyridin-2-yκN)diazenyl]aniline}zinc. Acta Crystallogr., Sect. E: Struct. Rep. Online. 67, 955-956.

Leesakul N., Runrueng W., Saithong S., Pakawatchai C. 2012. 2-{2-[4-(Dimethyl-amino) phenyl]diazen-1-ium-1-yl}pyridinium tetrachlorido-zincate. Acta Crystallogr., Sect. E: Struct. Rep. Online. 68, 837.

Li C., Zhang G., Yin Z. 2012. Dichloridobis(4-pyridylmethyl 1*H*-pyrrole-2-carboxy-late-κN)zinc. Acta Crystallogr., Sect. E: Struct. Rep. Online. 68, 323.

Li X., Gui J., Yang H., Wu W., Li F., Tain H., Hung C. 2008. A new carbazole-based phenanthrenyl ruthenium complex as sensitizer for dye-sensitized solar cell. Inorg. Chim. Acta. 361, 2835-2840.

Nag J.K.; Santra P. K.; Sinha C., Liao F. L.; Lu T. H. 2001. Synthesis, spectral and electrochemical studies of 2-(arylazo)heterocycle complexes of zinc(II) Single-crystal X-ray structure of [Zn(papm)Cl_2·CH_3OH](papm= 2-(phenylazo)pyrimidine). Polyhedron.; 20, 2253 – 2259.

Millington K. R., Fincher K. W., King A. L. 2007. Mordant dyes as sensitisers in dye- sensitised solar cells. Sol. Energy Mater. Sol. Cells. 91, 1618-1630.

Mondal T.K., Dinda J., Slawin A.M.Z., Derek Woollins J., Sinha C. 2007. Osmium-carbonyl complexes of naphthylazoimidazoles. Single crystal X-ray structure of [Os(H)(CO)$(PPh3)_2$(a-NaiEt)](PF_6){a-NaiEt = 1-ethyl-2-(naphthyl-a-azo)imidazole} Polyhedron. 26, 600–606.

Nazeeruddin Md. K., Kay A., Rodicio I., Humphry B. R., Mueller E., Liska P., Vlachopoulos N., Gräetzel M. 1993. Conversion of light to electricity by *cis*-X_2Bis(2,2′-bipyridyl-4,4′-dicarboxylate)ruthenium(II) charge-transfer sensitizers (X= Cl^-, Br^-, I^-, CN^-, and SCN^-) on nanocrystalline TiO_2 electrode. Am. Chem. Soc. 115, 6382-6390.

Nazeeruddin Md. K., Klein C., Liska P., Grätzel M. 2005. Synthesis of novel ruthenium sensitizers and their application in dye-sensitized solar cells. Coord. Chem. Rev. 249, 1460-1467.

Nazeeruddin Md. K., Zakeeruddin S. M., Lagref J. J., Liska P., Comte P., Barolo C., Viscardi G., Schenk K., Grätzel M. 2004. Stepwise assembly of amphiphilic ruthenium sensitizers and their applications in dye-sensitized solar cells. Coord. Chem. Rev. 248, 1317-1328.

OcaKoglu K., Zafer C., Cetinkaya B., Icli S. 2007. Synthesis, characterization, electrochemical and Spectroscopic studies of two new heteroleotic Ru(II) polypyridyl complexes. Dyes Pigments. 75, 385-394.

Pramanik A., Basu A., Das G., 2010. Coordination assembly of p-substituted aryl azo imidazole complexes: Influences of electron donating substitution and counter ions. Polyhedron. 29, 1980-1989.

Pramanik A., Das G. 2010. Aryl azo imidazole assisted self-assembly of d^{10} metal complexes: Influence of halogen substitution and counter ions. Polyhedron. 29, 2999-3007.

Sahin C., Tozlu C., Ocakoglu K., Zafer C., Varlikli C., Icli S. 2008. Synthesis of an amphiphilic Ruthenium complex with swallow-tail bipyridyl ligand and its application in nc-DSC. Inorg. Chim. Acta**.** 361, 671-676.

Samanta B., Chakraborty J., Shit S., Batten S.R., Jensen P., Masuda J.D., Mitra S. 2007. Synthesis, characterisation and crystal structures of a few coordination complexes of nickel(II), cobalt(III) and zinc(II) with N′-[(2pyridyl)methylene] salicyloylhydrazone Schiff base. Inorg. Chim. Acta. 360, 2471-2484.

Santra P.K., Sinha C., Sheen W.-J., Liao F.-L., Lu T.-H. 2001. Reaction of $Ru(PPh_3)_3Cl_2$ with 2-(arylazo)pyrimidines.Spectral and redox characterisation of the products. Part V. Single crystal X-ray structure of $Ru(PPh_3)_2$ (papm) Cl_2 (papm=2-(phenylazo)pyrimidine). Polyhedron. 20, 599-606.

Sharma A., Sharma R., Chaudhary P., Vatsyayan R., Pearce V., Jeyaba P., Zimniak P., Awasth S., Awasthi Y. C.2008. 4-Hydroxynonenal induces p53-mediated apoptosis in retinal pigment epithelial cells. Biochem and biophycal. 480, 85–94.

Shirvan S.A., Dezfuli S.H. 2012. Dichloridobis(pyrazine-2-carboxamide-κN^4)zinc(II). Acta Cryst. 68, 546.

SivaKumar R., Marcelis A. T. M., Anandan S. 2009. Synthesis and characterization of novel heteroleptic ruthenium sensitizer for nanocrystalline dye-sensitized solar cells. Photochem. Photobiol A: Chem. 208, 154-158.

Song H.-K., Park Y. H., Han C.-H., Jee J.-G. 2009. Synthesis of ruthenium complex and its application in dye-sensitized solar cells. Ind. Eng. Chem. 15, 62-65.

Tachibana Y., Nazeeruddin Md. K., Grätzel M., Klug D. R., Durrant J. R. 2002. Electron injection Kinetic for the nanocrytalline TiO_2 films sensitized with the dye $(Bu_4N)_2Ru(dcbpyH)_2(NCS)_2$. Chem. Phys. 285, 127-132.

Tan Z.-D., Tan F.-J., Tan B., Zhang C.-M. 2011. Dichloridobis[4-(1*H*-pyrazol-3-yl)-pyridine-κN^1]zinc. Acta Crystallogr., Sect. E: Struct. Rep. Online. 67, 1408.

Valdés-Martínez J., Muñoz O., Toscano R. A. π-π Stacking in bis(quinolinium) tetrachlorozincate dihydrate. Acta Crystallogr., Sect. E: Struct. Rep. Online. 61, 1590-1592.

Xu W., Shi J.-M., Zhang X. 2005. Tetraaquabis(thiocyanato-κ*N*) zinc(II) bis(methylpy razine 1,4-dioxide). Acta Crystallogr., Sect. E: Struct. Rep. Online. 61, 2194-2195.

APPENDIX

Table 1. Crystal data and structure refinement for [Zn(dmazpy)Cl_2].

Identification code	Zndm	
Empirical formula	C_{13} H_{14} Cl_4 N_4 Zn	
Formula weight	433.45	
Temperature	293(2) K	
Wavelength	0.71073 Å	
Crystal system	Monoclinic	
Space group	$P2_1/n$	
Unit cell dimensions	a = 7.4556(4) Å	α = 90°.
	b = 21.4126(10) Å	β = 99.8830(10)°.
	c = 11.1924(5) Å	γ = 90°.
Volume	1760.28(15) $Å^3$	
Z	4	
Density (calculated)	1.636 Mg/m^3	
Absorption coefficient	2.002 mm^{-1}	
F(000)	872	
Crystal size	0.184 x 0.172 x 0.037 mm^3	
Theta range for data collection	1.90 to 24.99°.	
Index ranges	-8<=h<=8, -25<=k<=25, -13<=l<=13	
Reflections collected	16401	
Independent reflections	3094 [R(int) = 0.0342]	
Completeness to theta = 24.99°	100.0 %	
Absorption correction	Semi-empirical from equivalents	
Max. and min. transmission	0.929 and 0.699	
Refinement method	Full-matrix least-squares on F^2	
Data / restraints / parameters	3094 / 0 / 201	
Goodness-of-fit on F^2	1.102	
Final R indices [$I>2\sigma(I)$]	$R1$ = 0.0362, $wR2$ = 0.0859	
R indices (all data)	$R1$ = 0.0435, $wR2$ = 0.0892	
Largest diff. peak and hole	0.566 and -0.207 e.$Å^{-3}$	

Table 2. Atomic coordinates (x 10^4) and equivalent isotropic displacement parameters (Å^{2}x 10^3) for [$(dmazpyH_2)^{2+}$ $(ZnCl_4)^{2-}$]. U(eq) is defined as one third of the trace of the orthogonalized U^{ij} tensor.

	x	y	z	U(eq)
Zn(1)	3154(1)	1310(1)	3117(1)	39(1)
Cl(1)	5337(1)	1010(1)	2033(1)	55(1)
Cl(2)	2706(1)	541(1)	4408(1)	49(1)
Cl(3)	513(1)	1494(1)	1811(1)	59(1)
Cl(4)	4108(1)	2165(1)	4215(1)	55(1)
N(1)	6142(3)	10374(1)	-1728(2)	39(1)
C(1)	5354(4)	10617(2)	-2788(3)	43(1)
C(2)	5437(5)	11238(2)	-2992(3)	47(1)
C(3)	6347(5)	11623(2)	-2089(3)	47(1)
C(4)	7169(5)	11373(2)	-1010(3)	45(1)
C(5)	7065(4)	10734(2)	-844(3)	39(1)
N(2)	7873(4)	10441(1)	213(2)	42(1)
N(3)	7673(4)	9829(1)	250(2)	42(1)
C(6)	8342(4)	9510(1)	1229(3)	37(1)
C(7)	9313(4)	9744(2)	2355(3)	42(1)
C(8)	9917(5)	9359(2)	3276(3)	45(1)
C(9)	9628(4)	8698(2)	3181(3)	43(1)
C(10)	8650(5)	8460(2)	2047(3)	50(1)
C(11)	8058(5)	8848(2)	1130(3)	46(1)
N(4)	10279(4)	8328(2)	4091(3)	58(1)
C(12)	11323(6)	8561(2)	5242(3)	78(1)
C(13)	10057(9)	7650(2)	4026(5)	102(2)

Table 3. Bond lengths [Å] and angles [°] for [$(dmazpyH_2)^{2+}$ $(ZnCl_4)^{2-}$].

Zn(1)-Cl(4)	2.2509(9)
Zn(1)-Cl(2)	2.2539(9)
Zn(1)-Cl(3)	2.2762(9)
Zn(1)-Cl(1)	2.2823(9)
N(1)-C(1)	1.336(4)
N(1)-C(5)	1.347(4)
C(1)-C(2)	1.352(5)
C(1)-H(1)	0.9300
C(2)-C(3)	1.388(5)
C(2)-H(2)	0.9300
C(3)-C(4)	1.366(5)
C(3)-H(3)	0.9300
C(4)-C(5)	1.385(4)
C(4)-H(4)	0.9300
C(5)-N(2)	1.382(4)
N(2)-N(3)	1.320(4)
N(3)-C(6)	1.315(4)
C(6)-C(7)	1.433(4)
C(6)-C(11)	1.433(4)
C(7)-C(8)	1.336(4)
C(7)-H(7)	0.9300
C(8)-C(9)	1.433(5)
C(8)-H(8)	0.9300
C(9)-N(4)	1.316(4)
C(9)-C(10)	1.442(5)
C(10)-C(11)	1.336(5)
C(10)-H(10)	0.9300
C(11)-H(11)	0.9300
N(4)-C(13)	1.461(6)
N(4)-C(12)	1.473(5)
C(12)-H(12A)	0.9600
C(12)-H(12B)	0.9600
C(12)-H(12C)	0.9600
C(13)-H(13A)	0.9600
C(13)-H(13B)	0.9600

C(13)-H(13C)	0.9600
Cl(4)-Zn(1)-Cl(2)	108.16(3)
Cl(4)-Zn(1)-Cl(3)	111.55(4)
Cl(2)-Zn(1)-Cl(3)	109.34(4)
Cl(4)-Zn(1)-Cl(1)	109.39(4)
Cl(2)-Zn(1)-Cl(1)	109.43(4)
Cl(3)-Zn(1)-Cl(1)	108.94(4)
C(1)-N(1)-C(5)	121.4(3)
N(1)-C(1)-C(2)	120.5(3)
N(1)-C(1)-H(1)	119.8
C(2)-C(1)-H(1)	119.8
C(1)-C(2)-C(3)	119.5(3)
C(1)-C(2)-H(2)	120.2
C(3)-C(2)-H(2)	120.2
C(4)-C(3)-C(2)	119.9(3)
C(4)-C(3)-H(3)	120.0
C(2)-C(3)-H(3)	120.0
C(3)-C(4)-C(5)	118.7(3)
C(3)-C(4)-H(4)	120.7
C(5)-C(4)-H(4)	120.7
N(1)-C(5)-N(2)	117.5(3)
N(1)-C(5)-C(4)	120.0(3)
N(2)-C(5)-C(4)	122.5(3)
N(3)-N(2)-C(5)	116.2(3)
C(6)-N(3)-N(2)	120.9(3)
N(3)-C(6)-C(7)	127.8(3)
N(3)-C(6)-C(11)	114.8(3)
C(7)-C(6)-C(11)	117.3(3)
C(8)-C(7)-C(6)	121.0(3)
C(8)-C(7)-H(7)	119.5
C(6)-C(7)-H(7)	119.5
C(7)-C(8)-C(9)	121.7(3)
C(7)-C(8)-H(8)	119.1
C(9)-C(8)-H(8)	119.1
N(4)-C(9)-C(8)	120.4(3)
N(4)-C(9)-C(10)	122.2(3)
C(8)-C(9)-C(10)	117.4(3)

C(11)-C(10)-C(9)	120.5(3)
C(11)-C(10)-H(10)	119.7
C(9)-C(10)-H(10)	119.7
C(10)-C(11)-C(6)	122.0(3)
C(10)-C(11)-H(11)	119.0
C(6)-C(11)-H(11)	119.0
C(9)-N(4)-C(13)	122.4(4)
C(9)-N(4)-C(12)	122.9(3)
C(13)-N(4)-C(12)	114.8(3)
N(4)-C(12)-H(12A)	109.5
N(4)-C(12)-H(12B)	109.5
H(12A)-C(12)-H(12B)	109.5
N(4)-C(12)-H(12C)	109.5
H(12A)-C(12)-H(12C)	109.5
H(12B)-C(12)-H(12C)	109.5
N(4)-C(13)-H(13A)	109.5
N(4)-C(13)-H(13B)	109.5
H(13A)-C(13)-H(13B)	109.5
N(4)-C(13)-H(13C)	109.5
H(13A)-C(13)-H(13C)	109.5
H(13B)-C(13)-H(13C)	109.5

Table 4. Anisotropic displacement parameters ($Å^2 x\ 10^3$) for $[(dmazpyH_2)^{2+}(ZnCl_4)^{2-}]$. The anisotropic displacement factor exponent takes the form: $-2p^2[\ h^2 a^{*2} U^{11} + ...\ + 2\ h\ k\ a^*\ b^*\ U^{12}\ ]$

U^{11}	U^{22}	U^{33}	U^{23}	U^{13}	U^{12}	
Zn(1)	42(1)	40(1)	34(1)	-4(1)	2(1)	
0(1)						
Cl(1)	55(1)	53(1)	62(1)	-15(1)	23(1)	-
7(1)						
Cl(2)	58(1)	47(1)	39(1)	5(1)	-1(1)	-
5(1)						
Cl(3)	52(1)	76(1)	42(1)	7(1)	-10(1)	-
1(1)						
Cl(4)	76(1)	34(1)	50(1)	-6(1)	-5(1)	
5(1)						
N(1)39(1)	45(2)	34(1)	-6(1)	6(1)	1(1)	
C(1)41(2)	51(2)	35(2)	-6(2)	2(1)	1(2)	
C(2)45(2)	58(2)	34(2)	4(2)	0(1)	6(2)	
C(3)50(2)	42(2)	48(2)	5(2)	7(2)	-4(2)	
C(4)45(2)	46(2)	40(2)	-9(2)	1(2)	-5(2)	
C(5)32(2)	53(2)	32(2)	4(1)	6(1)	6(1)	
N(2)46(2)	45(2)	36(1)	-1(1)	5(1)	3(1)	
N(3)44(2)	43(2)	38(1)	0(1)	8(1)	2(1)	
C(6)35(2)	42(2)	34(2)	-1(1)	9(1)	1(1)	
C(7)48(2)	42(2)	36(2)	-2(1)	6(1)	-5(2)	
C(8)46(2)	54(2)	36(2)	-3(2)	4(2)	-1(2)	
C(9)41(2)	52(2)	38(2)	6(2)	14(2)	8(2)	
C(10)	61(2)	39(2)	51(2)	-1(2)	15(2)	
0(2)						
C(11)	53(2)	45(2)	38(2)	-6(2)	5(2)	-
2(2)						
N(4)67(2)	62(2)	50(2)	14(2)	22(2)	21(2)	
C(12)	86(3)	106(4)	41(2)	18(2)	4(2)	
43(3)						
C(13)	168(6)	64(3)	82(3)	32(3)	37(3)	
34(3)						

Table 5. Hydrogen coordinates (x 10^4) and isotropic displacement parameters ($Å^2$x 10 ^{3}) for [$(dmazpyH_2)^{2+}(ZnCl_4)^{2-}$].

	x	y	z	U(eq)
H(1)	4745	10357	-3390	52
H(2)	4889	11405	-3732	56
H(3)	6396	12052	-2218	56
H(4)	7785	11627	-400	53
H(7)	9527	10170	2447	51
H(8)	10542	9524	3997	55
H(10)	8430	8034	1955	60
H(11)	7444	8684	404	55
H(12A)	12563	8632	5148	117
H(12B)	11289	8258	5869	117
H(12C)	10798	8945	5457	117
H(13A)	10044	7513	3208	154
H(13B)	8931	7537	4275	154
H(13C)	11052	7455	4552	154

Table 6. Torsion angles [°] for $[(dmazpyH_2)^{2+}(ZnCl_4)^{2-}]$.

C(5)-N(1)-C(1)-C(2)	-1.3(5)
N(1)-C(1)-C(2)-C(3)	-0.1(5)
C(1)-C(2)-C(3)-C(4)	0.8(5)
C(2)-C(3)-C(4)-C(5)	-0.2(5)
C(1)-N(1)-C(5)-N(2)	-178.5(3)
C(1)-N(1)-C(5)-C(4)	1.9(5)
C(3)-C(4)-C(5)-N(1)	-1.1(5)
C(3)-C(4)-C(5)-N(2)	179.3(3)
N(1)-C(5)-N(2)-N(3)	0.6(4)
C(4)-C(5)-N(2)-N(3)	-179.8(3)
C(5)-N(2)-N(3)-C(6)	-177.8(3)
N(2)-N(3)-C(6)-C(7)	0.8(5)
N(2)-N(3)-C(6)-C(11)	-178.6(3)
N(3)-C(6)-C(7)-C(8)	-179.9(3)
C(11)-C(6)-C(7)-C(8)	-0.4(5)
C(6)-C(7)-C(8)-C(9)	0.1(5)
C(7)-C(8)-C(9)-N(4)	178.2(3)
C(7)-C(8)-C(9)-C(10)	-0.1(5)
N(4)-C(9)-C(10)-C(11)	-177.9(3)
C(8)-C(9)-C(10)-C(11)	0.4(5)
C(9)-C(10)-C(11)-C(6)	-0.7(5)
N(3)-C(6)-C(11)-C(10)	-179.7(3)
C(7)-C(6)-C(11)-C(10)	0.7(5)
C(8)-C(9)-N(4)-C(13)	-178.5(4)
C(10)-C(9)-N(4)-C(13)	-0.2(6)
C(8)-C(9)-N(4)-C(12)	0.0(5)
C(10)-C(9)-N(4)-C(12)	178.3(4)

Table 7. Crystal data and structure refinement for [Zn(dmazpy)Cl_2].

Identification code	zndm2	
Empirical formula	$C_{13}\ H_{14}\ Cl_2\ N_4\ Zn$	
Formula weight	362.55	
Temperature	293(2) K	
Wavelength	0.71073 Å	
Crystal system	Monoclinic	
Space group	$P2_1/n$	
Unit cell dimensions	a = 7.7184(3) Å	$\alpha = 90^o$
	b = 13.6251(6) ล	$\beta = 95.3710(10)^o$
	c = 14.7582(6) ล	$\gamma = 90^o$
Volume	1545.22(11) ล^3	
Z	4	
Density (calculated)	1.558 Mg/m^3	
Absorption coefficient	1.929 mm^{-1}	
F(000)	736	
Crystal size	0.271 x 0.105 x 0.074 mm^3	
Theta range for data collection	2.04 to 25.00^o	
Index ranges	-9<=h<=9, -16<=k<=16, -17<=l<=17	
Reflections collected	16470	
Independent reflections	2724 [R(int) = 0.0288]	
Completeness to theta = 25.00^o	100.0 %	
Absorption correction	Semi-empirical from equivalents	
Max. and min. transmission	0.867 and 0.784	
Refinement method	Full-matrix least-squares on F^2	
Data / restraints / parameters	2724 / 0 / 183	
Goodness-of-fit on F^2	1.064	
Final R indices [$I>2\sigma(I)$]	$R1$ = 0.0302, $wR2$ = 0.0767	
R indices (all data)	$R1$ = 0.0376, $wR2$ = 0.0801	
Largest diff. peak and hole	0.322 and -0.210 e.Å^{-3}	

Table 8. Atomic coordinates (x 10^4) and equivalent isotropic displacement parameters ($Å^2$x 10^3) for [Zn(dmazpy)Cl_2]. U(eq) is defined as one third of the trace of the orthogonalized U^{ij} tensor.

	x	y	z	U(eq)
Zn(1)	2513(1)	2379(1)	952(1)	50(1)
Cl(1)	117(1)	3044(1)	323(1)	81(1)
Cl(2)	4921(1)	3214(1)	889(1)	66(1)
N(1)	2173(3)	1803(2)	2198(1)	51(1)
N(2)	2085(3)	316(2)	1353(1)	54(1)
N(3)	2474(2)	870(2)	696(1)	48(1)
C(1)	2061(4)	2278(2)	2991(2)	62(1)
C(2)	1670(4)	1796(3)	3759(2)	69(1)
C(3)	1387(4)	810(3)	3721(2)	74(1)
C(4)	1506(4)	312(2)	2919(2)	70(1)
C(5)	1924(3)	840(2)	2164(2)	52(1)
C(6)	2640(3)	429(2)	-134(2)	48(1)
C(7)	2345(3)	-562(2)	-322(2)	56(1)
C(8)	2545(3)	-934(2)	-1160(2)	57(1)
C(9)	3067(3)	-331(2)	-1870(2)	52(1)
C(10)	3348(4)	671(2)	-1671(2)	62(1)
C(11)	3151(4)	1034(2)	-830(2)	59(1)
N(4)	3289(3)	-698(2)	-2699(2)	59(1)
C(12)	3065(5)	-1738(2)	-2905(2)	76(1)
C(13)	3667(5)	-65(2)	-3453(2)	77(1)

Table 9. Bond lengths [Å] and angles [°] for [Zn(dmazpy)Cl_2].

Zn(1)-N(1)	2.040(2)
Zn(1)-N(3)	2.090(2)
Zn(1)-Cl(1)	2.1860(8)
Zn(1)-Cl(2)	2.1888(7)
N(1)-C(5)	1.326(3)
N(1)-C(1)	1.346(3)
N(2)-N(3)	1.288(3)
N(2)-C(5)	1.409(3)
N(3)-C(6)	1.380(3)
C(1)-C(2)	1.369(4)
C(1)-H(1)	0.9300
C(2)-C(3)	1.360(5)
C(2)-H(2)	0.9300
C(3)-C(4)	1.376(4)
C(3)-H(3)	0.9300
C(4)-C(5)	1.389(3)
C(4)-H(4)	0.9300
C(6)-C(7)	1.393(4)
C(6)-C(11)	1.404(3)
C(7)-C(8)	1.358(4)
C(7)-H(7)	0.9300
C(8)-C(9)	1.419(4)
C(8)-H(8)	0.9300
C(9)-N(4)	1.347(3)
C(9)-C(10)	1.409(4)
C(10)-C(11)	1.357(4)
C(10)-H(10)	0.9300
C(11)-H(11)	0.9300
N(4)-C(12)	1.456(4)
N(4)-C(13)	1.459(4)
C(12)-H(12A)	0.9600
C(12)-H(12B)	0.9600
C(12)-H(12C)	0.9600
C(13)-H(13A)	0.9600
C(13)-H(13B)	0.9600

C(13)-H(13C)	0.9600
N(1)-Zn(1)-N(3)	77.49(8)
N(1)-Zn(1)-Cl(1)	111.55(6)
N(3)-Zn(1)-Cl(1)	109.47(6)
N(1)-Zn(1)-Cl(2)	114.83(6)
N(3)-Zn(1)-Cl(2)	120.09(6)
Cl(1)-Zn(1)-Cl(2)	117.06(3)
C(5)-N(1)-C(1)	119.2(2)
C(5)-N(1)-Zn(1)	112.18(16)
C(1)-N(1)-Zn(1)	128.48(19)
N(3)-N(2)-C(5)	112.8(2)
N(2)-N(3)-C(6)	117.4(2)
N(2)-N(3)-Zn(1)	116.18(16)
C(6)-N(3)-Zn(1)	126.04(16)
N(1)-C(1)-C(2)	121.7(3)
N(1)-C(1)-H(1)	119.1
C(2)-C(1)-H(1)	119.1
C(3)-C(2)-C(1)	119.1(3)
C(3)-C(2)-H(2)	120.4
C(1)-C(2)-H(2)	120.4
C(2)-C(3)-C(4)	120.0(3)
C(2)-C(3)-H(3)	120.0
C(4)-C(3)-H(3)	120.0
C(3)-C(4)-C(5)	118.3(3)
C(3)-C(4)-H(4)	120.9
C(5)-C(4)-H(4)	120.9
N(1)-C(5)-C(4)	121.7(3)
N(1)-C(5)-N(2)	120.6(2)
C(4)-C(5)-N(2)	117.6(3)
N(3)-C(6)-C(7)	125.0(2)
N(3)-C(6)-C(11)	116.7(2)
C(7)-C(6)-C(11)	118.4(2)
C(8)-C(7)-C(6)	120.9(2)
C(8)-C(7)-H(7)	119.6
C(6)-C(7)-H(7)	119.6
C(7)-C(8)-C(9)	121.4(2)
C(7)-C(8)-H(8)	119.3

C(9)-C(8)-H(8)	119.3
N(4)-C(9)-C(10)	121.2(2)
N(4)-C(9)-C(8)	121.6(2)
C(10)-C(9)-C(8)	117.1(2)
C(11)-C(10)-C(9)	121.1(2)
C(11)-C(10)-H(10)	119.5
C(9)-C(10)-H(10)	119.5
C(10)-C(11)-C(6)	121.2(3)
C(10)-C(11)-H(11)	119.4
C(6)-C(11)-H(11)	119.4
C(9)-N(4)-C(12)	121.9(2)
C(9)-N(4)-C(13)	121.7(2)
C(12)-N(4)-C(13)	116.3(2)
N(4)-C(12)-H(12A)	109.5
N(4)-C(12)-H(12B)	109.5
H(12A)-C(12)-H(12B)	109.5
N(4)-C(12)-H(12C)	109.5
H(12A)-C(12)-H(12C)	109.5
H(12B)-C(12)-H(12C)	109.5
N(4)-C(13)-H(13A)	109.5
N(4)-C(13)-H(13B)	109.5
H(13A)-C(13)-H(13B)	109.5
N(4)-C(13)-H(13C)	109.5
H(13A)-C(13)-H(13C)	109.5
H(13B)-C(13)-H(13C)	109.5

Symmetry transformations used to generate equivalent atoms:

Table 10. Anisotropic displacement parameters ($Å^2 x\ 10^3$) for [Zn(dmazpy)Cl_2]—P21-n. The anisotropic displacement factor exponent takes the form: $-2\pi^2[\ h^2\ a^{*2}U^{11} + ...\ + 2\ h\ k\ a^*\ b^*\ U^{12}\ ]$

U^{11}	U^{22}	U^{33}	U^{23}	U^{13}	U^{12}	
Zn(1)	64(1)	44(1)	43(1)	2(1)	15(1)	-
1(1)						
Cl(1)	76(1)	80(1)	86(1)	18(1)	5(1)	
15(1)						
Cl(2)	74(1)	56(1)	73(1)	-7(1)	29(1)	-
13(1)						
N(1)57(1)	58(1)	41(1)	2(1)	11(1)	-4(1)	
N(2)63(1)	47(1)	52(1)	8(1)	12(1)	0(1)	
N(3)55(1)	45(1)	46(1)	5(1)	10(1)	2(1)	
C(1)66(2)	73(2)	49(2)	-3(1)	12(1)	-6(1)	
C(2)66(2)	99(3)	43(2)	2(2)	12(1)	-1(2)	
C(3)81(2)	94(3)	49(2)	23(2)	18(1)	6(2)	
C(4)82(2)	69(2)	61(2)	19(2)	19(2)	4(2)	
C(5)52(1)	60(2)	45(1)	11(1)	9(1)	3(1)	
C(6)56(1)	43(1)	47(1)	1(1)	10(1)	2(1)	
C(7)66(2)	43(1)	59(2)	7(1)	14(1)	1(1)	
C(8)67(2)	41(1)	64(2)	-4(1)	9(1)	-1(1)	
C(9)54(1)	49(2)	52(2)	-3(1)	7(1)	5(1)	
C(10)	86(2)	49(2)	54(2)	3(1)	23(1)	-
3(1)						
C(11)	87(2)	41(1)	51(2)	-1(1)	17(1)	-
6(1)						
N(4)72(1)	54(1)	53(1)	-7(1)	7(1)	6(1)	
C(12)	96(2)	65(2)	65(2)	-20(2)	4(2)	
5(2)						
C(13)	100(2)	76(2)	59(2)	0(2)	21(2)	
15(2)						

Table 11. Hydrogen coordinates (x 10^4) and isotropic displacement parameters ($Å^2$x 10^3) for [Zn(dmazpy)Cl_2].

	x	y	z	U(eq)
H(1)	2254	2951	3016	75
H(2)	1599	2137	4300	83
H(3)	1113	474	4237	89
H(4)	1311	-361	2882	83
H(7)	2007	-975	131	67
H(8)	2336	-1597	-1270	69
H(10)	3675	1090	-2122	74
H(11)	3358	1697	-714	71
H(12A)	3654	-2119	-2423	113
H(12B)	3545	-1883	-3467	113
H(12C)	1848	-1897	-2960	113
H(13A)	2709	374	-3598	116
H(13B)	3839	-461	-3976	116
H(13C)	4702	307	-3283	116

Table 12. Torsion angles [Å] for [Zn(dmazpy)Cl_2].

N(3)-Zn(1)-N(1)-C(5)	-6.78(17)
Cl(1)-Zn(1)-N(1)-C(5)	99.44(17)
Cl(2)-Zn(1)-N(1)-C(5)	-124.37(16)
N(3)-Zn(1)-N(1)-C(1)	178.0(2)
Cl(1)-Zn(1)-N(1)-C(1)	-75.8(2)
Cl(2)-Zn(1)-N(1)-C(1)	60.4(2)
C(5)-N(2)-N(3)-C(6)	-179.2(2)
C(5)-N(2)-N(3)-Zn(1)	-6.0(3)
N(1)-Zn(1)-N(3)-N(2)	7.23(17)
Cl(1)-Zn(1)-N(3)-N(2)	-101.47(16)
Cl(2)-Zn(1)-N(3)-N(2)	118.86(16)
N(1)-Zn(1)-N(3)-C(6)	179.8(2)
Cl(1)-Zn(1)-N(3)-C(6)	71.09(19)
Cl(2)-Zn(1)-N(3)-C(6)	-68.6(2)
C(5)-N(1)-C(1)-C(2)	-1.1(4)
Zn(1)-N(1)-C(1)-C(2)	173.8(2)
N(1)-C(1)-C(2)-C(3)	0.0(5)
C(1)-C(2)-C(3)-C(4)	0.4(5)
C(2)-C(3)-C(4)-C(5)	0.3(5)
C(1)-N(1)-C(5)-C(4)	1.8(4)
Zn(1)-N(1)-C(5)-C(4)	-173.9(2)
C(1)-N(1)-C(5)-N(2)	-178.0(2)
Zn(1)-N(1)-C(5)-N(2)	6.3(3)
C(3)-C(4)-C(5)-N(1)	-1.4(4)
C(3)-C(4)-C(5)-N(2)	178.4(3)
N(3)-N(2)-C(5)-N(1)	-0.2(3)
N(3)-N(2)-C(5)-C(4)	180.0(2)
N(2)-N(3)-C(6)-C(7)	2.9(4)
Zn(1)-N(3)-C(6)-C(7)	-169.6(2)
N(2)-N(3)-C(6)-C(11)	-176.9(2)
Zn(1)-N(3)-C(6)-C(11)	10.7(3)
N(3)-C(6)-C(7)-C(8)	-179.8(2)
C(11)-C(6)-C(7)-C(8)	0.0(4)
C(6)-C(7)-C(8)-C(9)	0.3(4)
C(7)-C(8)-C(9)-N(4)	179.1(2)

C(7)-C(8)-C(9)-C(10)	-0.7(4)
N(4)-C(9)-C(10)-C(11)	-178.9(3)
C(8)-C(9)-C(10)-C(11)	0.9(4)
C(9)-C(10)-C(11)-C(6)	-0.7(5)
N(3)-C(6)-C(11)-C(10)	-179.9(3)
C(7)-C(6)-C(11)-C(10)	0.3(4)
C(10)-C(9)-N(4)-C(12)	177.7(3)
C(8)-C(9)-N(4)-C(12)	-2.1(4)
C(10)-C(9)-N(4)-C(13)	-6.0(4)
C(8)-C(9)-N(4)-C(13)	174.2(3)

Symmetry transformations used to generate equivalent atoms:

Table 13. Hydrogen bonds for [Zn(dmazpy)Cl_2] [Å and^o].

D-H...A	d(D-H)	d(H...A)	d(D...A)	<(DHA)
C2—H2···Cl2#1	0.93	2.82	3.535(3)	134
C12—H12C···Cg2#2	0.96	2.92	3.784(4)	151

Symmetry codes: #1 : x−3/2, −y−1/2, z−1/2; #2 : −x, −y, −z.